MUONIUM CHEMISTRY IN CONDENSED MEDIA

by

CHI BIU WILLIAM NG

B.Sc., The University of British Columbia, 1978

A THESIS SUBMITTED IN PARTIAL FULFILLMENT OF

THE REQUIREMENTS FOR THE DEGREE OF

DOCTOR OF PHILOSOPHY

in

THE FACULTY OF GRADUATE STUDIES

(Department of Chemistry, U.B.C.)

We accept this thesis as conforming

to the required standard

THE UNIVERSITY OF BRITISH COLUMBIA

OCTOBER, 1983

In presenting this thesis in partial fulfilment of the requirements for an advanced degree at the University of British Columbia, I agree that the Library shall make it freely available for reference and study. I further agree that permission for extensive copying of this thesis for scholarly purposes may be granted by the head of my department or by his or her representatives. It is understood that copying or publication of this thesis for financial gain shall not be allowed without my written permission.

Department of CHEMISTRY

The University of British Columbia
1956 Main Mall
Vancouver, Canada
V6T 1Y3

Date Oct. 14, 1983

ABSTRACT

Muonium (μ^+e^-, chemical symbol Mu) consists of an orbital electron associated with a positive muon as nucleus. It can be regarded as a very light 'isotope' of the hydrogen atom because it has essentially the same Bohr radius and ionization energy. Thus it can be used as a sensitive probe of isotope effects and of H-atom reactions which cannot be studied by conventional techniques. Due to the unique nuclear spin properties of the muon, there are several techniques available for investigation. These include muon spin rotation (μSR), muonium spin rotation (MSR) and muonium radical spin rotation (MRSR) in transverse magnetic fields, as used in this study. Various fundamental aspects of muonium formation and of chemical reaction kinetics have been explored by the experiments presented in this thesis. These are summarized below.

(i) From the magnetic field dependence, it was verified that Mu does not react chemically with water to any significant extent. Its observed spontaneous slow spin relaxation arises from experimental artifacts such as magnetic field inhomogeneities and/or Mu-frequency beating. (ii) The MRSR technique was used to observe and identify muonium-substituted free radicals via their pair of precession frequencies in high transverse magnetic fields in pure benzene, pure styrene, and their mixtures. The results have implications regarding the mechanism of radical formation and selectivity. (iii) Both μSR and MSR experiments were performed on neopentane (liquid & solid) and concentrated KOH solutions. The μ^+ and Mu yields in these systems indicated that a spur model of Mu formation is neither appropriate nor adequate

to explain the results. (iv) In muonium solution kinetic studies, the reaction Mu + OH^-_{aq} was found to be relatively slow, with a substantial activation energy (E_a) and no kinetic isotope effect compared to H at room temperature. The reaction shows Mu behaving as a "muonic" acid. (v) Kinetic studies of the abstraction of D by Mu from DCO_2^- as a solute in water gave a large E_a. Upon comparison with HCO_2^-, the isotope effects (k_M/k_H and k'_H/k'_D) imply that quantum mechanical tunnelling does not dominate the abstraction of H and D atoms in HCO_2^- and DCO_2^- by either H or Mu at room temperature. (vi) The MSR technique was used to initiate a study of model biological systems (various solutes incorporated in cyclodextrins and micelles). The results demonstrated the sensitive and non-destructive nature of the MSR technique. (vii) Hydrocarbons were also investigated: including measuring their muon yields, their temperature dependence, the effect of an external electric field, and yields in solvent mixtures. Almost all the data obtained seem to be at variance with the expectations of significant intra-spur processes in Mu formation, but are consistent with that of a 'hot atom' mechanism.

TABLE OF CONTENTS

TABLE OF CONTENTS (cont'd) Page

TABLE OF CONTENTS (cont'd) Page

TABLE OF CONTENTS (cont'd) Page

LIST OF TABLES

LIST OF TABLES (cont'd)

LIST OF FIGURES

LIST OF FIGURES (cont'd)

LIST OF FIGURES (cont'd)

LIST OF FIGURES (cont'd)

ACKNOWLEDGEMENT

It is with the greatest pleasure to thank my research supervisor, Dr. David C. Walker, who has been both a very good friend and a tremendously patient advisor, for his helpful guidance and enlightening discussion. I must also give sincere thanks to Drs. Y.C. Jean (Univ. of Missouri-Kansas City) and T. Suzuki (Hachinole Institute of Technology, Japan) for being my experimental teachers during my early days at TRIUMF.

My whole-hearted gratitude must go to the delightful collaborations with Drs. Y. Ito (Univ. of Tokyo) and J.M. Stadlbauer (U.B.C. and Hood College, Maryland) during my graduate years. Furthermore, to Y. Miyake (Univ. of Tokyo), Dr. T. Nguyen (Univ. of Zurich), and R. Ganti (UMKC), their help during TRIUMF experiments are deeply appreciated.

Of course, this thesis could not have been completed without the many TRIUMF colleagues (J.H. Brewer, D.G. Fleming, D.M. Garner, R. Kiefl, G. Marshall, R.J. Mikula, and D.P Spencer). I am indebted to their many useful suggestions.

Finally, I must give all my thanks to my parents, whose support and patience provided me with energetic enthusiasm. It is with great respect that I dedicate to them this Ph.D. thesis.

CHAPTER 1

INTRODUCTION

1.A. Muonium, past and present.

Muonium (chemical symbol, Mu) is the atom consisting of a positive muon and an electron. The electron orbits the muon as its nucleus, therefore forming an analogous hydrogen atom. The muonium atom is viewed as the simplest system since both the muon and the electron are leptons [1], whereas the hydrogen atom (H) can now be considered as a four-particle system due to the advent of the theory of quarks [2]. In any event, chemically, the Mu atom can be regarded as an ultralight, radioactive isotope of the H atom. This is intrinsically obvious as the following table outlining the physical properties of the muon and Mu atom indicates [3,4,5].

Table 1.1

Physical parameters of the muon and the muonium atom.

Muon:	
Spin	1/2
Mass	$M_\mu = 206.77M_e = 0.11261M_p$
Mean lifetime	$\tau_\mu = 2.1971\times10^{-6}$ sec
Magnetic moment	$\mu_\mu = 3.1833\mu_p = 4.835\times10^{-3}\mu_e$
Muonium:	
Bohr radius	$a_M = 0.5317$ Å $= 1.0043a_o$(H)
Ionization potential	$I_p = 13.539$eV $= 0.9957$(H)
Hyperfine oscillation period	2.24×10^{-10} sec

The Bohr radii and the ionization potentials of both H and Mu are almost the same. In this sense, Mu is a true isotope of H. Its collisions with other atoms and molecules, especially chemical reactions, can be studied to examine with improved sensivity (relative to deuterium and tritium) such aspects as kinetic isotope effects and quantum mechanical tunnelling by comparing reactions of Mu with those of H.

In 1957, Garwin et al. [6] and Friedman et al. [7] made the first experimental observations of positive muons after the verification of the breakdown of the principle of parity invariance [8]. Although these two groups employed slightly different apparatus, their methods were forerunners of the present day μSR (muon spin rotation) technique. In the next few years, Hughes et al. [9] discovered free Mu atoms in argon gas and subsequently acclaimed it as an ultralight isotope of H atom [10]. Over the next decade, important experimental foundations of muon chemistry were paved by scientists studying the physical aspects of the muon and the muonium atom [11,12,13,14, 15]. In addition, a series of theoretical papers by Soviet groups led the way to fundamental understanding of the reaction and formation of Mu atoms [16,17,18]. During the 1970's, continuing experiments including measurements of the muon magnetic moment [19], the muon anomalous magnetic moment [20], and the hyperfine splitting of the Mu atom [1,21], helped to stablize and expand the field of muon and muonium chemistry immensely.

Muonium chemistry in condensed media was first studied by a group at Dubna [11,12,13] and then more extensively by a group at the Lawrence Berkeley Laboratory (LBL) [4,22,23]. It was not however until 1976 that

the first direct observation of Mu in water was achieved by Percival et al. at the Swiss Institute for Nuclear Research (SIN) near Zurich [24]. Since then, this group has continued to produce impressive data [25], including results in muonium-substituted transient radicals [26]. Here at TRIUMF, before 1978, the major investigation of Mu chemistry was centered around gas-phase studies [27,28]. However, since then, Jean et al. [29,30,31,32] have started and maintained a very competitive program of Mu chemistry in the condensed phase. In addition, recent direct observation of Mu in various hydrocarbons was successfully carried out at TRIUMF [33,34,35]. The applications of Mu as a nuclear probe in large macromolecular and biological systems [36,37,38,39,40] have also been a major concern here at U.B.C. Lastly, the recent use of Mu and Mu-substituted free radicals to study vinyl monomers [41] could give new insights about polymer initiation kinetics. As one can see, the field of Mu chemistry in the condensed phase is fast becoming of broad prospective and reaching into several conventional areas of chemical study.

1.B. Models of muonium formation.

At present, there are two models of muonium formation. One is referred to as the "HOT" model [4], while the other is called the "SPUR" model [42].

In the hot model, which was conceptualized earlier by physicists, essentially views an epithermal muon - with an energy up to several keV - abstracting an electron from the medium so that Mu is formed beyond the trail of ionizations (spurs) of the muon track. During its thermalization a certain

fraction of Mu reacts with the medium, some of which give diamagnetic muonic species or stay as free muons (P_D), some reach thermal energy as free Mu atoms (P_M) or as muonic free radicals (P_R), and some simply remain unobservable or lost (P_L) [43,44]. These fractions represent the relative probabilities of these reactions involved in the relevant energy range extending from several MeV, at which the muon enters the medium, down to thermal energies. However, in condensed media, these reaction probabilities are extremely difficult either to calculate or estimate; therefore making the hot model a very general and yet vague theory of muonium formation.

In radiation chemistry, a trail of spurs is a result of energy deposition to the medium from the passage and thermalization of a high energy charged particle, such as a positive muon. Typically, these spurs are regarded to result from the deposition, on average, of about 100eV of energy in a sphere of about 2 nm diameter in water. Therefore, these spurs are minute regions in the particle's track containing high concentrations of very reactive free radicals, electrons, positive ions, and excited molecules [45]. In positronium studies, Mögensen has postulated a spur model in which he argues that the positron (e^+) reaches thermal energy while still in the neighbourhood of reactive free radicals, electrons and ions generated in spurs in its thermalization track [46]. Recently, this has prompted an analogous "SPUR" model of Mu formation by Percival et al. [42]. The model pictures a muon being thermalized within the last spur of its own track in which it can either encounter a radiation-produced electron to become Mu or it can escape into the medium; at the same time, Mu can either perform intra-

spur reactions (including fast depolarization by a secondary solvated electron [47]) or escape from the spur. Therefore, this model attempts to explain the initial distribution of muons between diamagnetic and paramagnetic species simply based on the relative probabilities of reaction or escape of thermalized muons from the reactive species of the terminal spur. Although the spur model is more specific than the hot model, it is by no means a better theory of muonium formation. So far, there have certainly been more arguments against this spur model [28,33,34,35,48,49,50,51] than for it [43,44 52,53].

The two contrasting models, HOT and SPUR, have been in direct conflict for the proper mechanism of muonium formation in liquids. At this moment, both models are still under constant criticisms and investigations from the muon community and it is not yet so clear how Mu is formed, although the general consensus is that its formation could be some fractional contributions from both the HOT and SPUR theories. The schematics of the two models are illustrated in Figure 1.1. In the drawing, the time scales are mere differentiating guidelines between the two mechanisms and that the times of formation are only estimated.

1.C. Reaction dynamics in the liquid phase.

Contrary to gas phase studies, our knowledge of molecular motion and of molecular energy levels in liquids is not well developed. Therefore our approach toward encounters of molecules in solutions is quite different to that in gases. For example, N_2 gas molecules at STP occupy about 0.2% of

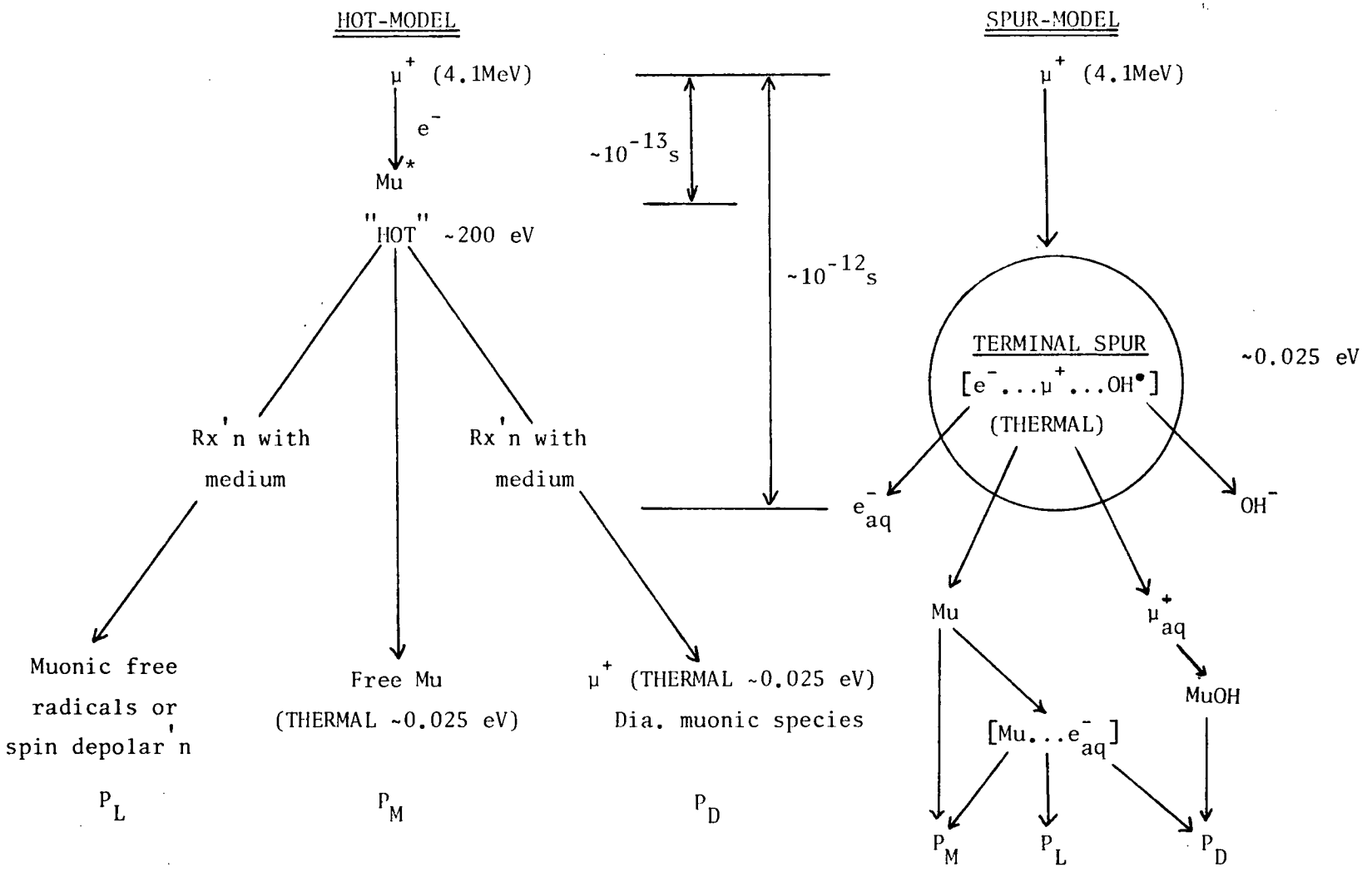

Figure 1.1: Diagrams showing the contrasting HOT and SPUR models for muonium formation in liquids.

the total volume while in the liquid this same figure rises to about 70% or more. This difference means that, while motion in gases is largely unhindered, molecules in solutions have to jostle their way past one another in order to make any substantial displacement. Clearly, the encounter frequency between two specified molecules initially separated is much smaller in solutions than that in gases. However, there is an important factor in this difference. In solutions, since molecules diffuse slowly into the region of a possible reaction partner, they also migrate slowly away from it. Therefore, once partners of a reaction move into each other's vicinity - into the same "solvent cage" - they collide with one another many times before escaping this solvent cage. In other words, once an encounter has occurred, the chance of undergoing a reaction is greatly enhanced compared to the gas phase. As a matter of fact, the time spent by a molecule in one of these solvent cages can be as long as 100 psec; and during this period, the molecule can make between 100 to 1000 collisions with its neighbouring molecules [54].

1.C.1. Types of reactions in solutions.

In order for molecule A to react with molecule B they must first come into contact with each other, and this requires the molecules to be in the same solvent cage where they are then referred to as the "encounter pair" [55]. The activation energy of a reaction (E_a) is now a complicated quantity (relative to gases) because the encounter pair is surrounded by solvent molecules and its reaction path is determined by all the neighbouring interactions. However, this situation can be depicted by the following reaction scheme:

$$A + B \underset{k_b}{\overset{k_d}{\rightleftharpoons}} \{A...B\} \xrightarrow{k_p} P \quad ; \qquad (1.1)$$

where {A...B} is the encounter pair, k_d and k_b are the diffusive-approach and separation rate constants, respectively, and k_p is the reaction rate constant giving product P. The steady state concentration of {A...B} can be found from the following rate equation:

$$\frac{d[\{AB\}]}{dt} = k_d[A][B] - k_b[\{AB\}] - k_p[\{AB\}] = 0 \quad , \qquad (1.2)$$

which gives:

$$[\{AB\}] = \left\{\frac{k_d}{(k_b+k_p)}\right\}[A][B] \quad . \qquad (1.3)$$

Substituting equation (1.3) into the rate expression for the formation of P gives the overall equation as:

$$\frac{d[P]}{dt} = k_p[\{AB\}] = \left\{\frac{k_p k_d}{k_b+k_p}\right\}[A][B] \quad . \qquad (1.4)$$

In equation (1.4) the overall rate law is second-order, and the bimolecular

rate constant, k_2 (experimentally observable, k_{obs}), is given as:

$$k_2 = \frac{k_p k_d}{(k_b + k_p)} \quad . \tag{1.5}$$

From equation (1.5), two limits can be recognized. If the rate of breakup of the encounter pair is much slower than the rate at which it forms products, that is $k_b << k_p$, then k_2 becomes equal to k_d,

$$k_2 \simeq \frac{k_p k_d}{k_p} = k_d \quad . \tag{1.6}$$

In this limit, the rate of the reaction is determined by the rate at which the species diffuse together through the medium. This is called the "diffusion controlled limit", and the reaction is diffusion controlled. Typically, these reactions have $k_2 \geq 10^9\ M^{-1}s^{-1}$ or E_a of about 17 kJ $mole^{-1}$ in water. For example, radical and atom recombination reactions are often diffusion controlled because the combination of species with unpaired electrons involves very little activation energy. The other limit arises when a substantial amount of activation energy is involved in the reaction step, and then $k_p << k_b$. This gives rise to the "activation controlled limit" and the overall rate constant becomes:

$$k_2 = k_p \left[\frac{k_d}{k_b} \right] = k_p K \quad , \tag{1.7}$$

where K is the equilibrium constant for the A, B and {A...B} species. In this case, the rate depends on the accumulation of energy in the encounter pair as a result of its interaction with the solvent molecules, and on their rate of passage over the reaction energy barrier.

In the diffusion controlled limit, the rate constant depends on the interaction distance and the relative diffusion coefficients. In general, it is given by equation (1.8) [56],

$$k_2 = 2\pi (10^{-3}) No (R_A + R_B)(D_A + D_B) \quad ; \tag{1.8}$$

where R_i and D_i are the effective reaction radii and diffusion coefficient of the i-th molecule, respectively; and No is Avogadro's number. The diffusion constant is normally [54] related to the solvent viscosity (η) and the molecular radius of the solute (r^*) through the Stokes-Einstein equation (1.9),

$$D = \frac{kT}{6\pi\eta r^*} \tag{1.9}$$

where k is Boltzmann's constant and T the absolute temperature. By assuming $r^* = R_i$ and by substituting equation (1.9) into (1.8), one obtains [57] the

well known Smoluchowski equation (1.10),

$$k_2 = \frac{No}{1000}\left(\frac{kT}{3\eta}\right)\left[\frac{(R_A+R_B)^2}{R_A \cdot R_B}\right] \quad . \qquad (1.10)$$

It is interesting to note that for two species of comparable size, the Smoluchowski equation becomes independent of molecular size. When the temperature dependence of viscosity is taken into account, the following equation (1.11) applies [58],

$$k_2 = \frac{No}{1000}\left\{\frac{kT}{3\eta}\right\}\left[\frac{(R_A+R_B)^2}{R_A \cdot R_B}\right]\exp\left(-\frac{E_\eta}{kT}\right) \qquad (1.11)$$

where E_η is the activation energy of viscosity.

1.C.2. Transition state theory applied to liquid phase reactions.

The idea that an "intermediate complex" was formed during transition from the initial reagents to the final products has been known for some time and it was first demonstrated by Bjerrum [59] and Brönsted [60] in 1925. However, their derivations using one dimensional coordinates cannot describe the great variety of kinetic features of reaction between complicated molecules. Various other groups [61,62,63] developed this idea further to suggest that the chemical reaction be considered as the movement of the reacting system along a potential energy surface or "phase space". The "transition

state theory" or the "activated complex theory" were independently formulated in 1935 by Eyring [64] and by Evans and Polanyi [65]. Their treatments of chemical reaction rates consider the movement of the configurational point over a potential energy surface such that the energy barrier between the initial and final states is minimized. The highest point along this path is referred to as the transition state or activated complex. The potential energy surface of most reactions is three-dimensional, and consists of two "valleys" connected by a saddle or a "pass" on the energy barrier (Figure 1.2a). The transition state is considered to be situated on the saddle point of this free energy surface [66]. The curve in Figure 1.2b illustrates the mapping of the potential energy surface E for the following reaction:

$$A + B \longrightarrow X^{\ddagger} \longrightarrow \text{Products} \quad . \tag{1.12}$$

along the reaction coordinate through the saddle point, which corresponds to the activated state. The section of the curve at the apex with an arbitrarily selected length $\Delta\ell$ corresponds to the activated complex ($X^{\ddagger}$). This approach led to considerable simplication of the equations for reaction rates and made it possible to examine the influence of the reactant structure and the nature of the solvent on the reaction rate.

Application of statistical mechanics to the activated complex theory [54] gives the following expression for the chemical reaction rate of equation (1.12) as:

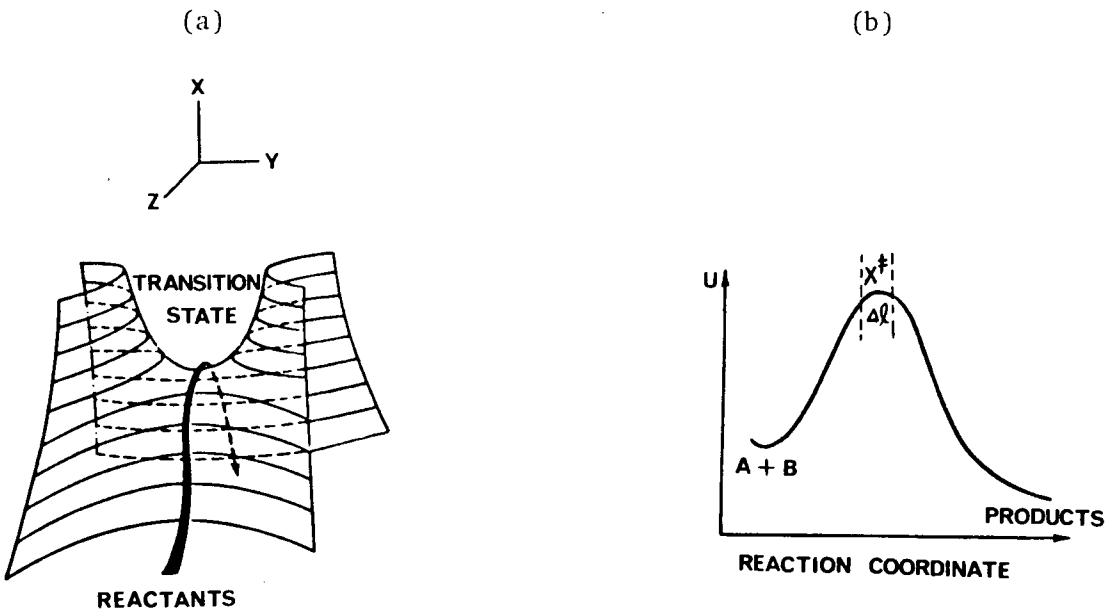

Figure 1.2: (a) Diagram of the reaction path through the energy barrier.
(b) Curve of the potential energy plotted against the reaction coordinate.
(after Entelis and Tiger [66])

$$k_2 = \kappa \left\{ \frac{kT}{h} \right\} \left[\frac{Q_X^{\ddagger}}{Q_A Q_B} \right] \exp\left(-\frac{\Delta\varepsilon_o}{kT} \right) \qquad (1.13)$$

where κ is a transmission coefficient allowing for the possibility that not all activated complexes lead to products since some may be reflected back to the reactants; $Q_X^{\ddagger}/(Q_A Q_B)$ is the partition function quotient permitting evaluation of molecular complexity; and $\Delta\varepsilon_o$ is the difference between the lowest energy levels of A and B, and $X^{\ddagger}$, which corresponds to the activation energy for the reaction.

1.C.3. Isotope effects and quantum mechanical tunnelling.

The application of the activated complex theory to the study of kinetic isotope effects has been quite satisfactory especially with the substitution of deuterium for hydrogen in reactant molecules. For example, if a reaction involves cleavage of an H-X bond, it is frequently found that deuterium substitution reduces the rate by a factor of ten at room temperature [54]. However, such a large kinetic isotope effect is confined to reactions involving hydrogen atoms and is rarely seen for other atoms. Using deuterium and tritium, experimentalists and theoreticians have been studying these mass-dependent effects in solution and gas kinetics for decades. Now, with Mu, a superlight isotope of H atom, one has a factor of nine in sensitivity and one can test severely the theory of absolute reaction rates. One can expect bigger isotope effects and therefore Mu can be used to investigate zero-point energy effects,

steric and orientational factors, quantum mechanical tunnelling, reaction mechanisms, and the dependence of translational diffusion on the reagents' volume and mass. It should be noted that since the muon has a lifetime of 2.2 μsec, there cannot be any stable Mu-containing compounds formed. This renders such discussions as spectroscopic and thermodynamic effects very difficult and limits our focus on kinetic isotope effects.

According to classical mechanics, a particle cannot cross a potential energy barrier if its energy is less than the barrier height. However, quantum mechanics states that a moving particle of atomic or electronic mass behaves as a wave packet and predicts that there is a finite probability for the crossing at lower particle energies and therefore can often make an important contribution to the overall reaction process. Mathematically, for a particle m encountering a barrier of height V with wavefunction ψ, its motion can be solved via the Schrödinger equation. The solution for m having energy E penetrating barrier V is a wavefunction ψ of the oscillating form [54] (see Figure 1.3). But once inside the barrier ($x>x_o$), ψ is non zero and decays according to:

$$\psi(x) = \alpha \cdot \exp\{-[2m(V-E/\hbar^2]^{\frac{1}{2}}x\} \quad . \tag{1.14}$$

Since $\psi(x)\neq 0$, this means there is a probability of finding m inside the barrier even when $E<V$. This phenonmenon in which a particle seemingly penetrates into the forbidden classical region is termed quantum mechanical tunnelling. The tunnelling probability is a sensitive function of the

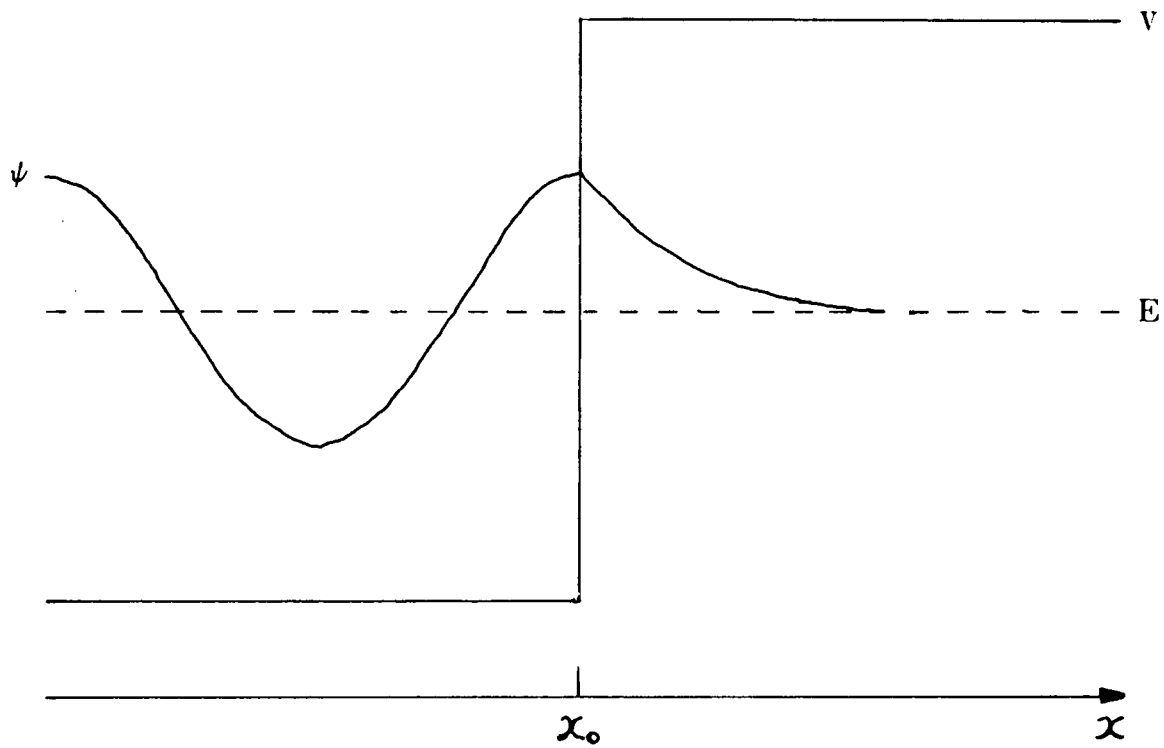

Figure 1.3: The dependence of a wave function (ψ) on the potential. .For $x<x_o$, ψ is oscillatory. For $x>x_o$, ψ decreases exponentially (after Pilling [34]).

barrier height and shape, and of the particle's mass and energy. The importance of tunnelling effects in chemical kinetics were recognized as early as 1933 by Bell [67], particularly for reactions involving a proton or hydrogen atom transfer. Since then, considerable research has been directed towards the design and execution of experiments that would provide examples of tunnelling effects in chemical processes. It has been observed that hydrogen atoms tunnel to an observable extent, and they do so more effectively than deuterium or tritium atoms because of their lighter mass [68]. This effect might be much more pronounced with the now much lighter Mu atom. Indeed, there is evidence from the muonium lifetime in neat methanol at low temperatures [69], and temperature dependence of Mu reacting with NO_3^- [70] that this is so. There are three major phenomenological manifestations of quantum mechanical tunnelling, curvature in Arrhenius plots, effect on Arrhenius pre-exponential factors and relative kinetic isotope effects. These can be investigated by measuring and comparing rate constants of Mu, ^1H, ^2H, and ^3H with various solutes as a function of temperature. It is for this reason, and for reaction kinetics in general, that the temperature dependence of Mu atom reaction rates with different substrates constitutes an important, fundamental, and interesting study in the field of muonium chemistry.

1.D. Description of thesis content.

Since this Ph.D. work is an on-going project from the M.Sc. thesis, it should be appropriate to describe briefly the M.Sc. projects [71]. The essential results were the temperature dependence measurements of five types of reactions of muonium atoms in aqueous solution between 2 and 92°C by the muonium spin rotation technique [70]. The results showed that for an electron transfer reduction with MnO_4^-, for an addition to π-bonds in maleic acid, and for a spin-conversion reaction with Ni^{2+}, the rate constants were all diffusion limited. An activation energy for diffusion of 17±2 kJ $mole^{-1}$ was found, while the A-factors varied somewhat in the range of 10^{13} $M^{-1}s^{-1}$. For these diffusion controlled reactions there was no kinetic isotope effect when compared with H atoms, so the diffusion coefficient, even for these very small light species, is mass independent. On the other hand, for the abstraction reaction with formate ions, there was a large kinetic isotope effect and the rate constant was activation controlled. The reaction between muonium and NO_3^- was also studied and tended to exhibit a curved Arrhenius plot even over this short temperature range. Such curvature was consistent with either a contribution from quantum mechanical tunnelling or alternative reaction paths. Other temperature dependence studies of both the muon and muonium atoms in CS_2, H_2O, and $CC\ell_4$ were also reported. In addition, the interactions of Mu with O_2 and with porphyrins in water were both investigated. In the case of O_2, the rate constant, which could be due to spin-conversion, was found to be 2.4×10^{10} $M^{-1}s^{-1}$ and was compared with the diffusion-controlled limit and the corresponding gas phase reaction [32]. For the

reaction of muonium with porphyrins, the rate constants with hemin and the protoporphyrin were found to be 2.7×10^9 and 6×10^8 $M^{-1}s^{-1}$, respectively [37]; the reaction mechanism was explained via Mu addition to the conjugated double bond for the protoporphyrin and reduction or partial spin-conversion for the hemin substrate.

In this Ph.D. thesis, not only will the muonium reactivity with various solutes be emphasized, but also its formation probability in neat solvents will be detailed. In chapter 3, the origin of muonium relaxation in pure water (λ_o) will be elucidated. In chapter 4, a novel technique, muonium-radical spin rotation, will be introduced. This is applied to study muonium selectivity in benzene-styrene mixtures [73]. In chapter 5, muon and muonium yields in concentrated hydroxide solutions [72] and neat neopentane [35] (liquid & solid) are discussed, while the following chapter gives the kinetics of Mu reacting with deutero-formate and hydroxide ions as a function of temperature [72] and the results compared with previous temperature dependence data. Finally, collaborative studies involving muonium formation in hydrocarbons [33,74], muonium kinetics in aqueous solutions of vinyl monomers, nickel (II) cyclam and cyanides [40,41,93,123], and muonium as a biological probe in micelles and cyclodextrins [36,38,39] are presented in chapter 7. It is hoped that the brief description of theories and techniques in this and the ensuing chapter will give the reader a better enjoyment of the presentation of results in the latter chapters. However, it is recommended that references [4,5,28,75] be read by those wishing to further understand the physics of the (muon-muonium-radical) spin rotation techniques in condensed media.

CHAPTER 2

THEORY AND EXPERIMENTAL METHOD

2.A. Theory of the experimental method.

Cosmic radiations that reach the surface of the earth are mainly in the form of highly energetic positive and negative muons. They are produced in the earth's atmosphere by incoming protons via pion (π°, π^+, π^-) intermediates. This combination of cosmic bombardment and atmospheric conversion is simulated in meson-facilities.

2.A.1. Muon production.

Muons are unstable particles and they are decay products of pions. At TRIUMF, the pions are generated by bombarding a ^{9}Be target (T2) with 450-500 MeV protons from the cyclotron to give the following nuclear reaction.

$$^9\text{Be} + {}^1\text{p} \longrightarrow {}^{10}\text{Be} + \pi^+ \qquad (2.1)$$

The pion then decays with a lifetime (τ) of 26 nsec to give a muon and a muon neutrino.

$$\pi^+ \longrightarrow \mu^+ + \nu_\mu \qquad (2.2)$$

Subsequently, the muon itself decays (τ=2.2 μsec) giving an easily detectable positron, an electron neutrino and muon anti-neutrino.

$$\mu^+ \longrightarrow e^+ + \nu_e + \bar{\nu}_\mu \qquad (2.3)$$

2.A.2. Muon polarization.

For the pion decay process (equation 2.2), the pion has zero spin and since all ν_μ in nature have negative helicity (the particle spin is represented in a left-handed sense to the direction of the particle momentum), this forces the muon to also have negative helicity according to the conservation law of angular momentum. In a fortunate but yet significant sense, this parity violation of "weak interactions" ensures and provides the experimenters with a beam of 100% polarized muons. As if one was not already blessed with luck, in the μ^+ decay (equation 2.3), again due to the non-conservation of parity implicit in the definite helicity of neutrinos, the e^+ emitted also tends to come off along the direction of μ^+ spin. As a result, the angular distribution of the positrons are anisotropic. In general, the number of positrons emitted at an angle θ relative to the muon spin is given by $1+a\cos\theta$ [76]. Here, 'a' is the so-called asymmetry parameter. It is a function of the emitted e^+ energy with an average value of 1/3 and a maximum value of 1 (for positrons of maximum energy, 52 MeV [4]). It is this variation of the positron distribution which allows one to observe the evolution of the muon polarization and which consequently gives one a sensitive way of measuring Mu reaction probabilities.

2.B. Experimental techniques.

Due to the nature and uniqueness of this relatively novel technique, all the experiments were carried out at the TRIUMF cyclotron (originally coined for TRI-University Meson Facility, but now governed by four universities - UA, SFU, UVIC & UBC). This meson facility, located on the U.B.C. campus, was completed in the fall of 1974. Its capability of producing two simultaneous beams of protons enabled the facility to include such fields of research as medium-energy nuclear physics and muon chemistry, as well as applied research, including medical radioisotope production, neutron activation analysis, pion cancer therapy, nuclear fuel research and positron emission tomography. Figure 2.1 depicts the TRIUMF site and shows the many available beam line channels, experimental beam ports and facilities. All the experiments in this thesis were conducted on the M-20 muon channel. Figure 2.2 shows the different mode of beam operation. In "conventional" mode, pions decay in flight to give two types of muons, forward and backward muons (in the pion rest frame, forward μ^+ decays in the pion momentum direction while backward μ^+ decays in the opposite direction). Usually, a backward muon beam was selected because of its clear separation from beam positron contamination. It has a penetration of 2 to 3 g cm^{-2} and momentum of about 80 MeV/c. It is especially well suited for Mu-radical experiments at high magnetic fields, reasons for which will be explained later. However, the necessity to study low pressure gases [77], or thin solids [78], or small quantities of liquids held in thin-walled cells [29] requires muons of much lower energy. In 1971, a new type of μ^+ beam (Arizona mode) using muons

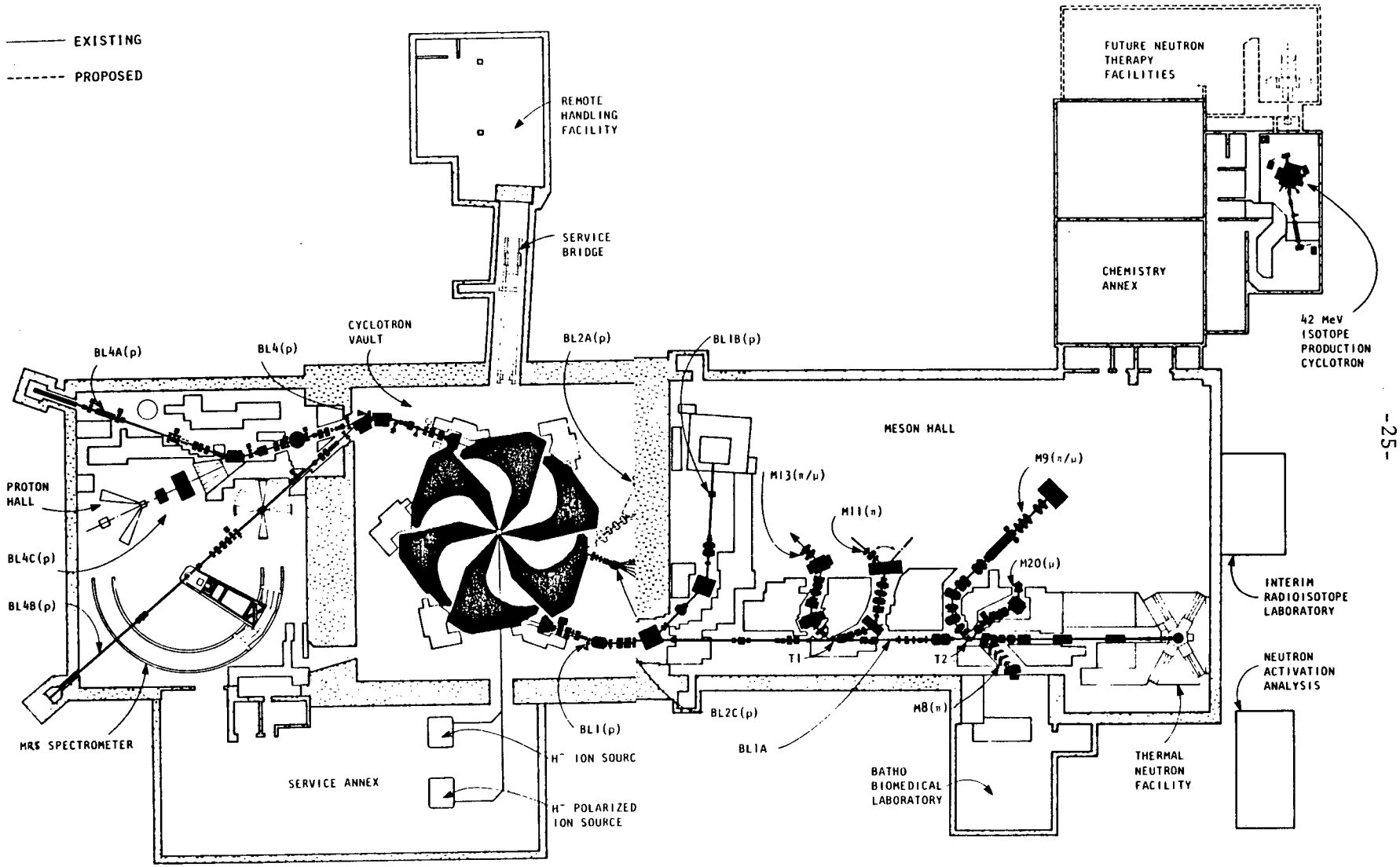

Figure 2.1: Schematic diagram showing the TRIUMF site at U.B.C.

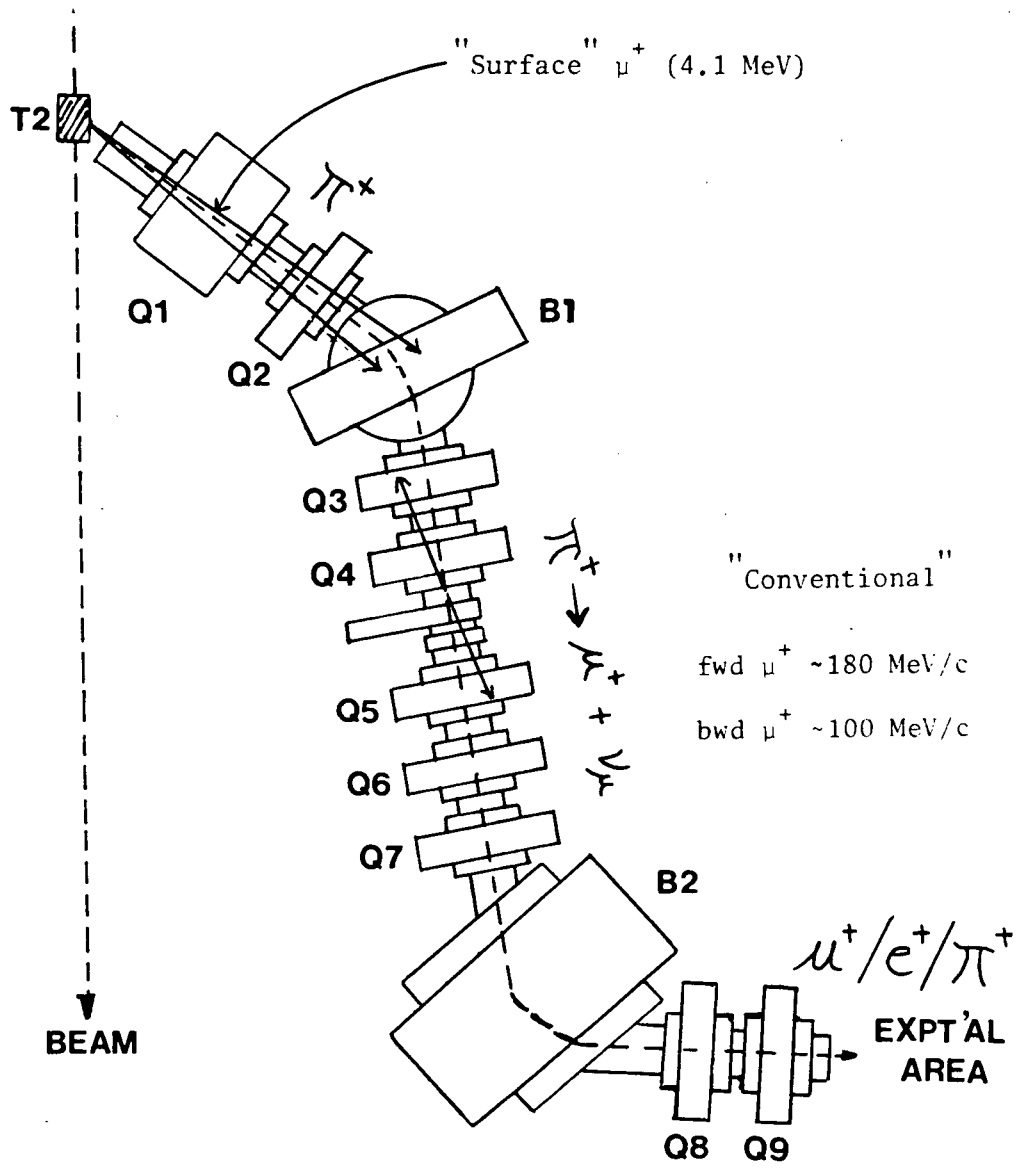

Figure 2.2: Schematic diagram showing the set-up of quadruple and bending magnets for the M20-muon channel at TRIUMF. It also differentiates between the types of muons available by tuning for high or low momentum.

from the decay of pions that stop near the surface of the production target (i.e. come to rest in T2 as in Figure 2.2) was investigated by a group from the University of Arizona operating at the Lawrence Berkeley Laboratory 184" cyclotron [79]. This was achieved by tuning for a momentum of less than 39 MeV/c, and the resulting beam gave a significant increase in muon stopping density over that of a conventional beam. At TRIUMF, our rapid interchange of targets and use of thin-walled sample cells necessitated the tune for this, so called, "surface" muon beam on the M20-beam channel. The use of either backward or surface muons depends on apparatus limitation, sample geometry and type of experiment. In general, the studies of muonium kinetic in aqueous solution employ surface muons while Mu-radical and hydrocarbon investigations require backward muons.

2.B.1. The μSR technique.

When a μ^+ stops in a target perpendicular to a magnetic field $(\vec{B})$, its spin (1/2) precesses at its Larmor frequency,

$$\omega_\mu = \gamma_\mu B \quad , \tag{2.4}$$

where γ_μ = 13.6 kHz/G. To observe this transverse field precession phenomenon, one can simply place a small positron counter in the plane of the μ^+ precession at an angle ϕ_o with respect to the initial muon spin direction; so at time t the angle between the μ^+ spin and e^+ detector when the μ^+ decays will be $\phi_o+\omega_\mu t$. As a result, the e^+ detection probability N(t) will be

proportional to $1+A_\mu \cos(\phi_o+\omega_\mu t)$, where A_μ is the experimental muon asymmetry (proportional to the muon polarization) and its magnitude depends on detector dimensions, target geometry and beam polarization. This method, the "μSR" (muon spin rotation) technique, allows one to monitor the magnitude and time dependence of the muon polarization for all muons in diamagnetic states, such as free μ^+ or MuH or MuCℓ, etc. The field dependence of the diamagnetic muon precession in $CC\ell_4$ is illustrated in Figure 2.3. The original "raw" histogram has the form of equation (2.5),

$$N(t) = N_o \cdot e^{-t/\tau_\mu}[1+A_D e^{-\lambda_D t}\cos(\omega_D t+\phi_D)] + BG \quad , \qquad (2.5)$$

where N_o is a normalization factor, BG is the time-independent background, τ_μ is the muon lifetime (2.2 μsec), A_D is the experimental diamagnetic asymmetry or amplitude, λ_D is the exponential decay rate constant, ω_D is the precession frequency, and ϕ_D is the initial phase of the diamagnetic muon precession.

2.B.2. The MSR technique.

In 1976 [24] it was found, provided the liquid is relatively pure and oxygen free, that Mu can be observed directly by the MSR (muonium spin rotation) technique. This method is a result of hyperfine interaction between the magnetic moment of the muon and that of the electron (hyperfine field = B_o = 1585G) giving rise to two net spin states of F=0 (singlet) or F=1 (triplet). Classically, the observable spin state is that of the triplet

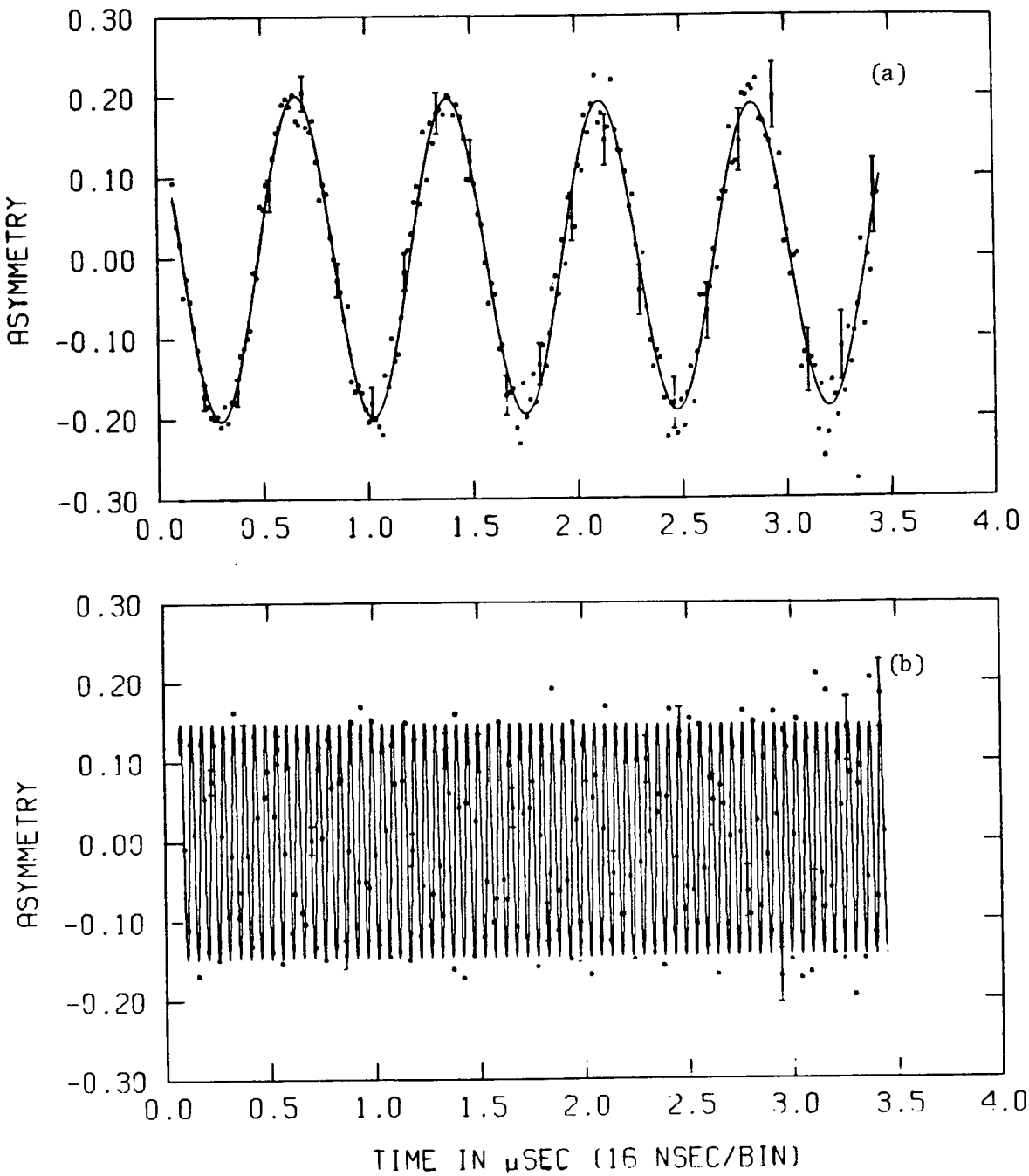

Figure 2.3: Time histograms showing the field dependence of the diamagnetic precession signal at (a) 100G and (b) 1500G for target solution of $CC\ell_4$. The line is the computer fit to the muon components in equation (2.5).

which precesses in weak fields at 1.39 MHz/G, about 103 times faster than the free muon in the same magnetic field. Experimentally, the positron detection probability in this MSR method now acquires another term of the form $\theta=\phi_o+\omega_M t$ with a new empirical amplitude A_M. Therefore, one has the Mu precession superposed upon the μ^+ precession, while both are superposed upon the exponential decay of the muon. In addition, there might be exponential damping on the Mu oscillatory term due to possible phenomenological depolarization and/or chemical reaction. Here, the positron time distribution takes the form of,

$$N(t) = N_o e^{-t/\tau_\mu}[1+A_D\cos(\omega_D t+\phi_D)+A_M e^{-\lambda_M t}\cos(\omega_M t-\phi_M)] + BG \qquad (2.6)$$

where λ_M is the Mu-decay rate constant. The "raw" and "asymmetry" MSR histograms are displayed in Figure 2.4. It should be noted that the triplet frequency that one observes in the MSR method is degenerate at low fields. At higher fields there is a lifting of this degeneracy as evident from the Breit-Rabi diagram in Figure 2.5. This phenomenon will be investigated in the ensuing chapter. However, explicit time-dependent solutions to the muon polarization in muonium are given in references 4, 5, 28 and 75.

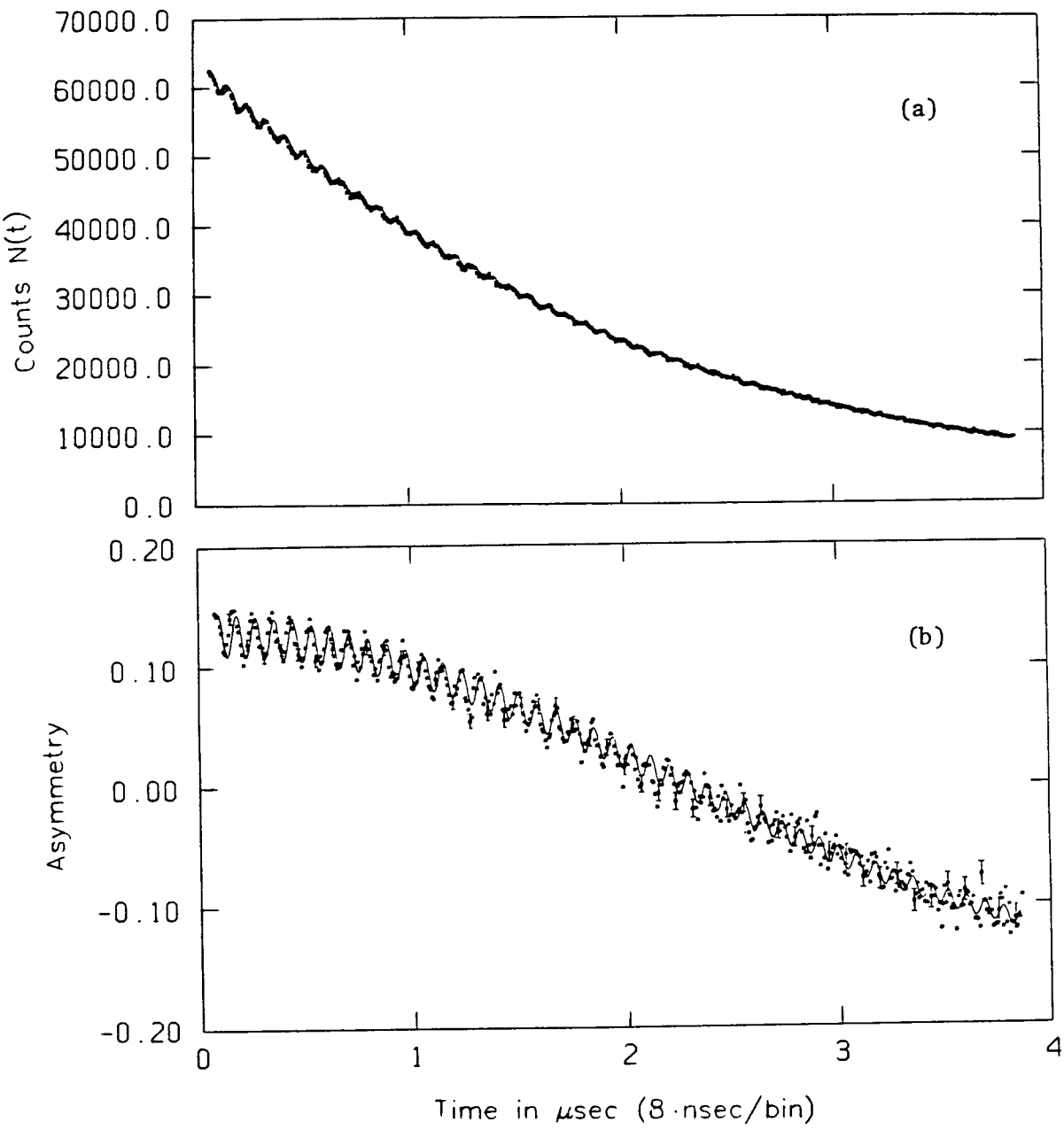

Figure 2.4: "Raw" and "asymmetry" MSR histograms of water. The lines in plots (a) and (b) represent the computer's best fits to equations (2.6) and (2.15), respectively.

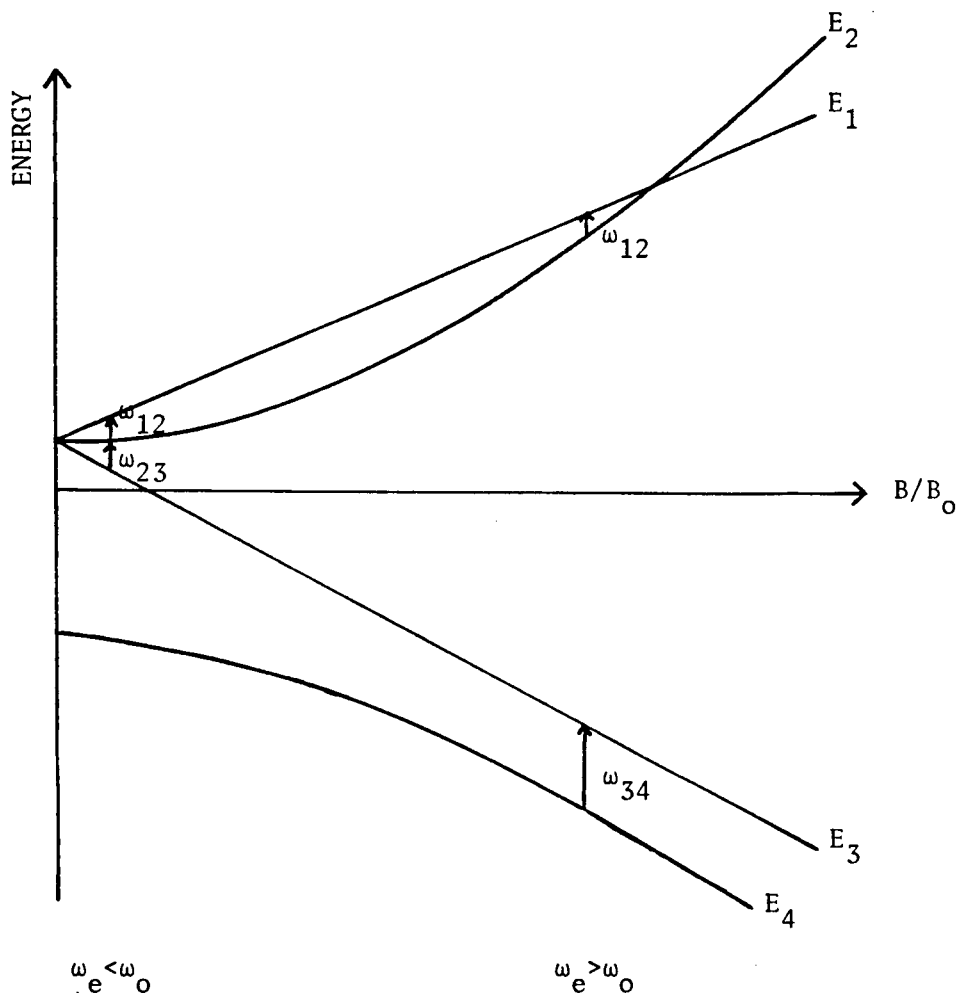

Figure 2.5: Breit-Rabi diagram for a two-spin-½ system (ω_e=electron Larmor frequency). At low fields, $\omega_e<\omega_o$, ω_{12} & ω_{23} are degenerate, giving rise to the characteristic Mu-precession in the MSR method. At high fields, $\omega_e>\omega_o$, ω_{12} & ω_{34} are observable in the MRSR method.

2.B.3. The MRSR technique.

When a Mu-atom adds to a double-bonded system such as benzene,

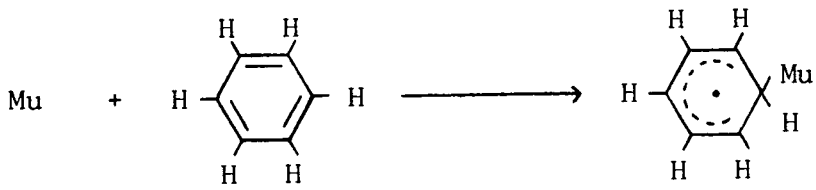

(2.7)

a radical compound will be formed; in this case, a cyclohexadienyl radical, $\cdot C_6H_6Mu$. At low magnetic fields, there are many transitions with the muon polarization distributed among them. This complexity delayed the direct observation of Mu-radicals until 1978 [26]. By applying much higher magnetic fields ($B \geq 2$ kG), the vast amount of radical frequencies collapsed to give just 2 transitions (Figure 2.5, ω_{12} & ω_{43} for $\omega_e > \omega_o$). The numerical solution to this problem was solved by Roduner et al. [80]. It was shown that by applying high transverse magnetic fields, the muon hyperfine coupling constant (A_μ) in the radical is given by

$$A_\mu = \omega_{12} + \omega_{43} \tag{2.8}$$

Figure 2.6 shows (a) the raw histogram, while (b) and (c) give the power spectrum of the Fast Fourier transform (FFT) in frequency space for styrene at several fields. It can be seen that the diamagnetic muon frequency changes linearly with field, while A_μ remains constant with field. This decoupling method of applying high magnetic fields to observe Mu-radicals is called the

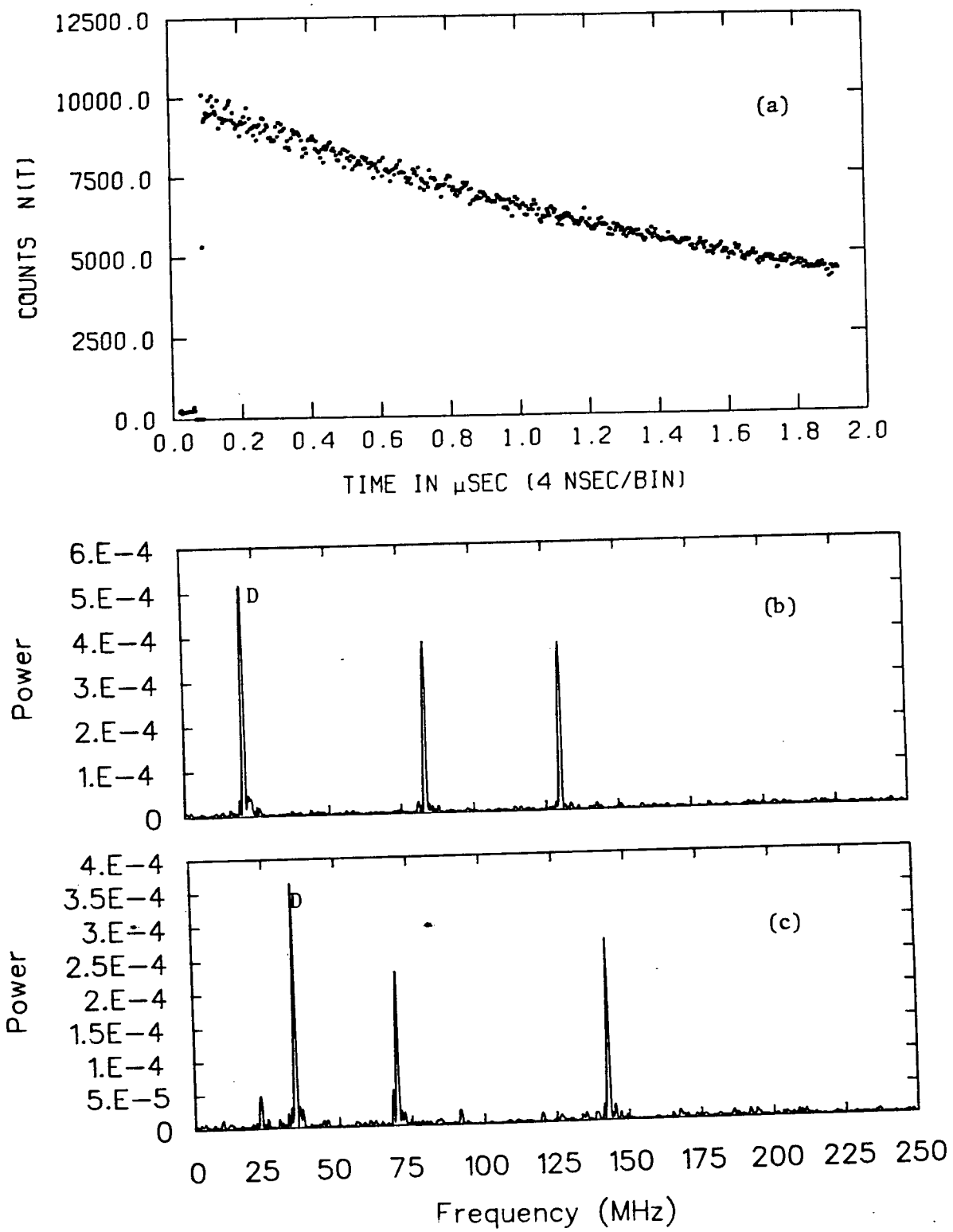

Figure 2.6: Muonium radical in styrene showing (a) the raw histogram at 1500G, and FFT spectra at (b) 1500G and (c) 2500G.

Muonium-radical spin rotation (MRSR) technique. Here, the general form of the histogram is given by

$$N(t) = N_o e^{-t/\tau_\mu}[1+A_D\cos(\omega_D t+\phi_D)+\Sigma_i R_i(t)]+BG \qquad (2.9)$$

and

$$R_i(t) = A_{Ri} e^{-\lambda_i t}\cos(\omega_i t+\phi_i) \qquad (2.10)$$

where $R_i(t)$ represents various contributions of the i-th radical amplitude (A_{Ri}) at the i-th frequency (ω_i) with relaxation rate λ_i. These three techniques (μSR, MSR, MRSR) are shown as FFT spectra in Figure 2.7.

2.C. Electronic logic and experimental set-up.

The basic methods (μSR, MSR, and MRSR), whether employing surface or backward muons, involve nuclear physics counting logistics. It requires starting an ultrafast digitizing clock when a muon enters the target sample and stopping the clock when (and if) the muon's decay positron is detected in the positron counters within several muon lifetimes. This measured time interval is stored in a time histogram in a PDP-11/40 mini-computer. The process is repeated until sufficient statistics in a time spectrum, such as that in Figure 2.4(a), are obtained. Typical electronic logistics are shown in Figure 2.8. However, more detailed explanations of the electronic and computer logistics can be found in reference [75].

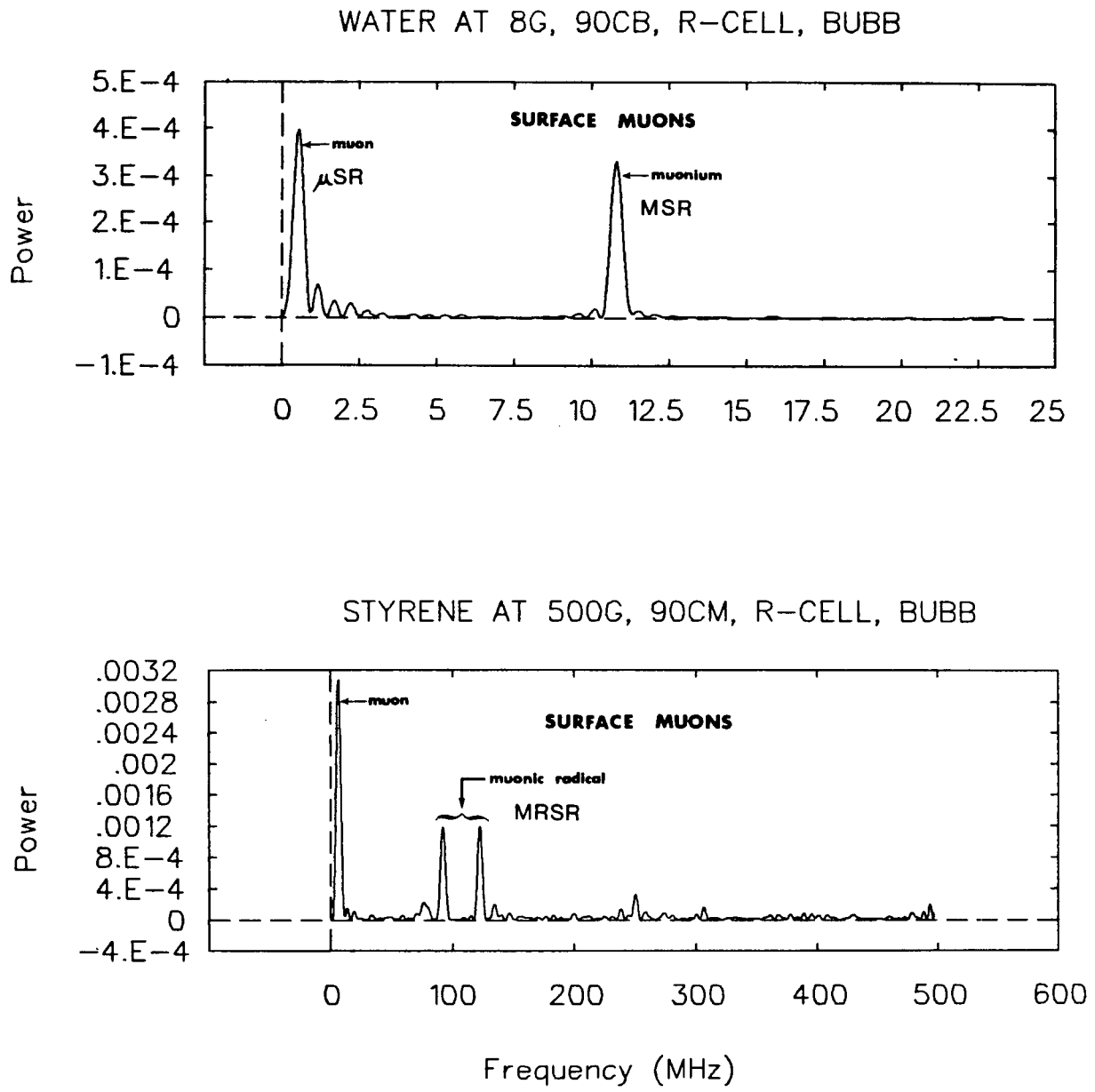

Figure 2.7: FFT spectra showing precession frequencies of the three techniques (μSR, MSR, MRSR).

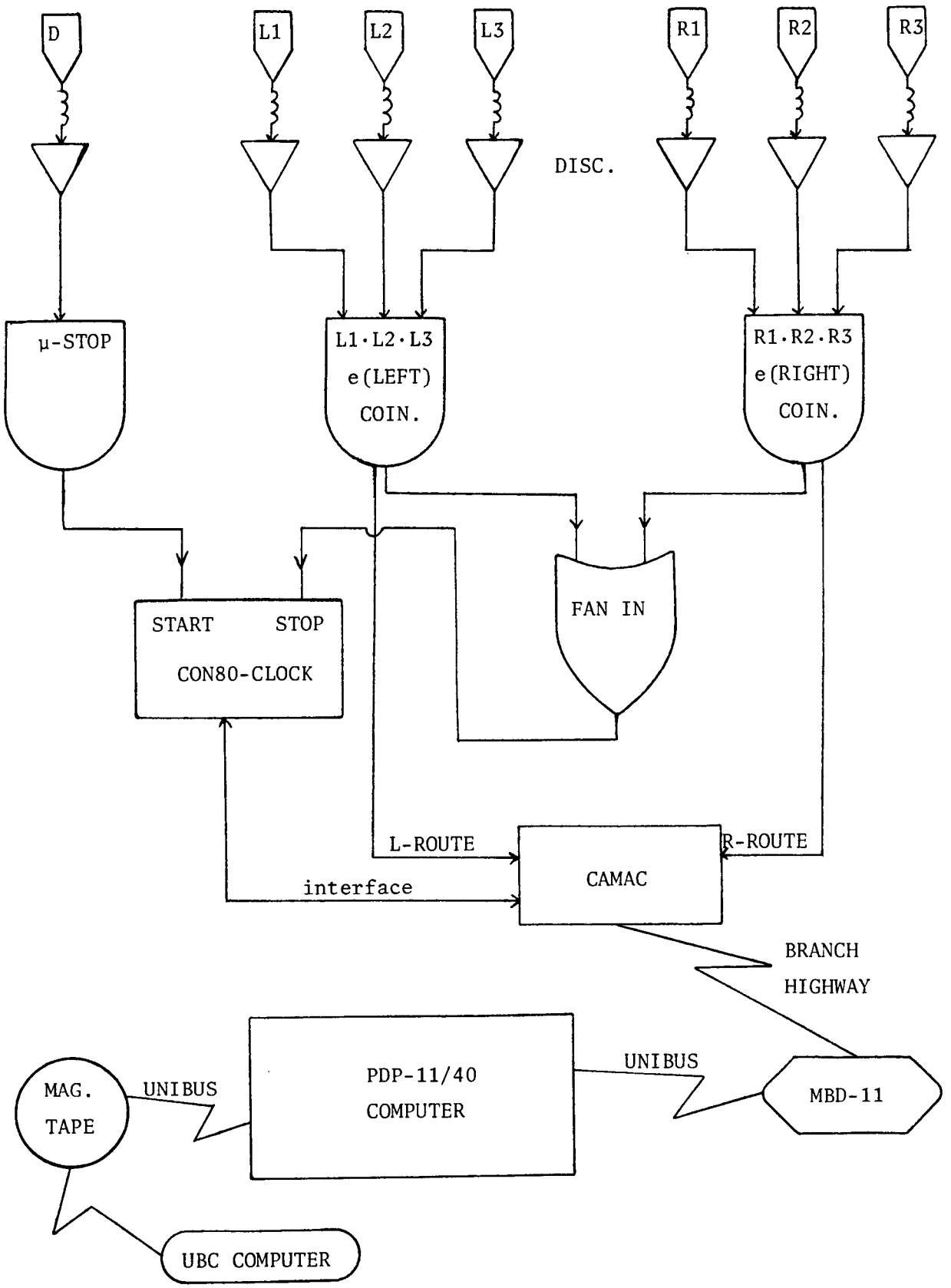

Figure 2.8: Simplified schematic diagram showing data acquistion system at TRIUMF.

2.C.1. Surface muon set-up.

The counters and target arrangement for surface muons are shown in Figure 2.9. Incident muons which are collimated to 1½" beam by lead bricks, trigger the thin (TM) counter (~15 mil) sending a "μ-stop" signal to the "start" input of a time digitizing converter (TDC) clock; then decay positrons detected either by the left (L1·L2·L3) or the right (R1·R2·R3) coincidence telescopes trigger a signal to the "stop" input of the TDC clock. The resultant time interval is then routed to the appropriate left or right histograms. Each histogram is divided into 2048 bins of 2 ns/bin. The "snout" was simply an extension beam pipe used to bring the low energy surface muons as close to the targets as possible. The 2"-carbon absorbers between the e^+ counters served to reduce "accidentals" and to discriminate against low-energy decay positrons, thereby raising the experimental asymmetry [4,27,75]. The magnetic field is provided by either a pair of helmholtz coils 24" in diameter or sets of rectangular (20"x40") helmholtz coils, both of which can generate fairly homogeneous fields (up to ~800G) transverse to the muon spin direction. As drawn in Figure 2.9, there are two possible positions for the target samples. The common set-up is for the target to be placed at a 45° angle to the muon beam. Since the 4.1 MeV muons will be stopped within 1 mm in most liquids, the left histogram can be used to measure absolute asymmetry values. Most μSR and room-temperature MSR experiments are carried out in this mode of operation. For reasons which will be explained in section 2.D., the temperature cell is placed perpendicular to the incident μ^+ beam. Not shown in the diagram are the

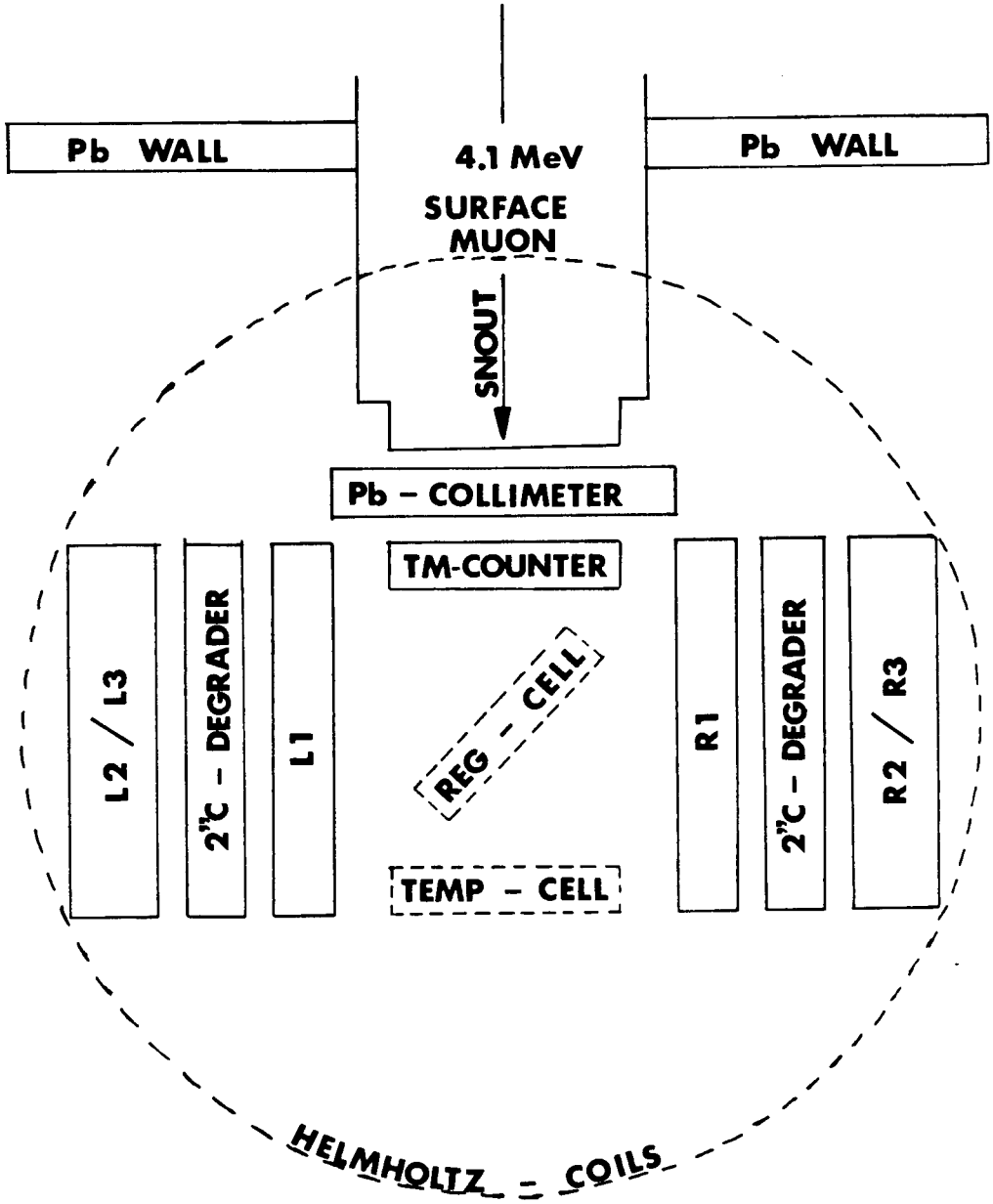

Figure 2.9: Diagram of surface muon apparatus geometry. The magnetic field is physically out of the paper which is called the transverse field method. See text for explanation.

many lead-bricks which must be "painfully" stacked around the counters to prevent contaminations from beam positrons which seriously interfere with the time histograms of decay positrons.

2.C.2. Backward muon set-up.

The experimental set-up for backward-muon beam is depicted by Figure 2.10. The difference between this and the surface-muon set-up arises from the higher energy of the arriving backward muons (~29 MeV). For clarity, the diagram shows only one set of positron detectors. In reality, there are usually 3 sets of these e^+ counters giving "forward", "backward", and "perpendicular" histograms. As shown, A is lead shielding, DEG is a remotely adjustable water block to degrade the muon energy, B is a set of lead collimators, C & D are the muon "start" counters; S is the sample, T is a temperature box; H are the magnetic field coils (up to 4kG) giving a field out of the paper so that the longitudinally polarized muon precesses in the plane of the paper; E & K are the positron "stop" counters. As is evident from the diagram, backward muons can pass through the sample. Therefore, in order to distinguish decay positrons from muons, one must use electronic logistics (vetos) to separate the two particles. For a good event in the MSR or MRSR histogram, the muon "start" signal is registered by $C \cdot D \cdot \overline{E}$ while the decay e^+ "stop" signal by $E \cdot K \cdot \overline{D}$. This set-up is used for experiments involving Mu-radicals and hydrocarbons. For MRSR experiments, histograms are usually of 3000 bin length with 1 nsec/bin packing. The smaller bin packing increases the frequency range and sensitivity which is necessary for observing high frequencies up to 500 MHz.

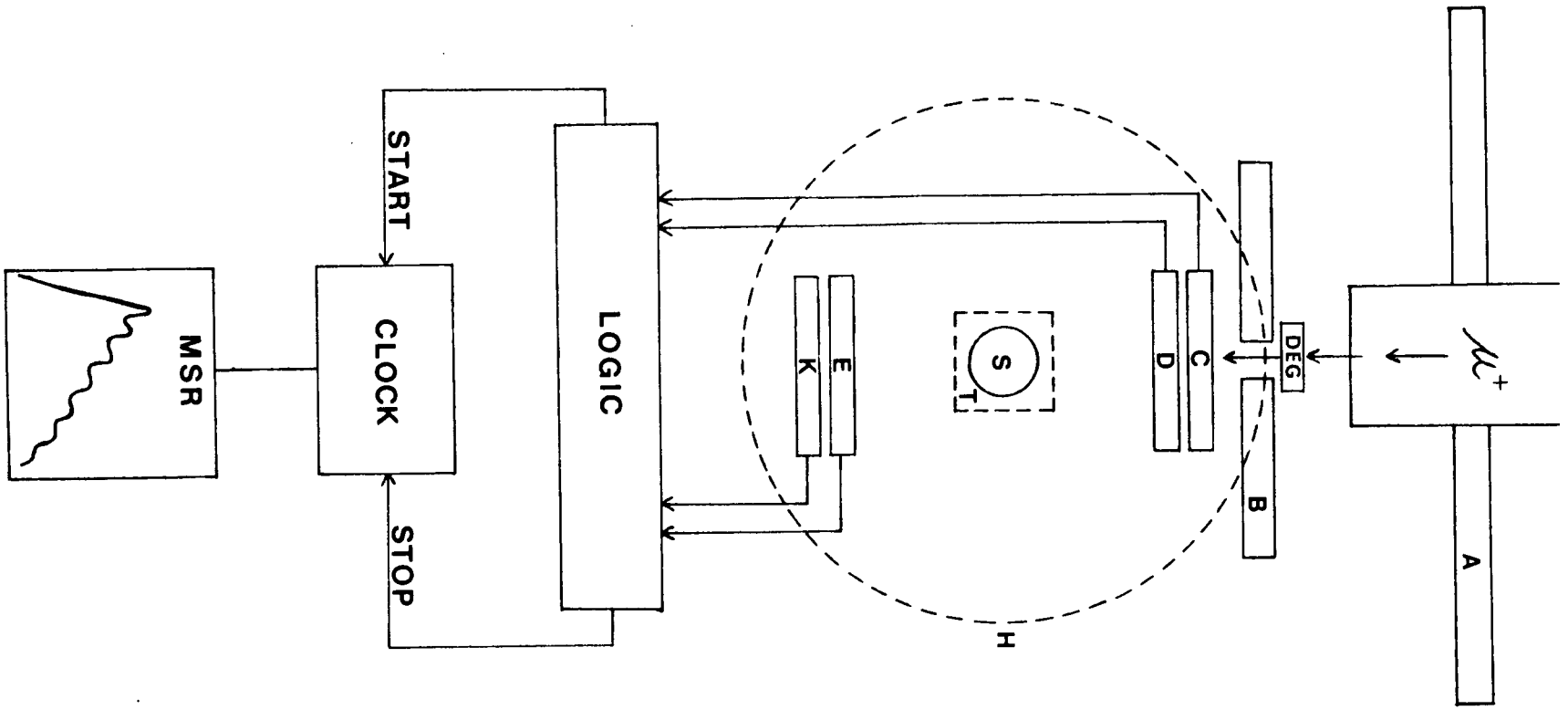

Figure 2.10: Experimental set-up for backward muon experiments. See text for explanation.

2.D. Sample preparation and target-holders.

All solid chemicals were either of reagent or analytical grade and were used without further purification. However, the water used was always carefully purified and triply-distilled before using for aqueous concentrations. In the case of hydrocarbons such as neopentane, styrene and benzene, they were all purified by shaking with H_2SO_4, washing with a base, drying overnight by zeolite, and distilled at least twice several days before an experiment. All hydroxide MSR experiments were titrated with potassium hydrogen phthalate to obtain concentration values to within 1%. Analogously, the DCO_2^- solutions were obtained by titrating formic-acid-d_2 (98 atom %D) with a base of known concentration. For the micelle and cyclodextrin samples, the chemicals were specially obtained from the Strem Chemical Company and freshly prepared just before experiment without further purification. With μSR experiments involving solvent mixtures, the neat solutions were of spectrograde standard and were used directly from the manufacturers' containers.

2.D.1. Surface muon sample holders.

All MSR experiments involving kinetics in aqueous solutions and most μSR hydrocarbon projects were carried out with surface muons. The low energy muons can be conveniently stopped in thin walled cells. For most aqueous MSR experiments (except the temperature dependence measurements), the liquid samples were contained in a specially designed plastic cell (see Figure 2.11a). The body of the cell was made of teflon and was cylindrical, 100 mm in diameter and 6 mm deep. Its "muon windows" consisted of very thin sheets

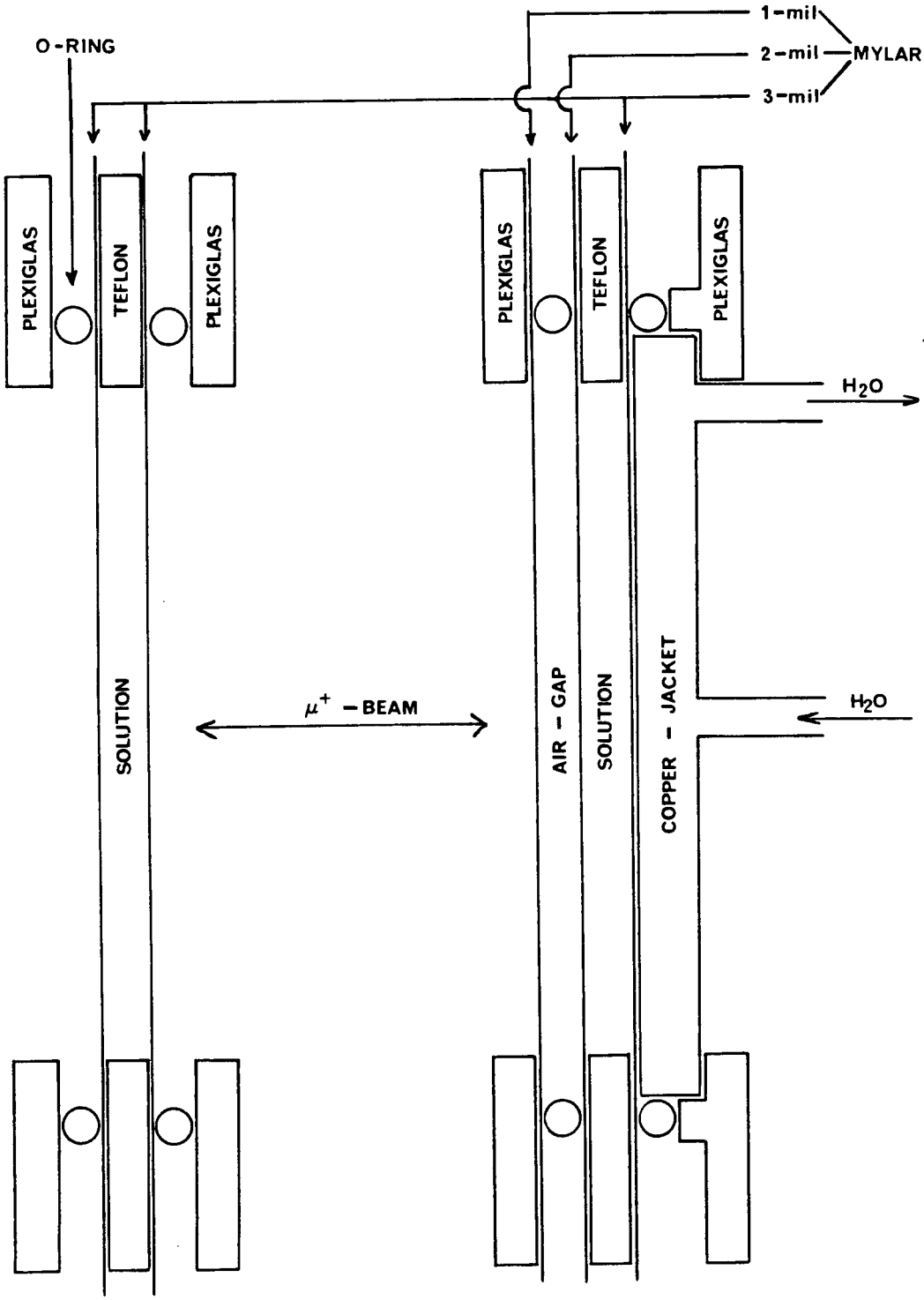

Figure 2.11: Side view of (a) regular teflon cell, and (b) temperature teflon cell for surface muon experiments.

of mylar (0.076 mm). The windows were held onto the teflon cell by rubber pressure rings which was held together with screws and plexiglass plates to avoid possible air diffusion. Tiny holes were drilled into the teflon body and sealed with teflon plugs. Tygon tubings were attached to the plugs so the solutions can be deoxygenated with high purity He gas before and during each experimental run. It should be noted that the fraction of muons stopped in the mylar window was less than 5% and therefore did not affect the MSR results to any significant extent. Since the incident surface muons were completely stopped within the first 0.5 mm of aqueous solution with the cell placed at angle of 45° to the beam, the left-histogram gives close to absolute asymmetry values. Most aqueous and non-aqueous μSR experiments were also done with this mode of operation with the exception that not all the samples were degassed to remove residual O_2 [32].

For the temperature dependence measurements, a special temperature-regulated cell was designed (Figure 2.11b). Similar to the regular cell, the reaction vessel was made of teflon with thin mylar windows (two pieces of mylar, total of 0.076 mm separated by an air gap of 5 mm) at the front to let the weakly penetrating muons into the medium and to prevent excessive heat exchange with surrounding elements. For temperature regulation, a copper jacket was pressed against the rear mylar window of the cell through which water was flowed from a thermostated bath at selected temperatures from 0 to 96°C (see Figure 2.12). Copper-constantan thermocouples sticking into the solution through sealed teflon plugs continuously monitored the temperature of the solution which was actually being bombarded by muons.

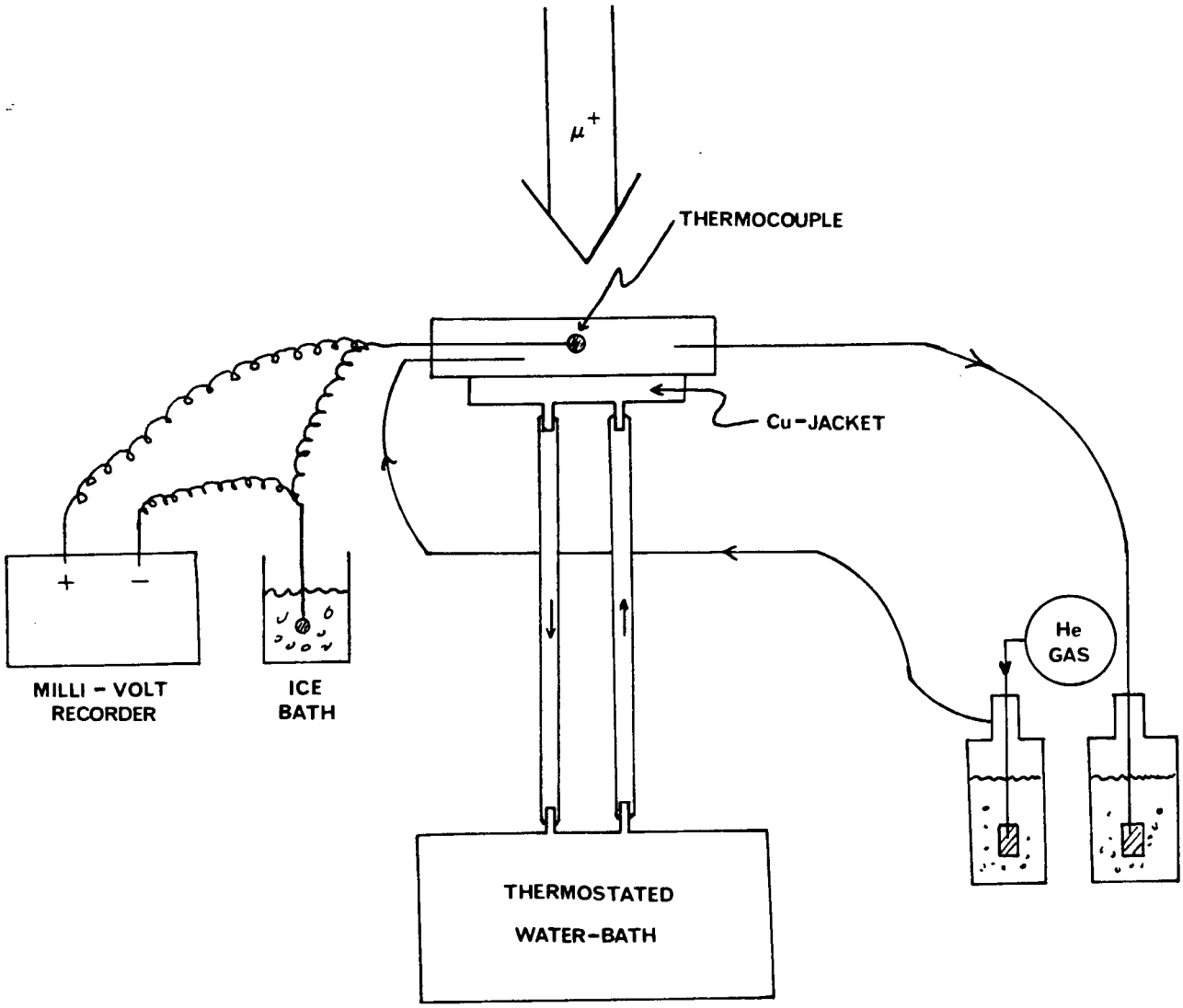

Figure 2.12: Schematic diagram of the surface muon temperature-dependence experimental set-up.

There was a small temperature gradient (1°C between front and back) even though the cells were only 6 mm deep and the solution was being continuously stirred by the deoxygenating He gas. Moreover, there was never more than a 5°C difference between the bath and cell temperature, so possible errors in the temperature scale in the Arrhenius plots were small. Also, in order to avoid unknown variations in the impurity levels, the same solution was studied at several temperatures whenever this could be done without having to change the solute concentration. In several cases, the bubbling solution was left untouched and only the bath temperature varied. Furthermore, the highest temperature experiment was invariably done first to ensure that any extra impurities which may be leached from the cell at the elevated temperature would be common to all solutions and hence to the background λ_o ("background" muonium relaxation constant). Notice in Figure 2.9 that the temperature targets were placed perpendicular to the muon beam and behind the e^+ detectors. The reason for this is that in the 45°-mode operation, beam positrons (higher energy than decay e^+ from μ^+) are scattered efficiently by copper and this produces a strong cyclotron signal at 23 MHz. This phenomenon effectively smears out the slower MSR signal (~11 MHz at 8G) in the right histogram. Therefore, the perpendicular geometry was the best site for the cells in the temperature experiments.

2.D.2. Backward muon sample holders.

Due to the higher energy of backward muons, thicker containers (relative to surface muons) must be used to ensure maximum muon stops in the sample. For hydrocarbons such as neopentane, the samples were deoxygenated by freeze-pump-thaw cycles and then vacuum-sealed in a 70 ml round-bottomed glass bulb (~45 mm diameter). The adjustable water degrader was used to stop muons in the middle of the sample. Temperature control was achieved in a closed styrofoam box (Figure 2.10, symbol T) through which cold He gas was passed at a variable rate. Temperatures ranging from room temperature to -150°C were obtained and determined by a thermocouple in contact with the glass-bulb wall. Throughout the experiment, the temperature was monitored continuously with a mV-chart recorder. The temperature was maintained within at least 2°C of the quoted values for all MSR hydrocarbon experiments.

For the MRSR experiments, some were done in sealed-deoxygenated glass cells. However, most were contained in 50 ml round-bottom flasks connected with teflon stopcocks and deoxygenated by bubbling with pure He gas before and during the experiment. Appropriate prebubblers ensured that evaporation did not significantly alter the compositions of various mixtures.

2.E. Data analysis.

In condensed phase studies, the highest muon asymmetry obtained is that of $CC\ell_4$. Its value is also equal to that found in metals such as aluminum and copper [28]. For this reason, its value has been used as a normalizing standard for all other solvents. In this thesis, the value of P_D is taken

as the observed muon asymmetry in the liquid of interest divided by the asymmetry found under identical conditions in $CC\ell_4$.

$$P_D = \frac{A_D}{A_{CC\ell_4}} \tag{2.11}$$

i.e. P_D represents the fraction of incident muons which are observed in diamagnetic states. P_D values are usually obtained by the μSR technique under a transverse field of 80G. For the case of muonium, P_M (the muonium fraction) is twice the value of the Mu-experimental-amplitude divided by the muon asymmetry in $CC\ell_4$.

$$P_M = \frac{2A_M}{A_{CC\ell_4}} \tag{2.12}$$

The factor of two arises from the fact that half of the muonium ensemble (singlets) are depolarized by the extremely fast hyperfine frequency (ω_o = 4464 MHz) and remains unobservable in the MSR technique. To obtain P_M, MSR experiments are usually carried out at fields of 8 to 9 G.

In most solvents, the sum of P_M and P_D is usually less than 1. The difference $(1-P_M-P_D)$ is referred to as the "missing fraction", P_L, which at present is attributed to either unobservable muonium radical formation or rapid spin depolarization perhaps by intra-spur spin-exchange reactions [25,47,52]. For observable muonium radical amplitudes obtained in the MRSR

experiments, they are also normalized to $CC\ell_4$ at fields of 1500 to 3400 G.

$$P_R = \frac{\sum_i A_{Ri}}{A_{CC\ell_4}} \qquad (2.13)$$

By measuring P_D, P_M & P_R for a particular sample using the above three techniques, one can obtain the various fractions of diamagnetic, muonium, or radical contributions formed. In muonium kinetics involving aqueous solutes and hydrocarbons, both μSR and MSR experiments are done to obtain P_D and P_M, respectively. Whereas for radical experiments, the MRSR and μSR techniques are used to deduce P_R and P_D.

2.E.1. Analysis of μSR and MSR spectra.

In μSR experiments about 10^6 events are required for a surface μ^+ spectrum, while about 1½ times as many are needed for a backward μ^+ spectrum. The need for extra events is due to the lower beam polarization of backward muons. Typical asymmetry values are shown in the following table.

TABLE 2.1

Typical asymmetry values for backward and surface muons.

Substance	Surface μ^+		Backward μ^+	
	A_D	A_M	A_D	A_M
$CC\ell_4$	0.33	0	0.20	0
H_2O	0.20	0.033	0.12	0.020

As one can see, in an MSR experiment, one needs many more events, about 10^7 events per histogram for surface muons. However, other considerations such as number of discernable precessions (depends on decay rate) and background are also factors in determining the amount of data that one should accumulate. Usually, one must compromise between experimental time (very limited at TRIUMF since there are many users from four different universities) and sufficient statistics.

Representative μSR and MSR histograms are shown in Figure 2.3 and 2.4. The lines are the computer fits to equation (2.5) and (2.6) using the linear-least squares fitting program MINUIT [81] compiled on an IBM 12-megabyte Amdahl 470 V/8 computer. In the asymmetry histograms, as mentioned previously, the BG, N_o and the muon decay are removed to display more vividly the amplitude signals. The equations for μSR and MSR asymmetry histograms are given by the following equations.

$$A(t) = A_D e^{-\lambda_D t} \cos(\omega_D t+\phi_D) \tag{2.14}$$

$$A(t) = A_D \cos(\omega_D t+\phi_D)+A_M e^{-\lambda_M t} \cos(\omega_M t-\phi_M) \tag{2.15}$$

In μSR experiments, one is usually interested in A_D. Occasionally, such as solids, one also abstracts the parameter λ_D. For MSR experiments, the parameters of interest are A_M and λ_M. It should be noted that equation (2.5) fits 6 parameters while equation (2.6) fits 8 parameters. By experience, initial guesses are given to the computer as the starting points, then the

MINUIT program fits all parameters. This process usually takes very little CPU time to reach convergence.

Typical MSR asymmetry histograms for aqueous solute studies are shown in Figure 2.13. The parameter λ_M varies with the addition of a reactive solute S at concentration [S] in accordance with equation (2.16),

$$\lambda_M = \lambda_o + k_M[S] \quad , \tag{2.16}$$

where λ_o is the "background" muonium relaxation constant found in pure water (or other media such as neat hydrocarbon solvents). The linear relationship of λ_M and [S] is illustrated in Figure 2.14. It is worth emphasizing that never more than one muon at a time is in the solution, so $(\lambda-\lambda_o)$ represents a pseudo first-order rate constant as in equation (2.16) and a plot of λ versus [S] gives the slope as k_M, which then represents the bimolecular rate constant for reaction of Mu with substrate S. Furthermore, the time scale over which the relaxation was observed (0.2-20 μsec) is much later than the slowing down process of the muon, so k_M is indeed a thermal rate constant. It must be noted that solute concentrations for the experiments were selected so that the value of λ_M falls within the working range of ~$5x10^6$ to ~$2x10^5$ s^{-1} where the χ^2-minimization of data points is statistically reliable.

For temperature dependence measurements, the extracted muonium rate constant (k_M) changes with temperature. This can be expressed by the familiar Arrhenius equation,

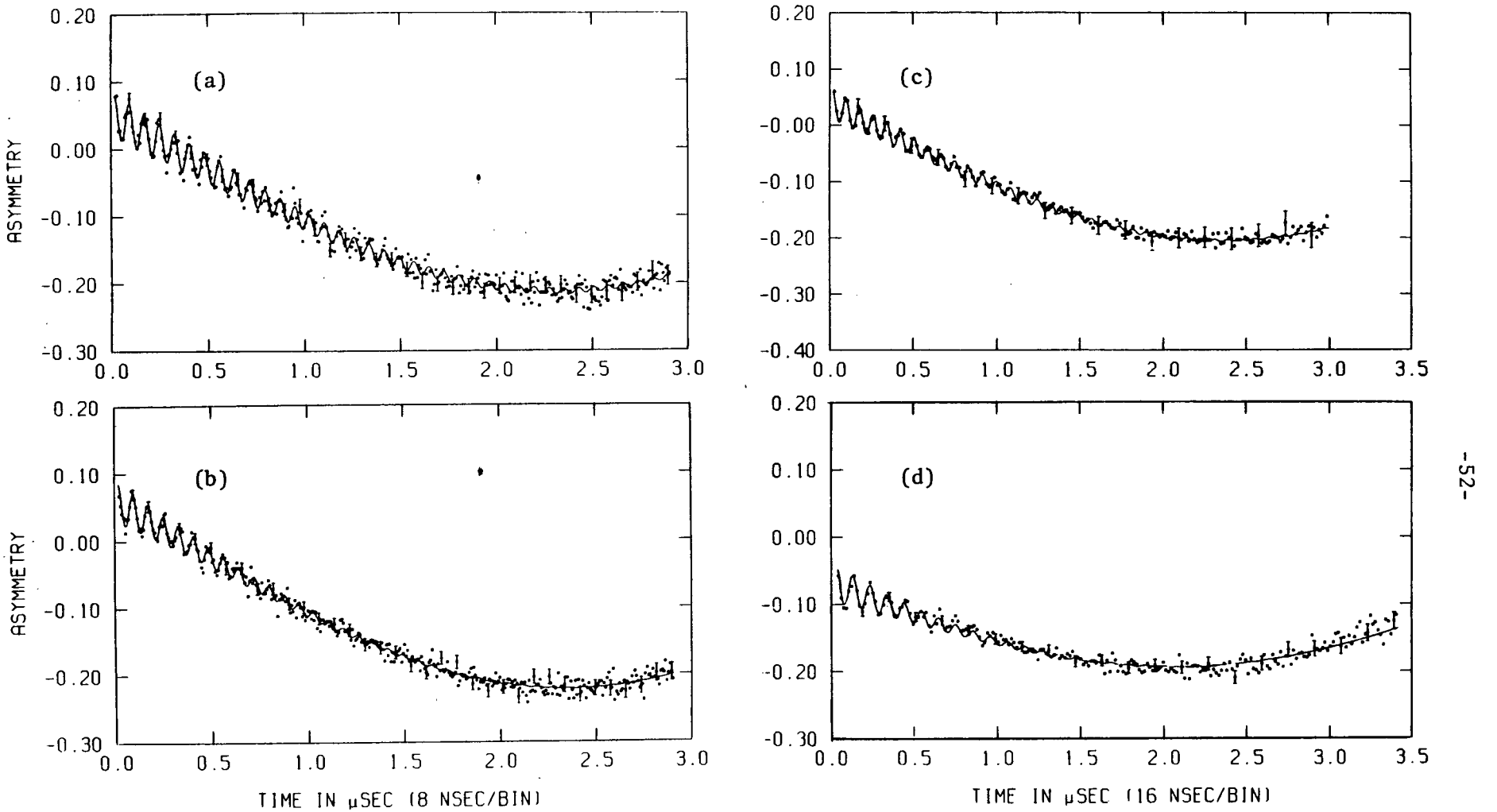

Figure 2.13: Typical MSR asymmetry histograms showing the decay of muonium signal at 9 gauss for 5×10^{-5} M $KMnO_4$ at (a) 3°C, (b) 58°C, and for (c) 3.5×10^{-4} M $NaNO_3$, (d) 1.4×10^{-3} M $NaNO_3$, both at 1°C. The lines drawn are the computer's best χ^2-fit of the data points to equation (2.6).

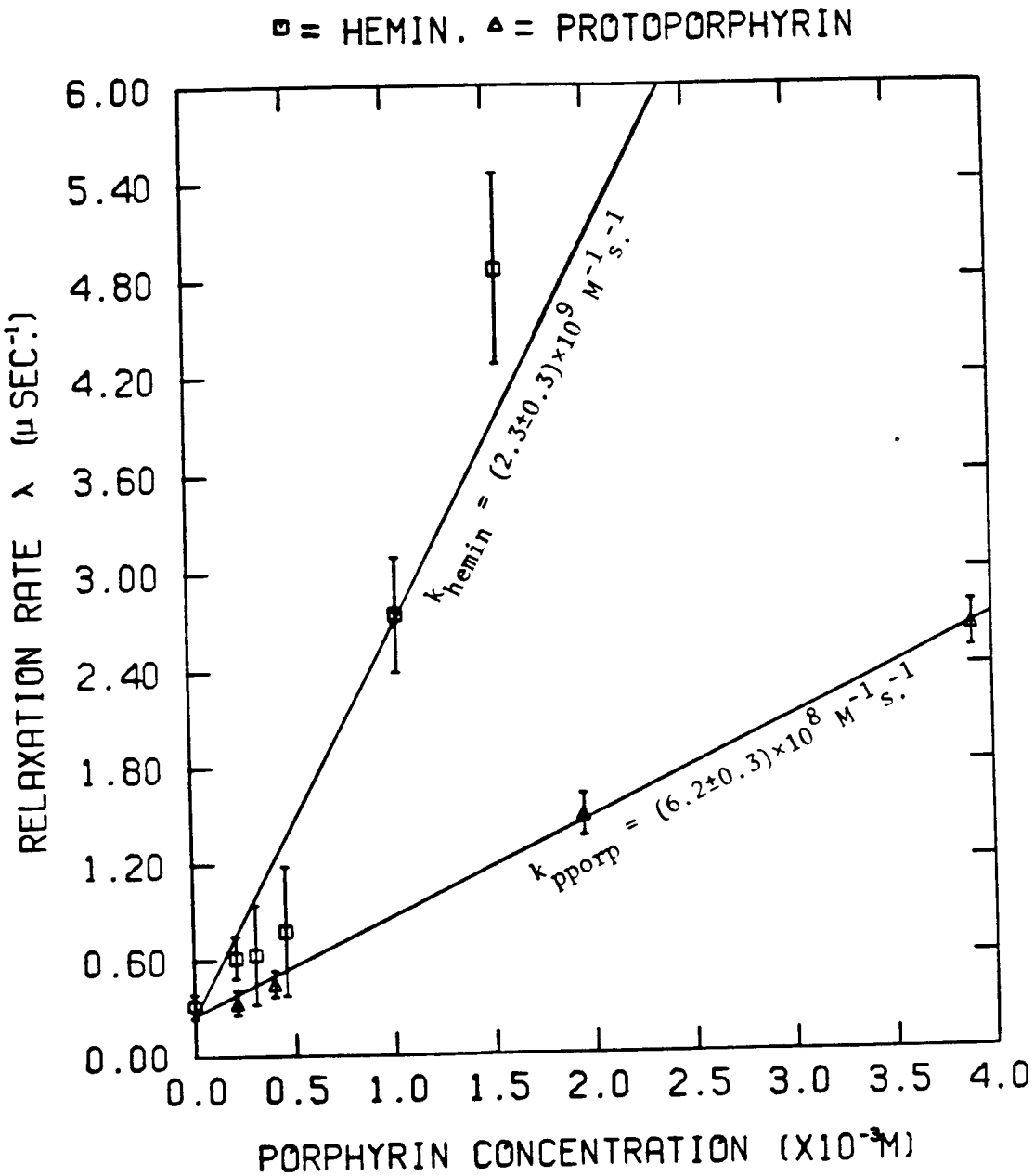

Figure 2.14: Plot of observed Mu-decay constants (λ_M) against solute concentrations (hemin and protoporphyrin) at room temperature to obtain k_M.

$$k_M = A \cdot \exp(-E_a/RT) \quad . \tag{2.17}$$

A plot of ln k_M against 1/T yields the slope as the activation energy (E_a/R) and the intercept as the pre-exponential factor (A). Again, these parameters are obtained via the MINUIT fitting of the data points assuming a linear relationship between ln k_M and 1/T.

In general, the statistical errors from the computer fits were less than the variations found from one experiment to another due to unknown random errors arising from small changes in cell positions, field inhomogeneities, impurity levels, solute concentrations, etc. Sometimes they were less, even, than the difference in values between left and right detectors. Realistic "probable errors" in k_M values may be about 20%. Indeed, the values of k_M in this thesis are always within ~20% of previously published values where these were available from the work of other groups from TRIUMF [29] or SIN [25].

2.E.2. Analysis of MRSR spectra.

Due to the many frequencies and their small amplitudes in MRSR experiments, at least 10-20 million events are required to discern all signals. For samples containing just one Mu-radical, the spectra consist of the diamagnetic frequency and a pair of frequencies whose sum corresponds to the A_μ value of the Mu-radical. Figure 2.15 displays Mu-radicals in neat styrene and benzene solutions. The formulation of the raw histogram is given by equation (2.9). As the number of frequencies increases, MINUIT-analysis of expression (2.9) in time-space becomes increasingly difficult. Therefore,

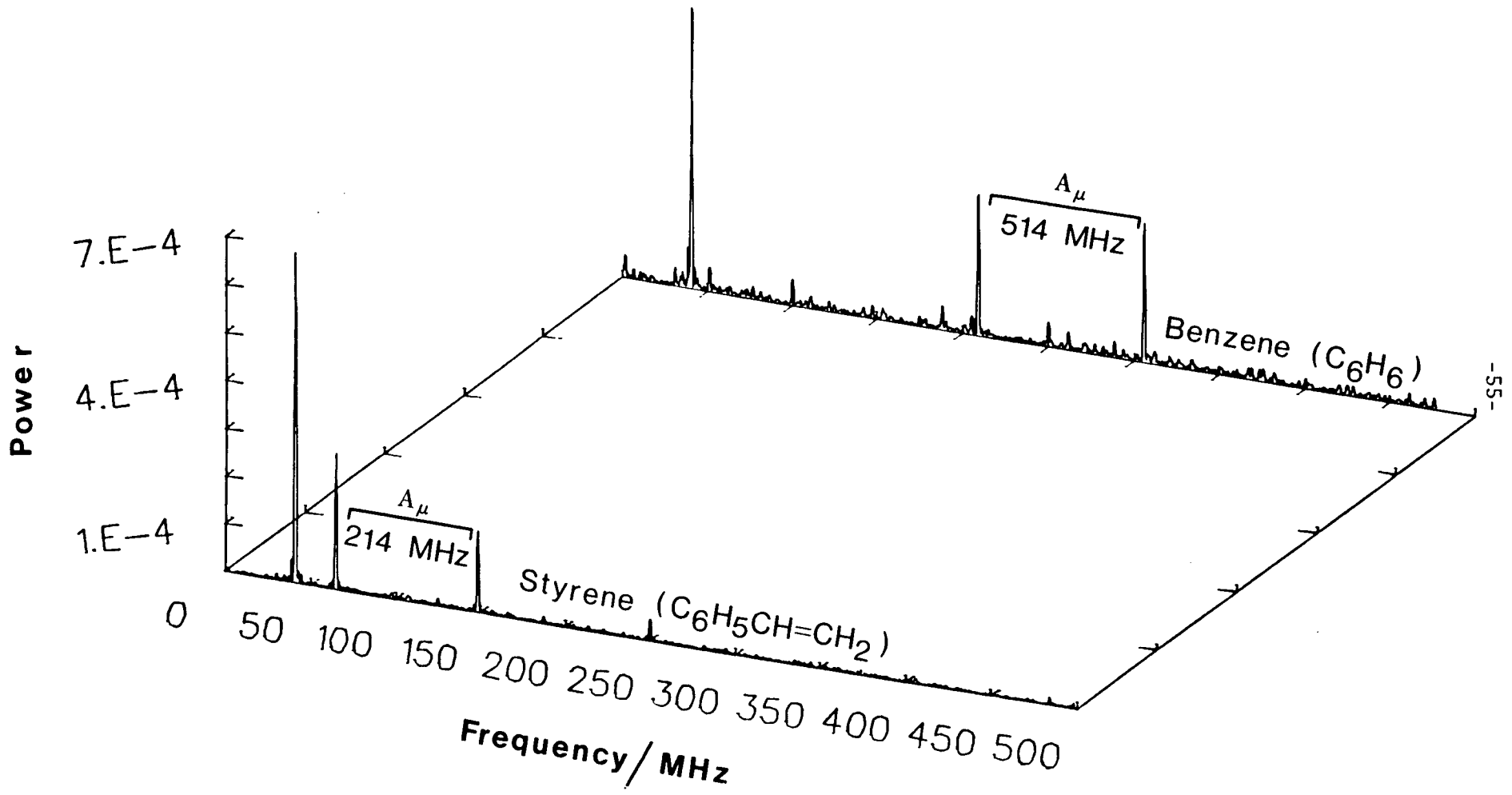

Figure 2.15: FFT diagrams showing Mu-radical formation in neat styrene and neat benzene at 3400G.

it is appropriate to apply Fast Fourier Transform (FFT) techniques to the raw histogram and analyze in frequency space [80,82]. However, in order to compare experimentally observable amplitudes, it is necessary to apply corrections (details of which are given in Appendix I) for the reduction in signal caused by the finite response time of the detection system (1.3 ns) and for limitations imposed by the small number of bins per cycle (especially for high frequencies). In this thesis, the parameters of interest are the amplitudes (A_{Ri}) and A_{μ}. Normalization (after corrections) of the amplitudes was achieved by comparison with the diamagnetic asymmetry in $CC\ell_4$ at 80G as defined by equation (2.13). Due to the many corrections needed for the MRSR experiments, P_R values are not expected to be better than ±20%. However, even considering the many corrections it is encouraging that P_R's in this thesis agree within 10% for similar samples performed by groups from SIN [82] and CERN (Synchro-cyclotron in Geneva, Switzerland) [83].

There was no attempt made to interpret the initial ϕ_i or λ_i, both of which are difficult to analyze precisely. The former parameter depends critically on an accurate determination of the experimental zero time, while the latter varies in a non-systematic manner between 0.5 and 3 μs^{-1}. The values of ϕ_i and λ_i for Mu-radicals will not be discussed further in this thesis.

CHAPTER 3

ORIGIN OF λ_o IN WATER:

A MAGNETIC FIELD DEPENDENCE STUDY

Since the discovery of Mu in water by Percival et al. [24], λ_o values of about 0.25×10^6 s^{-1} have been obtained in MSR experiments by groups from SIN and TRIUMF. There are many possible origins of this observed Mu background relaxation constant in water. (i) It may arise from reaction of Mu with impurities (such as residual O_2 or organic impurities). This was deemed unlikely due to adequate deoxygenation with helium gas during experiment and the many careful distillations days before beam time. Also, the small E_a (zero or at most 0.6 kcal $mole^{-1}$) obtained from the temperature dependence measurement of λ_o ruled out these chemical reactions since any such reactions would give a much higher E_a [71]. (ii) Another possible origin of λ_o involves intra-spur reactions of Mu with species produced at the end of μ^+ track. This was eliminated earlier [29] based on arguments that such intraspur processes would not follow first order kinetics [84] nor last longer than 10^{-6} sec [85]. It was further indicated that the radiation dose levels (mainly from positrons accompanying the muons) of less than 10^2 rad produced within the experimental timescale could not possibly account for sufficient production of H_2O_2 concentration to give diamagnetic products via reaction of Mu with H_2O_2,

$$Mu + H_2O_2 \longrightarrow MuOH + OH. \qquad (3.1)$$

(iii) The only other possible reaction of Mu is that with solvent water molecules. This will be commented upon later in section 3.A.2. Two further possible origins of λ_o are due to (iv) magnetic field inhomogeneities, and (v) collisional broadening, or Mu-frequency beating. Since (i) and (ii)

have been discounted, one can write the various possible origins to λ_o by the following expression,

$$\lambda_o = \lambda'_o + \lambda_{\Delta H} + \lambda_{FB} \qquad (3.2)$$

where λ', $\lambda_{\Delta H}$ and λ_{FB} represent the contributions to λ_o from solvent reaction, field inhomogeneities and frequency beating, respectively. Contribution via magnetic field inhomogeneities can be either eliminated experimentally by using a combination of high-quality magnets and correction field coils, or corrected-for after measurement by careful mapping of ΔH around the target sample area. On the other hand, the contribution to λ_o via Mu frequency beating (Mu-FB) can be measured directly by MSR experiments at several low fields and then fitted-out by appropriate MSR expressions. It is this so called "two-frequency"-MSR technique that one will be using to investigate λ_{FB} in this chapter.

First of all, what is this Mu-FB phenomenon? At very low magnetic fields ($B \leq 12G$), the classical Mu precession frequency ($\omega_- \equiv \omega_M$) is characterized by the two degenerate transitions, ω_{12} and ω_{23}, shown by the region of $\omega_e << \omega_o$ in Figure 2.5. However, at $B > 15G$, ω_{12} & ω_{23} are no longer degenerate. Therefore, it is now inappropriate to describe the Mu-amplitude signal by the degenerate (no beating) expression, equation (2.15). Notice that λ_M in equations (2.6) and (2.15) is referred to as λ_o in neat solvents. In order to account for this non-degenerate Mu phenomenon, one uses the full expression describing both amplitudes arising from ω_{12} and ω_{23} [86].

$$A_{FB}(t) = \frac{A_M}{2} e^{-\lambda_o t} \{(1+\delta)\cos(\omega_{12}t-\phi_M) + (1-\delta)\cos(\omega_{23}t-\phi_M)\} \quad (3.3)$$

where, $$\delta = x(1+x^2)^{-\frac{1}{2}} \quad (3.4)$$

Here, x is defined as $2\omega_+/\omega_o$ ($\omega_\pm = \frac{1}{2}[|\omega_e| \pm |\omega_\mu|]$). In equation (3.3), ω_{12} and ω_{23} are represented by:

$$\omega_{12} = \omega_- - \Omega \,, \quad (3.5a)$$

and $$\omega_{23} = \omega_- + \Omega \,; \quad (3.5b)$$

where,

$$\Omega = \frac{\omega_o}{2} [(1+x^2)^{\frac{1}{2}} - 1] \,; \quad (3.6)$$

and ω_- is the classical Mu-precession frequency at very low fields ($B<<B_o$). It should be mentioned that equation (3.3) is valid up to about 150G [4,75] and the difference between ω_{23} and ω_{12} gives 2Ω. To properly analyze non-degenerate MSR histograms, one must then use the following expression,

$$N(t) = N_o e^{-t/\tau_\mu} [1 + A_D\cos(\omega_D t + \phi_D) + A_{FB}(t)] + BG \quad (3.7)$$

As one can now see, the contribution of λ_{FB} to λ_o in equation (3.2) can be computer-analyzed by using equation (3.7). This Mu-FB phenomenon can be seen clearly be measuring Mu in quartz at 17G (Figure 3.1). Therefore, by measuring Mu as a function of low magnetic fields, one can then extract λ_{FB} from λ_o by applying this two-frequency expression to MSR histograms.

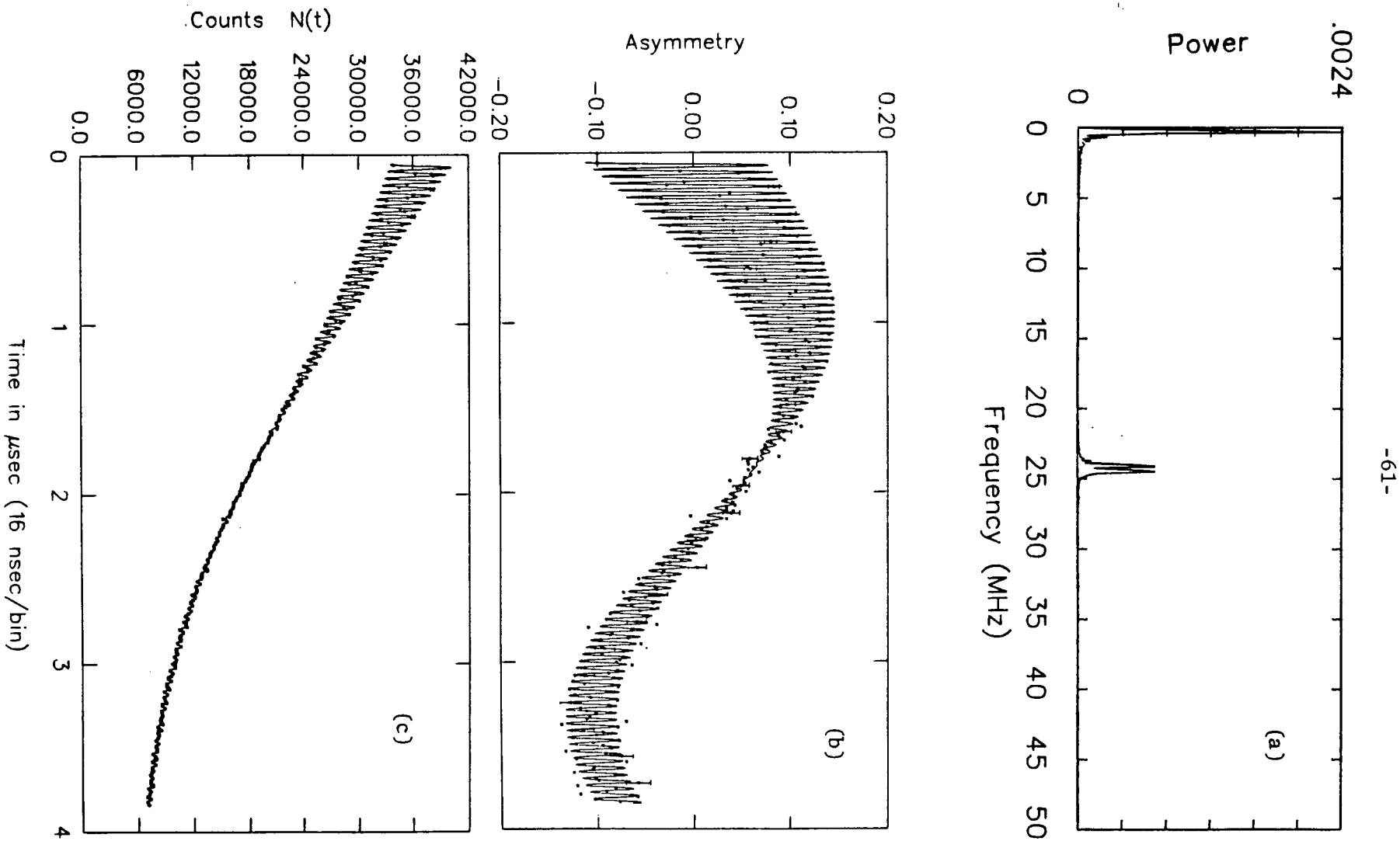

Figure 3.1: MSR measurement of Mu in quartz at 17G. (a) FFT spectrum showing ω_{12} and ω_{23} around 24 MHz, the much lower frequency belongs to the diamagnetic signal. Corresponding: (b) asymmetry and (c) time histograms showing the beating effect of ω_{12} and ω_{23} in time-space. The line is computer drawn by fitting the data points with equation(3.7).

3.A.1. Results.

The magnetic field dependence of Mu in water was investigated at three low fields (~4, 6, & 9G) using the surface muon-MSR technique. The regular teflon cell containing the pure water sample was continuously bubbled with He gas and left untouched while the field was varied from one experiment to another. In order to adequately observe the beating effect of Mu at low fields, the gate was set to 8 μsec and each experiment was allowed to collect at least 8 million events. Typical MSR histograms at low fields are shown in Figure 3.2. The data was analyzed over the full 8 μsec spectrum with equation (2.6) and equation (3.7). The χ^2 values (quality of fit to data points, best fit is when χ^2=1) for all fits were about 1.05. All parameters in equation (2.6) and equation (3.7) remain the same for both fits with the exception that λ_o decreases and remains constant for the non-degenerate analysis relative to the degenerate analysis. The results are given in Table 3.1 and illustrated in Figure 3.3. It can be seen clearly from Figure 3.3 that if one does not consider Mu-degeneracy for slow Mu relaxations, the Mu-FB effect appears as an extra contribution to λ_o and the effect increases for progressively higher fields. As shown in Table 3.1, the Mu-FB contribution to λ_o is simply the difference between the two fitted values (λ_{FB}). It is interesting to note that λ_{FB} seems to increase rapidly with field and suggests a power dependence of about 4. In addition, the magnetic field around the target sample area was mapped carefully with a Hall-probe. The measurement indicated an average field inhomogeneity (ΔH) of about 10mG within a 10 cm cube at the center of the coils.

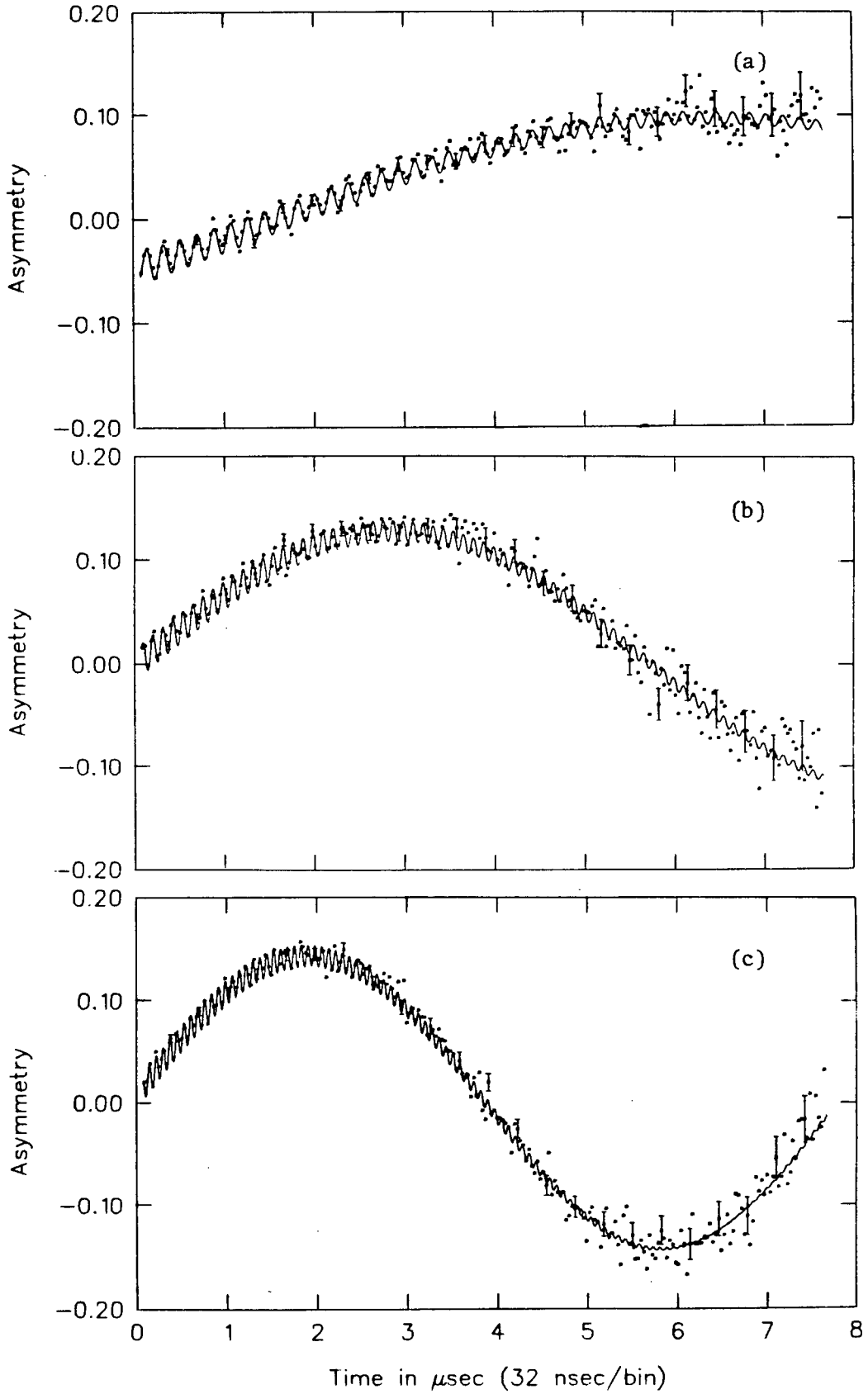

Figure 3.2: MSR histograms of Mu in water fitted with equation (3.7) at (a) 3.85G, (b) 6.44G, and (c) 9.38G.

TABLE 3.1

λ_o values obtained by fitting with and without consideration of Mu-degeneracy at low magnetic fields.

B/gauss	$\lambda_o/10^6$ s^{-1}		$^{\dagger}\lambda_{FB}/10^6$ s^{-1}
	§Degenerate-fit	$^{\partial}$Non-degenerate-fit	
3.85	0.109±0.055	0.111±0.050	0.002
6.44	0.136±0.063	0.109±0.037	0.027
9.38	0.230±0.051	0.099±0.069	0.131

$^{\S}\lambda_o$ is obtained by fitting the data with equation (2.6).

$^{\partial}\lambda_o$ is obtained by fitting the data with equation (3.7).

$^{\dagger}\lambda_{FB}$ is defined as the absolute difference between the degenerate and non-degenerate values.

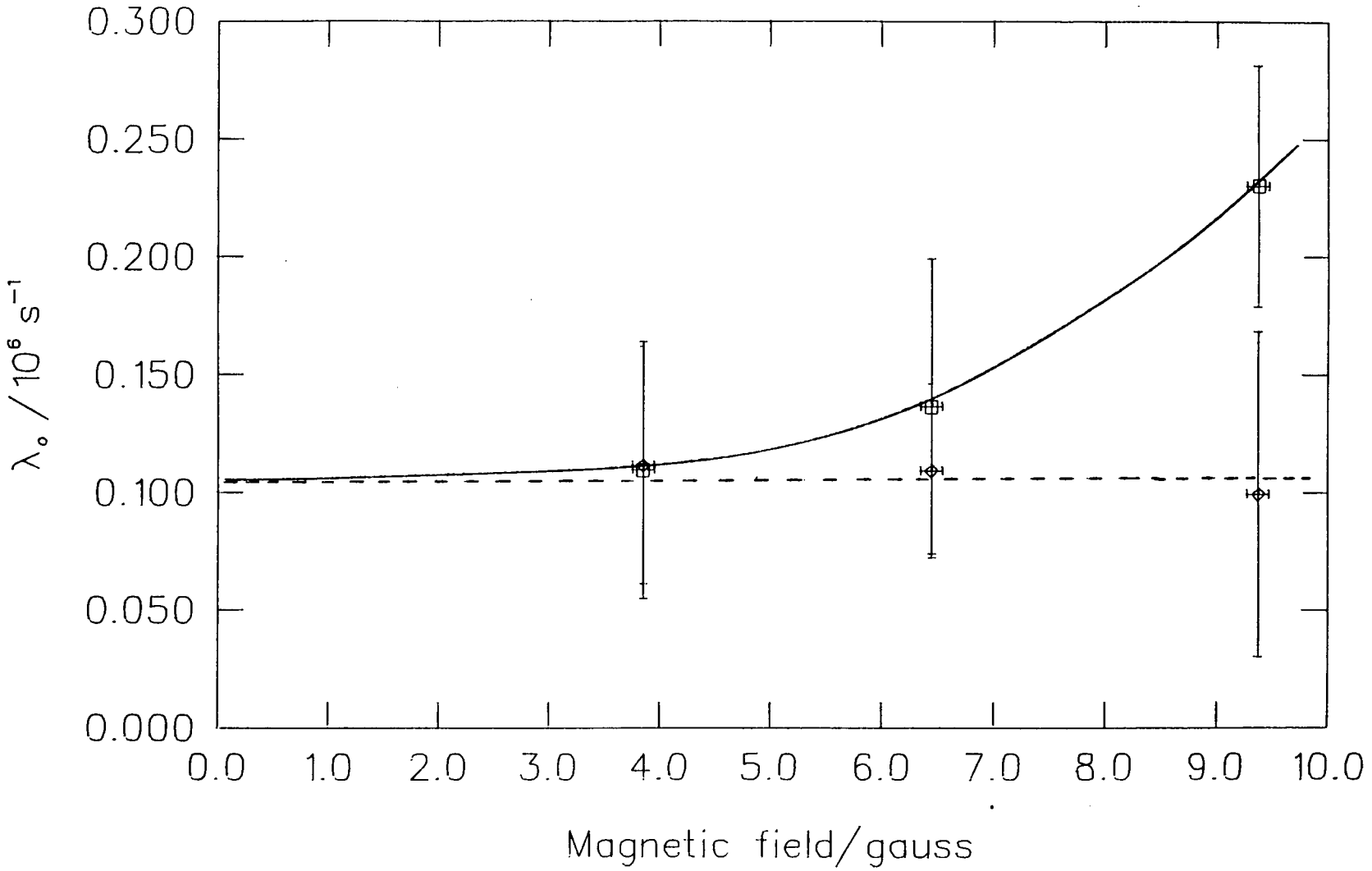

Figure 3.3: Magnetic field dependence of λ_o for water. (□) represents the value obtained by the degenerate expression, equation (2.6), while (◇) was by the non-degenerate equation (3.7).

3.A.2. Discussion.

It is obvious that the Mu-FB effect contributes to λ_o. In the higher field range (B≈9G), λ_{FB} comprises almost 60% of the λ_o value. Therefore by subtracting this phenomenon, λ_o ($=\lambda'+\lambda_{\Delta H}$) becomes 0.11×10^6 s^{-1}. A similar non-degenerate expression to equation (3.7) was used to fit low field MSR histograms by Percival et al. [87]; however, the authors did not find any difference for λ_o between the degenerate and non-degenerate fits. Perhaps their inability to see the λ_{FB} contributions was due to combinations of small data gate ($\leq$4 μsec), insufficient statistics, and low asymmetry of backward muons. In order for the computer to properly fit (or "see") the beating effect, one must collect over long gate times (at least $\geq$8 μsec), have high Mu-asymmetries, and certainly a vast amount of data points, especially for the longer time range.

It was interesting to note that λ_{FB} varies approximately as B^4. This λ-fourth-power dependence on the value of the external field was qualitatively predicted by Nagamine et al. [88] from the University of Tokyo Meson Science Laboratory (UT-MSL) at KEK (National Institute of High Energy Physics) in Japan. However, the exact analytical dependence of λ_{FB} upon the magnetic field is not well known. At present, the gas-chemistry group at TRIUMF has concluded that the functional form of the dependence is neither exponential nor Gaussian and they are now performing Monte-Carlo simulations to extract the exact λ_{FB} dependence upon B. In any case, from this chapter's result, it is clear that λ_{FB} has a strong dependence upon B and this is demonstrated especially at relatively high fields (~10G).

The field inhomogeneity ΔH was measured around the target sample area and an average value of about 10 mG was obtained. Since ΔH causes dephasing of the coherent Mu precession with a rate of $\gamma_M \Delta H$ [88], a corresponding dephasing rate of 0.09×10^6 s^{-1} will be expected for the ΔH contribution to λ_o (i.e. $\lambda_{\Delta H}$). Thus, the present result after subtraction of λ_{FB} and $\lambda_{\Delta H}$ from λ_o gives a lower limit value for equation (3.2) of

$$\lambda_o' \simeq 0.02 \times 10^6 \ s^{-1} \ . \qquad (3.8)$$

Within statistical and systematic errors, this value of λ_o can be probably considered as zero. This suggests that λ_o in water is simply an experimental artifact due to a combination of magnetic field inhomogeneities and the physical phenomenon of Mu-frequency beating.

Let's consider that λ_o is non-zero and has a value corresponding to equation (3.8). If this is so, this number will be the contribution λ' due to the reaction of Mu with water solvent molecules. The following are possible reactions giving rise to diamagnetic species such as MuOH, MuH or MuO [29].

$$Mu + H_2O \longrightarrow H + MuOH \qquad (3.9a)$$

$$Mu + H_2O \longrightarrow OH + MuH \qquad (3.9b)$$

$$Mu + H_2O \longrightarrow H_2 + MuO \qquad (3.9c)$$

These reactions do not involve diffusion of the reacting species since the

water molecules are already present at a concentration of 55M! This places an upper limit on k_M (reaction rate constant of Mu with H_2O molecules). Using $\lambda_o = k_M[H_2O]$, one obtains $k_M \leq 3.6 \times 10^2\ M^{-1}s^{-1}$. Since this is an upper limit (i.e. λ_o can be smaller), it is not inconsistent with the corresponding k_H of about $10^{-4}\ M^{-1}s^{-1}$ [89] for the reaction,

$$H + H_2O \longrightarrow H_2 + OH . \qquad (3.10)$$

Considering all the errors and difficulties involved in the MSR measurements of small Mu-relaxation rates, this indicates that Mu does not react with solvent water molecules.

The fact that λ_o in water is of such a small value is much blessing for the Mu-chemist studying kinetics of various solutes in aqueous solutions. If λ_o was greater than 1 μs^{-1}, the range of concentrations (see Figure 2.14) that one could investigate would be very much smaller and place tremendous uncertainty in the evaluation of k_M. However, it should be emphasized (contrary to Nagamine et al. [88]) that the λ_o value one uses for extraction of k_M in equation (2.16) should be the value obtained by each group fitting with equation (2.6). Although one can extract λ_{FB} from λ_o by fitting with equation (3.7), this can not be done for higher λ's (similar to the case of slower relaxation at short data gate). Since λ_{FB} is the same at constant magnetic field, this will have to be subtracted out from concentration-λ's $\geq 1\ sec^{-1}$. This is equivalent to fitting with the degenerate expression, equation (2.6), for all concentrations including pure H_2O. This is further illustrated in Figure 3.4. In other words, k_M values for various solutes in

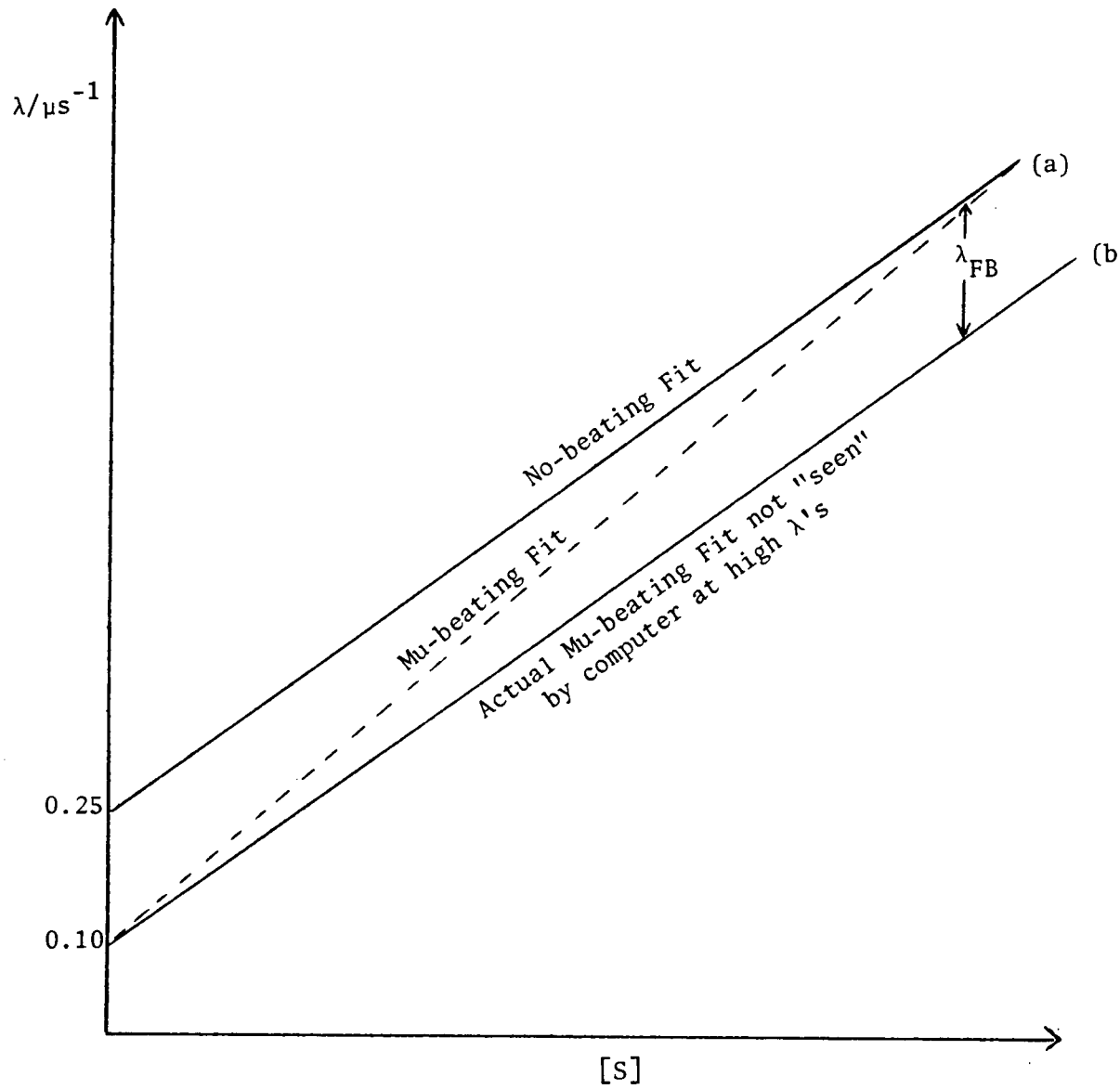

Figure 3.4: Diagram of expected λ dependence vs. [S] fitted with (a) equation (2.6) and (b) equation (3.7). Both methods should give the same k_M. However, equation (2.6) is a much simpler expression to use for data analysis in the MSR technique.

aqueous solution should be obtained by using λ_o's and λ's fitted with equation (2.6) for one particular set of experiments.

It should now be of particular interest to use this two-frequency MSR technique to investigate λ_o of various solvents (i.e. neopentane, MeOH, etc.) to see if Mu really does react with these compounds. However, MSR experiments with these solvents are extremely difficult due to impurity problems. Non-reproducibility of λ_o with different samples of the same hydrocarbon delays such attempts with neat solvents. However, the investigation of Mu in hydrocarbons will be further elaborated in later chapters.

CHAPTER 4

MUONIUM RADICALS IN BENZENE, STYRENE, AND THEIR MIXTURES

As was explained in section 2.B.3., muonium-containing free radicals can be observed in unsaturated molecules by applying high-enough transverse magnetic fields. Since the initial direct discovery of Mu-radicals in 2,3-dimethyl-2-butene [26], more than 80 of these species have been observed by groups from SIN, CERN, and TRIUMF. The MRSR technique can be used to study kinetic isotope effects or initiation kinetics, selectivity of Mu-reactions based on inter- and intra-molecular exchanges, effects of group substitutions, and formation of Mu-radicals and Mu itself. In pure styrene, it was shown [41] that only one Mu-radical is observed in a solution of neat styrene ($C_6H_5CH=CH_2$) on the MRSR timescale (between 10^{-9} - 10^{-5} sec). Similarly, only one pair of radical frequency lines is observable for pure benzene [41,90]. In the case of styrene, there are six possible radicals that can be formed by the Mu addition to the double bonds of the vinyl or phenyl groups, yet only one radical is observed. Is this selectivity a result of intra-molecular rearrangement to the most stable radical following random primary attack, or is it a matter of kinetic competition in forming the initial radical? Of course, in the case of benzene, all positions of Mu-attack are equivalent, therefore only one Mu-radical frequency pair is possible. The radical frequencies for separate solutions of neat styrene and neat benzene at 3400G are shown as FFT spectra in Figure 2.15. Also, the field dependence of the diamagnetic and radical frequencies are illustrated in Figure 2.6.

In ESR studies, H-atom addition to the phenyl group of polystyrene gives a primary splitting of a_p=45G [91] which is translated into

A_p=126MHz. On the other hand, it has been calculated [92] that A_p for an ESR radical observed in the backbone of polystyrene should give a value of 56 MHz. To calculate the equivalent MRSR-A_μ (A'_μ) from A_μ obtained in styrene (213.4±0.2 MHz) [41], the difference between the magnetic moments of the proton and muon is considered; thus

$$A'_\mu = A_\mu \left(\frac{\mu_p}{\mu_\mu}\right) . \qquad (4.1)$$

This gives a value of 67.0 MHz for A'_μ in the styrene radical (see Table 1.1 for ratio of μ_p to μ_μ). By comparison to the ESR values, it is clear that the observable radical in styrene belongs to the Mu addition to the vinyl bond of styrene. For example,

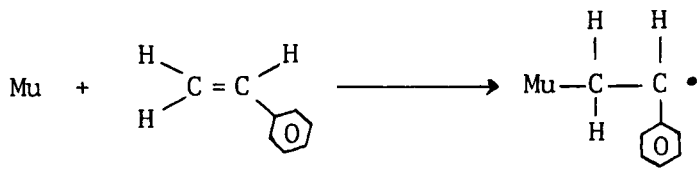

(4.2)

Therefore, there is no net insertion of Mu into the phenyl ring, yet benzene itself readily forms cyclohexadienyl radicals as shown by equation (2.7) (A_μ = 514.6±0.2 MHz) [26,93]. Similarly, there are three radicals (o-, m- & p- with A_μ ~ 490-512 MHz) formed in comparable yields in both toluene and ethylbenzene [82,83].

At present, there are four models of Mu-radical formation [94]:

$$Mu^{*} + S \longrightarrow \text{radical} \qquad \text{(I)}$$

$$Mu + S \longrightarrow \text{radical} \qquad \text{(II)}$$

$$\mu^{+} + S \longrightarrow [S_{\mu}^{+}] \xrightarrow{e^{-}} \text{radical} \qquad \text{(III)}$$

$$e^{-} + S \longrightarrow S^{-} \xrightarrow{\mu^{+}} \text{radical} \qquad \text{(IV)}$$

These models differ in the nature of the radical precursor. In models I and II, the precursor is assumed to be Mu, with model I being hot and model II thermal [22,95]. However, for models III and IV, the precursor is diamagnetic, be it $[S\mu^{+}]$ in (III) or μ^{+} in (IV) [96]. As one can see, the models of Mu-radical formation are just as tentative and even more variable than that of Mu formation itself. Therefore in this chapter, it is appropriate to investigate mixtures of benzene and styrene in an effort to seek answers to questions about intra- and inter-molecular exchanges, and possibly about "hot" or "thermal" Mu attacks. It should be mentioned that since the completion of this project [73], a paper reporting similar experiments (from CERN) has appeared [96]. However, the results only agree moderately and the discussions differs substantially.

4.A.1. Results.

Backward muon set-ups were used to obtain MRSR spectra of styrene, benzene, and their mixtures. A magnetic field of 3.4 kG was chosen for all experiments. Twenty million events were collected for at least one of the three spectra. Already spectrograde samples were redistilled just before experiments and were contained in glass cells. Before and during the data

taking, the samples were bubbled with high purity helium. To ensure evaporation did not significantly alter the compositions, appropriate bubblers were used to saturate the He gas before entering the sample solutions.

The value of A_μ, A'_μ and A_p for styrene and benzene are listed in Table 4.1. Figure 4.1 shows the FFT spectra of the MRSR experiment at 3.4kG for the 80% benzene/20% styrene mixture. It consists of the diamagnetic peak (D) and two pairs of radical peaks (S_1 & S_2 for styrene, B_1 & B_2 for benzene) whose frequencies are given in Table 4.2. These are the same as found separately in pure styrene or benzene, and their sums correspond to those in Table 4.1 and other published hyperfine coupling constants [26,41]. In order to compare amplitudes (as detailed in Appendix I), it is necessary to apply corrections for the reduction caused by the finite response time of the detection system (~1.3 nsec) and for limitations imposed by the small number of bins per cycle after analysis in Fourier space (section 2.E.2.). The correction factors used for the four radical frequencies are given in Table 4.2. After corrections, the amplitudes were normalized against the diamagnetic asymmetry in $CC\ell_4$ at 80G. P_D values of 0.17 and 0.15 at 80G were found for pure benzene and styrene respectively, in good agreement with previous results [41,96]. No free muonium atoms were found in any of these systems (i.e. P_M=0). Figure 4.2 shows how the corrected, normalized radical yield of the cyclo-hexadienyl Mu-radical (R_B) and the phenylethyl Mu-radical (R_S) vary with the volume-fraction of the mixtures. When plotted against mole- or mass-fraction the plots are similar. However, it is more appropriate to use volume-fraction since it is probably the best way to represent the

TABLE 4.1

Hyperfine coupling constants of styrene and benzene

		Mu-R		H-R
Monomer	Radical	A_μ/MHz	A'_μ/MHz	A_p/MHz
Styrene	$C_6H_5\dot{C}HCH_2Mu$	213.4	67.0	56.0
Benzene	$\dot{C}_6H_6Mu$	514.6	161.6	133.7[†]

[†] Taken from reference [97].

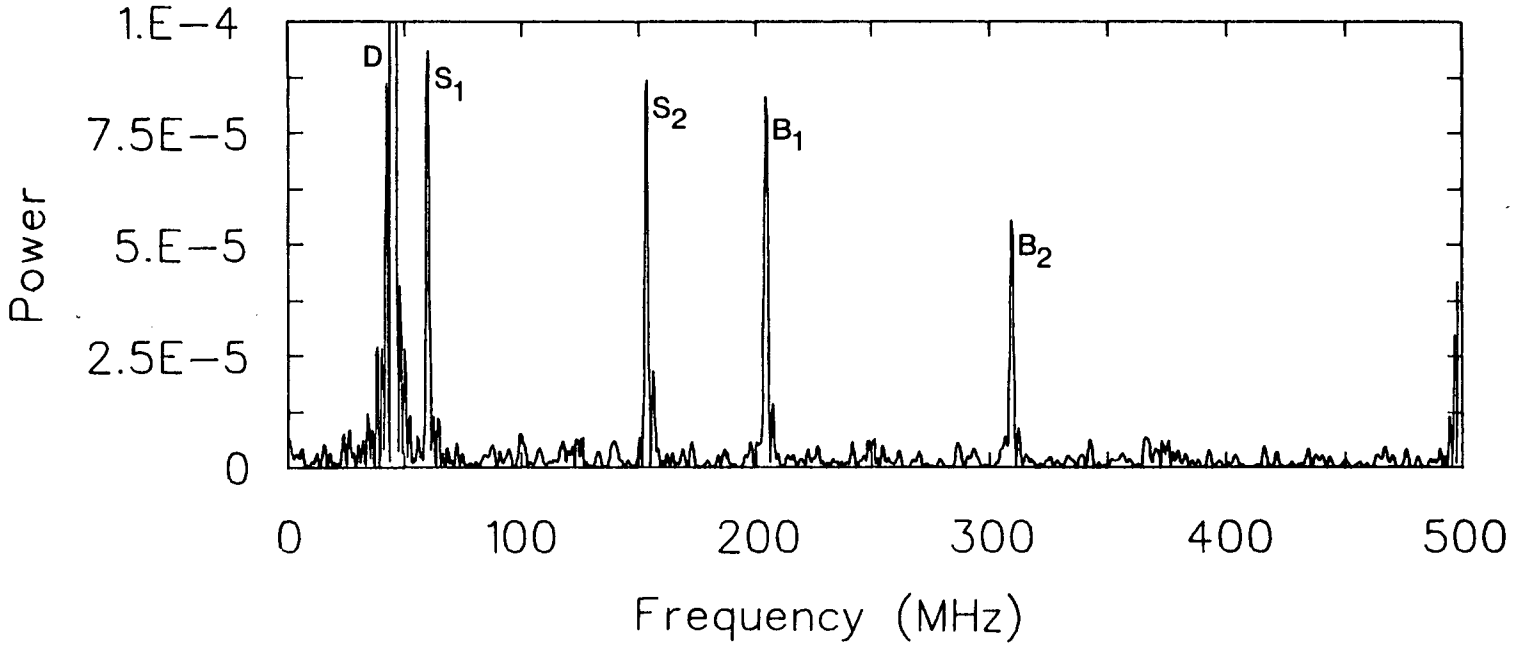

Figure 4.1: FFT spectrum of 20% styrene by volume in benzene obtained from the 3.4kG MRSR histogram. Peak D represents the diamagnetic signal (46 MHz), S_1 and S_2 (sum = 215 MHz) represent the Mu-radical from styrene, B_1 and B_2 (sum = 514 MHz) represent the Mu-radical from benzene. (power is proportional to the amplitude squared)

TABLE 4.2

Radical frequencies at 3.4 kG in styrene (S_1 and S_2) and benzene (B_1 and B_2) and correction factors needed to calculate the amplitudes. Column X gives the observable fraction due to the timing resolution of the detection system, and Y is the observable fraction due to the packing fraction (or number of bins per cycle) used in the analysis.

Radical	Frequency/MHz	X	Y
S_1	60	0.97	0.99
S_2	154	0.82	0.96
B_1	205	0.71	0.94
B_2	310	0.46	0.86

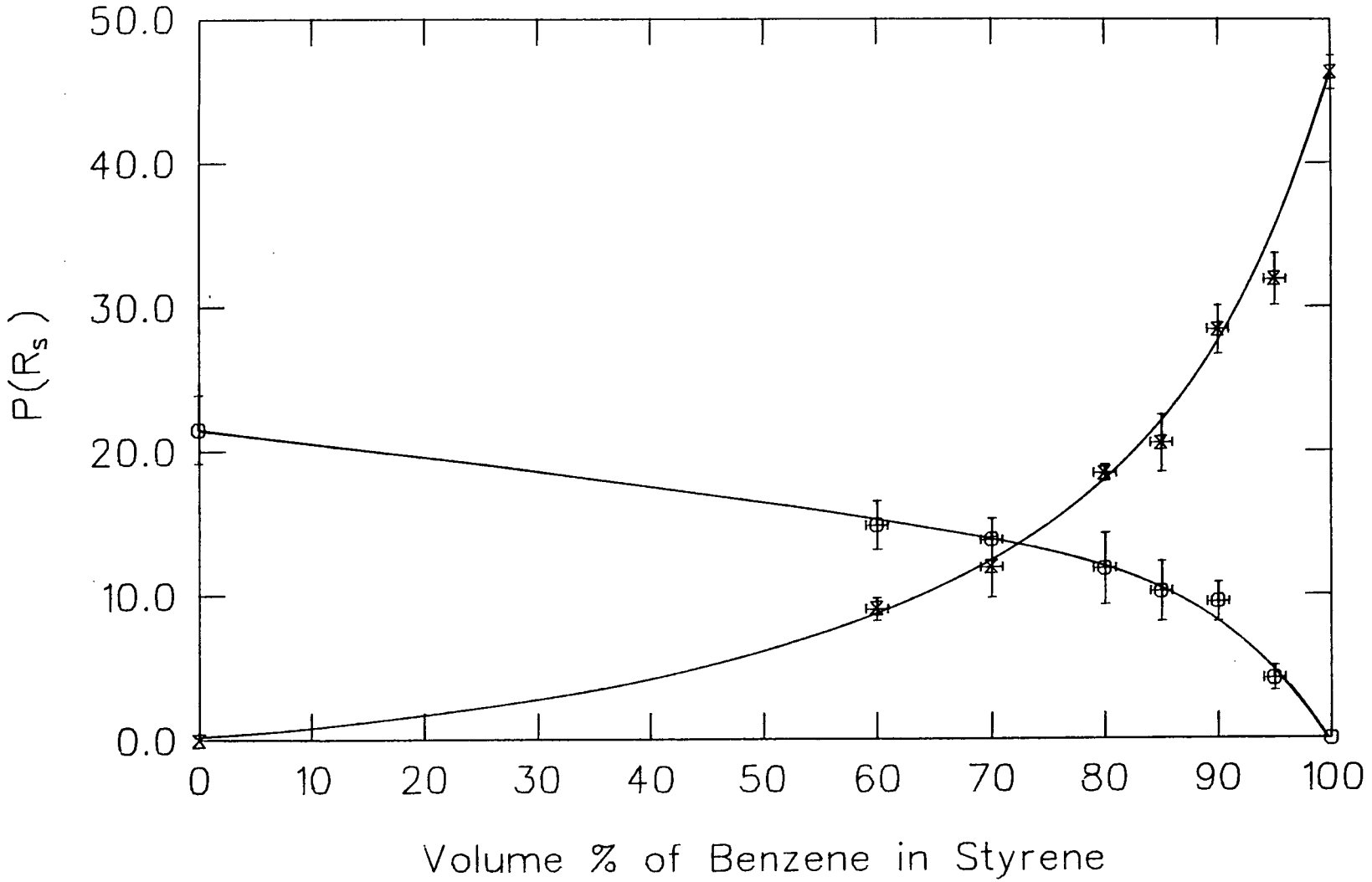

Figure 4.2: Plot of normalized, corrected radical yields against the volume-percent of the benzene/styrene mixture. Upper curve (o) gives $P(R_S)$, lower curve (⧖) $P(R_B)$.

fraction of time spent by the radical precursor in contact with benzene or styrene molecules. The total yields (P_D, P_R & P_L) against volume fraction of the mixtures are illustrated in Figure 4.3. Notice that in the plot, P_R is the sum of $P(R_S)$ and $P(R_B)$. The lines are drawn by eye to show the dependence of P_D and P_R+P_D with composition.

4.A.2. Discussion.

It is clear from the FFT mixture spectra (Figure 4.1) that the two radical frequency pairs are the same as those in the separate neat liquids (compare Table 4.1 and Table 4.2). Since both Mu-radicals can be observed in each mixture within the time window of $\sim 10^{-9}$ to 3×10^{-6} sec, it implies that there is no fast inter-molecular conversion during this time scale. The fact that they can be seen at all in the MRSR technique places an upper limit of Mu-radical formation of $<<10^{-9}$ s. In any case, the observable time-scale, including the fact that the styrene radical signal is fairly long lived ($\lambda \sim 1\ \mu s^{-1}$), means that the cyclohexadienyl radical does not initiate polymerization of styrene, so its rate constant (k_p) for initiating styrene polymerization must be less than $\sim 10^4\ M^{-1}s^{-1}$.

The radical yield plot in Figure 4.2 indicates some sort of kinetic competition, since on a volume basis there is not an equal probability of forming R_B and R_S. Let's consider the following reactions:

$$X + B \xrightarrow{k_B} P(R_B) \qquad (4.3a)$$

$$\text{and} \quad X + S \xrightarrow{k_S} P(R_S)\ ; \qquad (4.3b)$$

where X is the precursor (be it Mu, hot or thermal, or a μ^+ ion); then,

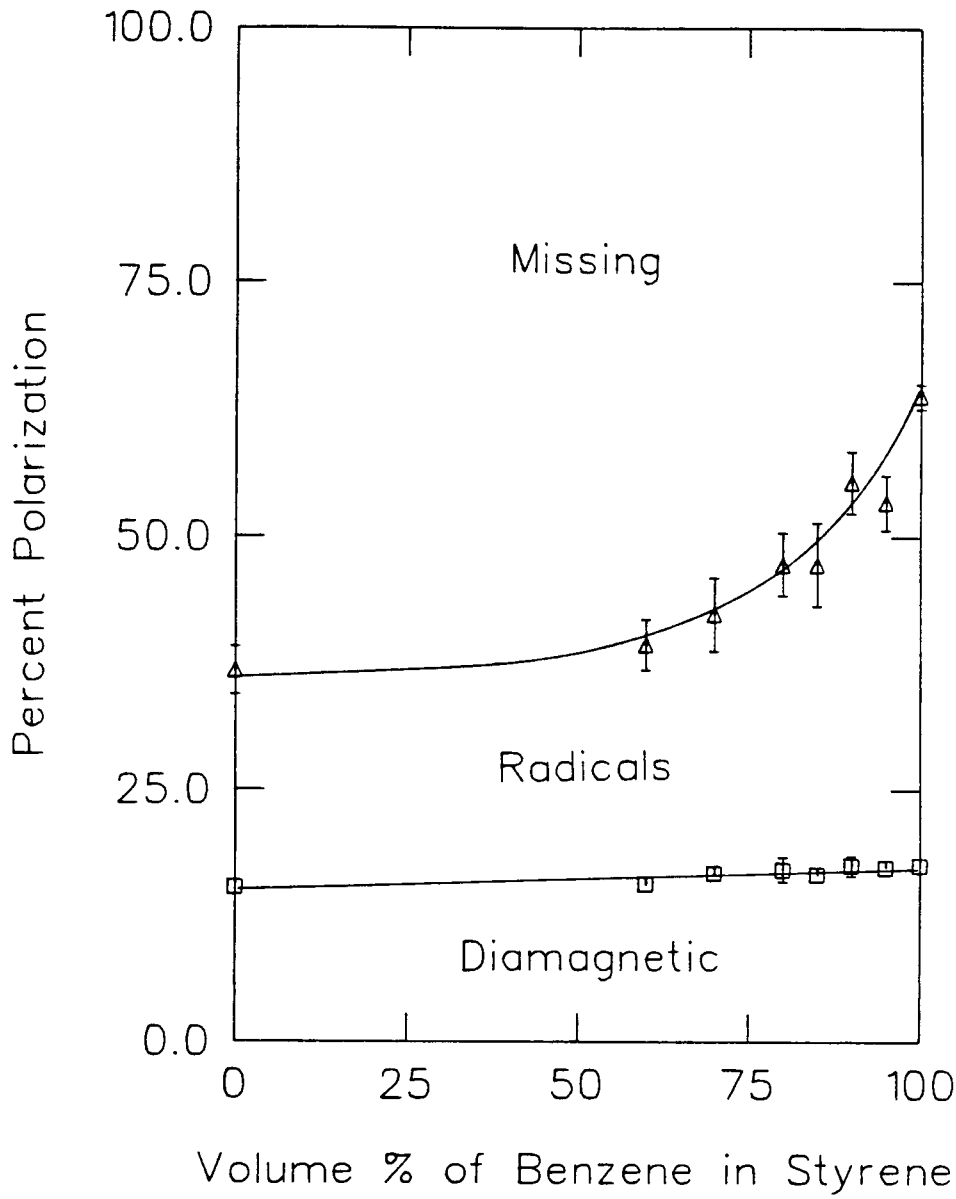

Figure 4.3: Plot of total yields (P_D, P_R & P_L) against volume fraction of the benzene-styrene mixtures. Note that P_R is the sum of $P(R_S)$ and $P(R_B)$. The line is drawn by eye to show the dependence of P_D and P_R with composition. (□) P_D alone, (△) P_D+P_R.

providing k_B and k_S remains invariant over the full composition range, the inverse fractional yields are given by:

$$1/P(R_B) = 1/P^o(R_B)\ \{1 + k_S[S]/k_B[B]\} \qquad (4.4a)$$

and

$$1/P(R_S) = 1/P^o(R_S)\ \{1 + k_B[B]/k_S[S]\}\ , \qquad (4.4b)$$

where $P^o(R_B)$ and $P^o(R_S)$ are the fractions of Mu adding to benzene and styrene, respectively. Figure 4.4 displays the linear dependence of equation (4.4). This strongly corroborates the occurrence of a direct competition between benzene and styrene for a common precursor. Both lines give a ratio of $k_S/k_B = 8\pm1$. This ratio is more than twice the value obtained by Cox et al. [96]. Their k_S/k_B value of (3.5 ± 0.15) was determined by assuming a constant precursor yield of 0.35 (i.e. $P^o(R_B) = P^o(R_S)$). Indeed, such an assumption can possibly cause a poor fit to their data. However, considering the many corrections that are needed in analyzing MRSR spectra and the fact that both groups (CERN and TRIUMF) used different sets of apparatus and electronics, there is probably as good a correlation between the two ratios as could be expected at this stage.

It can be seen from Figure 4.3 that a large missing fraction, P_L, is present in the neat solutions and their mixtures. Since there were no free Mu-atoms observable at low fields, this suggests that P_L does not stem from P_M. However, no corrections have been made here to the radical yields for any decay of the radicals during or prior to the observation window; nor for any possible dephasing by prior precession of precursor X if the absolute

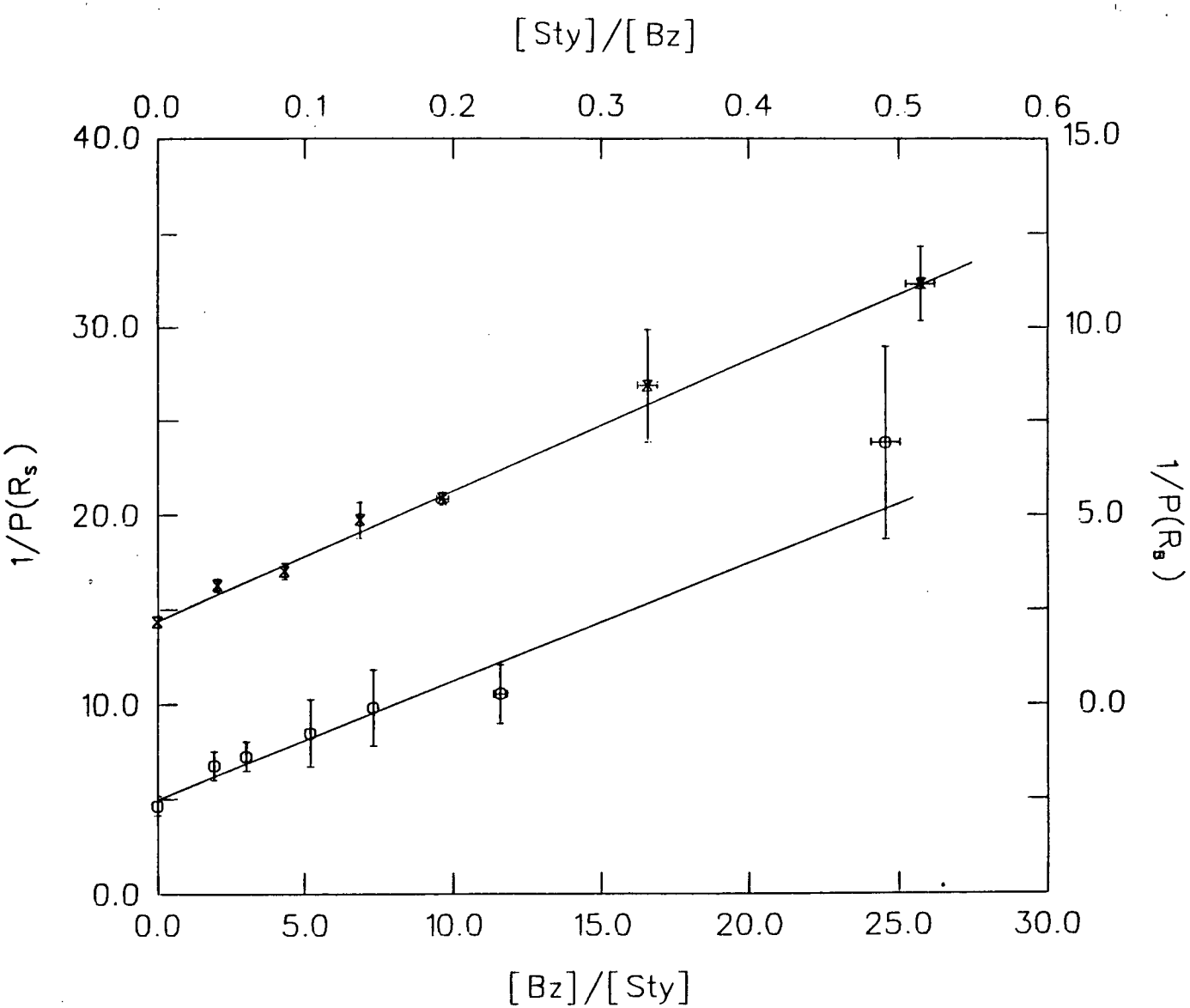

Figure 4.4: Kinetic competition plots: upper curve (X) represents $1/P(R_B)$ versus [S]/[B] and lower curve (o) represents $1/P(R_S)$ versus [B]/[S].

rate constants k_S and k_B are not high enough [95] (i.e., see chapter 5, OH^-), nor for any depolarization of the "singlet" muonium through the hyperfine interaction. The observed P_R could be smaller than the initial radical fractions, and thus contribute to P_L, for any of these reasons.

A selectivity ratio of 8 based on competition in the primary radical-forming step between the different solvent molecules can be accounted for, as above. However, the identity of precursor X (diamagnetic or Mu) cannot be established unequivocally with such competition experiments above [94]. In principle, measurements of the initial Mu-radical phases may be used for such a determination. However, Roduner [94], using relative phases, concluded Mu to be the main direct radical precursor in various solvent mixtures, while Cox et al. [96] found the opposite result (i.e. X is diamagnetic) by measuring absolute phases. Such variance of interpretation may be likened to that of hot and spur models of Mu-formation. The identity of precursor X will probably require more and different types of experiment.

Regardless of the above controversy, one can discuss the possibility of hot or thermal X addition to the mixtures. Comparatively, hot additions of X should be less selective than that of a thermal process; but is a selectivity ratio of 8 sufficiently large to force one to favour a thermal-X addition? Intriguingly, if X was a thermalized Mu atom, and if this same k_S/k_B ratio applies to Mu reactions in dilute aqueous solution, then k_M for the benzene reaction of Mu would be only 1.4×10^8 $M^{-1}s^{-1}$ because k_M for styrene is 1.1×10^9 $M^{-1}s^{-1}$ [41]. This rate for benzene is barely fast enough to retain phase coherence in the muon spin as the radicals are formed in these mixtures.

Furthermore, it would imply an inverse isotope effect (k_M/k_H = 0.16 [99]) which is hitherto unknown for an addition reaction.

Due to the above inexplicable isotope effect, one should devise an alternative explanation. Roduner [94] has investigated the degree of transfer of muon polarization via amplitude and phase effects and obtained a value of $k_M = (8.9\pm0.6)\times10^9\ M^{-1}s^{-1}$ for Mu addition to neat benzene. Applying the selectivity ratio of 8, one obtains $k_M \sim 7\times10^{10}\ M^{-1}s^{-1}$ for Mu addition to neat styrene (Table 4.3). Such a high k_M should retain all of its muon polarization [95] if a magnetic field dependence study is carried out. Such an experiment is in the preliminary stages at TRIUMF. Table 4.3 lists the k_M, k_H and k_S/k_B values for reactions in water, neat solvents, and gases. It is interesting that the selectivity ratio (k_S/k_B) is bigger for H than for Mu by a factor of two. Such a result, with Mu being less selective than H, is an agreement with other free radical data from SIN [94,100]. This suggests either of two possibilities: that the precursor X is epithermal or that the effect is due to the tunnelling ability of the lighter Mu atom which reduces its selectivity. These cannot be distinguished at this time. It would be of particular interest if such MRSR mixture experiments and Mu-kinetic studies were carried out in the gas phase.

Finally, there is also the intriguing question of why only one radical structure is observed in styrene (but not in toluene, for instance). The factor of eight favouring styrene over benzene may be consistent with the greater rate of attack at the vinyl side chain than in the benzene ring. This would account for observing only the vinyl addition aduct for styrene if

TABLE 4.3

Various k_M and k_H values for benzene and styrene

	$k_M/M^{-1}s^{-1}$		$k_H/M^{-1}s^{-1}$	
	(in water)[a]	(in neat solvent)	(in water)[b]	(in gas phase)[c]
styrene (S)	1.1×10^9	$[\sim 7 \times 10^{10}]^{\dagger}$	$[\sim 2 \times 10^9]^{\partial}$	$[\sim 8 \times 10^8]^{\partial}$
k_S/k_B	1	8	2	16
benzene (B)	$\sim 1 \times 10^9$	$[8.9 \times 10^9]^{\#}$	1×10^9	5.01×10^7

$^{\partial}$ Since k_H is not available for styrene, the numbers are inferred from H-atom reacting with ethylene.

$^{\#}$ Taken from reference [94].

† Inferred from the experimentally selectivity ratio in chapter 4.

[a] k_M values of styrene in water was taken from reference [93], while benzene came from preliminary TRIUMF data.

[b] Values taken from reference [99].

[c] Values taken from reference [98].

one cannot also resolve the small remaining polarization distributed three ways among the ortho, para and meta vinylcyclohexadienyl frequencies. In addition, one cannot observe the $C_6H_5CHMu\dot{C}H_2$ radical either. Two explanations can be forwarded, either it is not formed initially or it simply disappears too quickly on the μSR time-scale. The former event would suggest an even higher primary selectivity than the obtained value of 8 since k_S would be based on attack on just one carbon site (out of up to 8 in styrene) compared to any one of 6 equivalent sites in benzene. In the latter case - where the observed selectivity accrues from the disappearance of the other primary radicals - one needs to contemplate whether the disappearance arises from intramolecular rearrangement to the most stable radical configuration (equation (4.2)), or whether the other radicals are lost by reaction with reactive species from the muon track or with styrene itself. From gas phase studies [98], intramolecular relaxation to the most stable radical seems appropriately selective for these observations. Therefore, as suggested by Table 4.3, even though the Mu-addition reaction producing radicals is fast (close to diffusion controlled limit for styrene), possible intramolecular rearrangements within the MRSR time-scale can induce phase incoherence of the radical signals causing low radical yields and the resulting large missing fractions.

4.A.3. Conclusion

From these MRSR experiments in mixtures of benzene and styrene, one can derive the most stable structures. In this case, intramolecular rearrangement gives rise to the only observed radical in styrene and the selectivity ratio

(k_S/k_B) of 8 in the mixture. The possibilities of tunnelling and epithermal reactions warrant further investigations into the many formation models of Mu-radicals. It is certainly clear that many more experiments are necessary to resolve some of these controversial, and yet most interesting issues, regarding the role of Mu-radical formation in liquids.

CHAPTER 5

MUON AND MUONIUM YIELDS

Both models, hot and spur, of muonium formation seem to be in constant consideration by the muon community. Many experiments were performed in the past several years in an attempt to clarify the arguments. Percival et al. [43], shortly after their discovery of Mu in water, proposed the spur model of muonium formation. Based upon their model, they explained the concentration and field dependence of the diamagnetic fraction (P_D) in the presence of electron scavengers. Walker [51] proposed many arguments against such a spur model based on radiation chemistry effects. In this chapter, muon and muonium yields in neopentane and concentrated hydroxide solutions will be used to further investigate the proper mechanism of Mu-formation in condensed media.

5.A. Muonium atoms in liquid and solid neopentane.

Hydrogen atoms are difficult to observe in liquid hydrocarbons; therefore it is particularly useful to use Mu as an isotope of H to study this subject. Long-lived Mu has been detected in water, and also in alcohols [42] and saturated hydrocarbons [33], although their lifetimes are comparatively reduced. There are three major reasons to study neopentane. (i) This compound has all of its hydrogen atoms present in methyl groups, thus Mu could be long-lived since abstraction of such H is slow. (ii) The molecule is almost spherical and therefore its quasifree electrons are enormously mobile [101]. This means that neopentane will have an unusually large free ion yield in radiolysis, despite its low dielectric constant. On the basis of the spur model [43], then, one would expect its Mu-yield to be dramatically different

from both water and hexane. (iii) Since neopentane has a convenient melting point and a simple solid structure, it is therefore an appropriate and interesting medium in which to study the effect of phase transitions on the various muon yields.

4.A.1. Results.

Neopentane was carefully purified, deoxygenated, and vacuum sealed in a 70 ml round glass bulb as described in section 2.D.2. About 10^7 backward muon events were collected on each of three positron counters for the sample held at four temperatures between 209 and 295 K (melting point = 253 K). P_M and λ_M values were obtained at 8G by fitting the data with equation (2.6), while P_D was obtained at 80G with equation (2.5). The muonium and muon precessions are displayed in Figure 5.1. Table 5.1 gives the values of λ_o ($\lambda_M=\lambda_o$ since this value is the observed Mu-decay rate constant in the neat solvent), P_M, P_D and P_L in the liquid and solid phases of neopentane.

5.A.2. Discussion.

These results have three major aspects of interest. First, Table 5.1 provides muon yields in a hydrocarbon which has physical properties different from both linear hydrocarbons and saturated weakly polar alcohols and ethers. This is particularly interesting with regard to radiation chemical free ion yields of these liquids [102]. As shown in Table 5.2, neopentane provides a medium due to its sphericity and non-polarizability [101] in which quasifree electrons are exceptionally mobile. The table indicates that for solvents

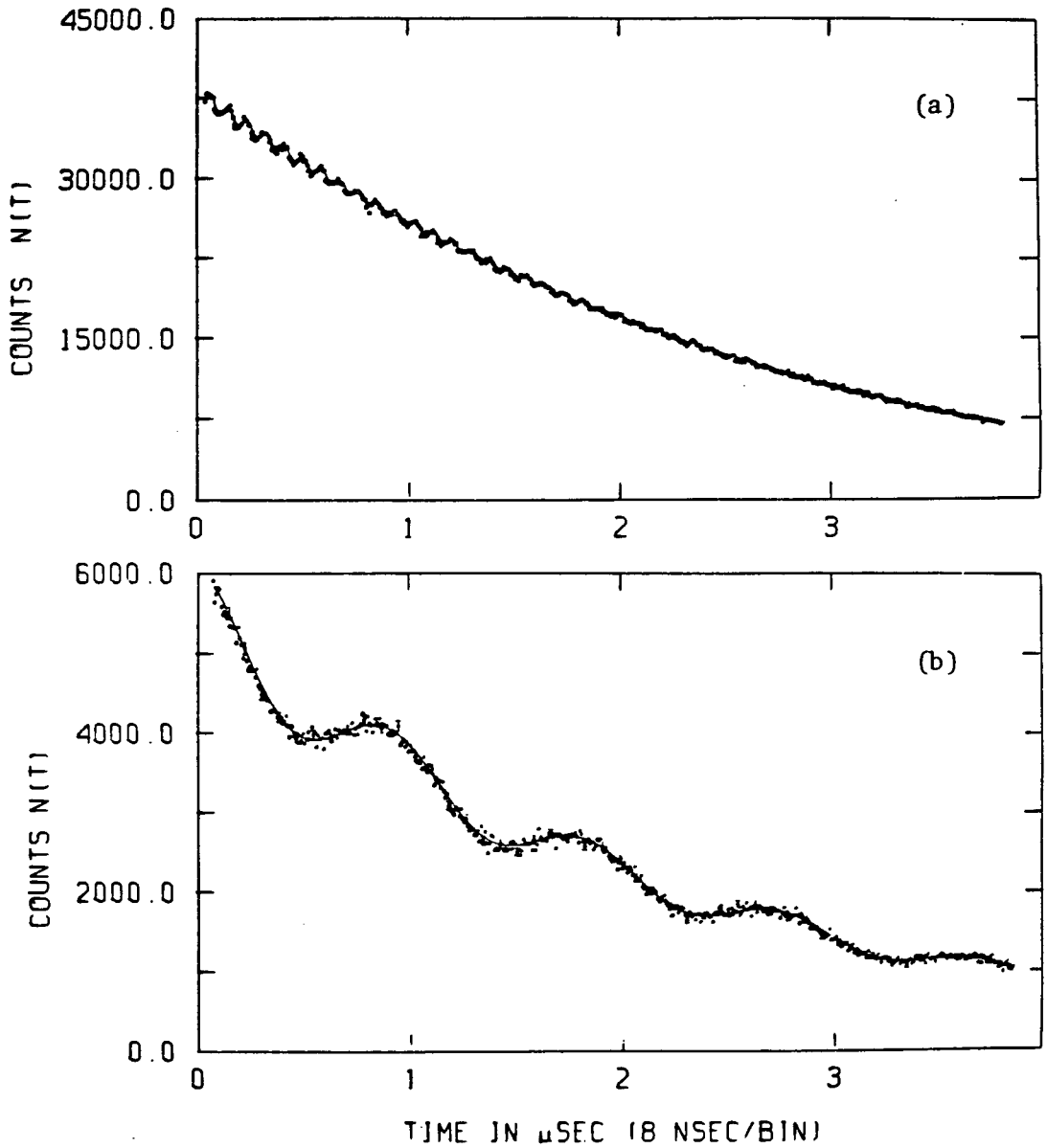

Figure 5.1: Raw histograms (dots) and computer fits (lines) for liquid neopentane at 295 K; (a) showing the muonium precession with 8G transverse magnetic field; and (b) showing the diamagnetic muon precession at 80G.

TABLE 5.1

Values of λ_o, P_M, P_D and P_L in neopentane in liquid and solid phases.

Phase	T/K	$\lambda_o/10^6 s^{-1}$	P_M	P_D	P_L[a]
Liquid	295±3	0.26±0.03	0.18±0.02	0.55±0.02	0.27±0.03
Liquid	259±2	0.30±0.07	0.14±0.02	0.60±0.02	0.26±0.03
Solid	238±2	0.17±0.06	0.14±0.01	0.59±0.02	0.27±0.03
Solid	209±2	0.33±0.13	0.19±0.02	0.61±0.02	0.20±0.04

[a] $P_L = 1-P_M-P_D$, as explained in section 2.E.

TABLE 5.2

Physical properties affecting electron escape from spurs, and P_M, P_D and P_L values obtained for four pure liquids at 295 K.

Liquid	G_{gi}/G_t [a]	μ [b]	ε [c]	V_o [d]	P_M	P_D	P_L	Ref.
Neopentane	0.97	70	1.8	-0.39	0.18	0.55	0.27	This work
c-hexane	0.99	0.4	1.8	+0.01	0.20	0.69	0.11	[33]
Methanol	0.62	0.0006	33	NA	0.23	0.62	0.15	[42]
Water	0.38	0.002	78	NA	0.20	0.62	0.18	[33,42]

[a] Fraction of total radiation-produced electrons (G_t=4.5) which do not escape intraspur neutralization to become free ions.

[b] Mobility in $cm^2V^{-1}s^{-1}$ [103].

[c] Static dielectric constant.

[d] Conduction band energies of electrons in the liquid at 295 K.

ranging from c-hexane to water, with completely different polarity, solvating power, and spur electron survival probabilities, the muon yields are essentially the same. This leads one again [33] to conclude that the spur model of muonium formation does not account for the muon yields in different liquids. Instead, one inclines to the view that Mu formation might depend on the probability of hot Mu* emerging from the epithermal stages of the track without having undergone a hot atom abstraction or substitution reaction. Perhaps the probability of such hot atom reactions occurring relative to thermalization is very similar for all saturated molecules composed of fully hydrogenated C and O atoms.

A second major interest lies in the fact that the yields barely change at the liquid-solid phase transition, or with temperature over the range studied. For certain, there is no marked break in the yields at the melting point. As shown by Table 5.3, this is in sharp contrast to the results in water [43] and the noble gases Ar, Kr, and Xe [86] (only the Ar data is shown for comparison). Unlike neopentane, these other media show a complete absence of P_L in the solid phase, with P_M increasing noticeably as the material was solidified. Percival [44] proposed that P_L in water arises from the depolarization of Mu by some paramagnetic species in the muon's terminal spur. However, this cannot explain the results in Tables 5.2 and 5.3. An "expanding track model" was proposed by Walker [51] to account for P_L in non-polar as well as polar liquids. In this model, thermalized Mu is visualized to stop some distance (perhaps $\leq 10^2$ Å) beyond the last spur of the muon's track of ionization and excitation. However, as these paramagnetic and transient species diffuse

TABLE 5.3

The effect of phase (and temperature) on the various muon yields in neopentane, water and argon.

Medium	Phase	T/K	P_M	P_D	P_L	Ref.
neopentane	liquid	295	0.18	0.55	0.27	This work
neopentane	solid	209	0.19	0.61	0.20	This work
water	liquid	295	0.20	0.62	0.18	[43]
water	solid	272	0.52	0.48	0	[43]
argon	liquid	85	0.48	0.02	0.50	[86]
argon	solid	77	0.91	0.008	0.08	[86]

apart, their expanding track overlaps with Mu, which is diffusing randomly. Within ≃ 10 nsec, Mu then has a chance to react with these radiolysis products in the expanding muon track and results in a loss of Mu-amplitude. Since the majority of these species are hydrated electrons (e_{aq}^-) and OH radicals (OH·) in water, or free radicals in organic media, the track could have expanded to ~10^2 Å in 10^{-8} sec at which time their concentration will be ~10^{-3} M (calculated on diffusion coefficients of 5×10^{-5} cm^2s^{-1}). Since spin conversions have k_M~10^{10} $M^{-1}s^{-1}$ [30], this implies that there will be a reasonably large probability of reaction between Mu and these expanding track species within <10^{-7} sec. This explains P_L in liquids such as argon (Table 5.3) at 85K, since depolarization of Mu by these track species will cause a lowering of P_M and contribute to P_L. In solids, the diffusion should be sufficiently slow that the expanding track requires >10^{-5} sec to overlap with Mu, whose motion could also be suppressed at low temperatures or even be trapped in some sites of the solid matrix. So, within the MSR time scale, one can observe this P_L as P_M and therefore no missing fraction appears. In view of this expanding track model, one can now attempt to rationalize P_L observed in neopentane by assuming that the muon track still expands rapidly in the solid, and there may not be any trapping sites available for Mu. For neopentane, this is reasonable since its solid state is of a plastic nature. According to Livingstone et al. [104], neopentane behaves as a "liquid-like" crystal between -133 and -20°C. Indeed, the translational and vibrational motions of the liquid state are still retained to a large extent in the solid state form even at these low temperatures. For instance, light particles

such as Mu are expected to be just as mobile in solid neopentane as in the liquid phase since it was found that the electron mobility in plastic crystals of neopentane was approximately twice as large as that in the liquid [105]. This can explain the presence of P_L in solid neopentane and its absence in solid argon and ice based on the expanding track model.

A third point of interest in the above results is the value of λ_o obtained in neopentane (see Table 5.1). This indicates that neopentane has a λ_o-value close to the smallest found for any system at TRIUMF or SIN (see chapter 3). Indeed, it is the same as that found for water in chapter 3. As in section 3.A.2., considering a $\lambda_{\Delta H}$ contribution of 0.09×10^6 s^{-1}, λ_o for neopentane becomes

$$\lambda_o \leq 0.17 \times 10^6 \ s^{-1} \ . \qquad (5.1)$$

Using this value of λ_o, one obtains $k_M < 2 \times 10^4$ $M^{-1}s^{-1}$ for the abstraction reaction,

$$Mu + C(CH_3)_4 \longrightarrow MuH + C(CH_3)_3\dot{C}H_2 \ . \qquad (5.2)$$

By analogy, the corresponding H-atom reaction has a rate constant, k_H, of 1×10^6 $M^{-1}s^{-1}$ [106]. The smaller k_M value for Mu as compared to H was explained by the possible endothermicity of reaction (5.2) [107]. In contrast the corresponding H-atom is exothermic (~1 kJ $mole^{-1}$) [108]. This difference stems from the higher zero-point energy of Mu-bonds compared to H-bonds. However, if

one considers the Mu-FB as in chapter 3, one can probably conclude, as in the case of λ_o in water, that Mu does not react in neopentane and that the λ_o-value obtained is simply an experimental artifact due to physical phenomena in the aforementioned chapter. Similar magnetic field experiments to investigate λ_o in neopentane are being planned for future beam times at TRIUMF.

5.B. Muon yields in concentrated OH^- solutions.

It was noted by Percival et al. [43] that the reaction,

$$Mu + OH^-_{aq} \longrightarrow e^-_{aq} + MuOH \qquad (5.3)$$

has a rate constant at room temperature of 1.7×10^7 $M^{-1}s^{-1}$ (the kinetics of this reaction were investigated and will be discussed in chapter 6). This rate means that Mu in hydroxide solutions having pH greater than 12 will not be observable on the MSR timescale of about 10^{-6} sec. Also, as no Mu-radicals are produced in KOH/H_2O systems, the only yield at high pH is the diamagnetic fraction, P_D. This section will give results of muon yields at high OH^- concentrations which have bearing on the validity of both spur and hot models of muonium.

5.B.1. Results.

Experiments with the highly concentrated OH^- solutions were done at 80G at room temperature. Analar grade KOH pellets were dissolved in triply distilled deionized water. The concentrations of solutions were checked after

dilution by titration with a standard acid, potassium hydrogen phthalate. The mole, mass, and volume fractions were evaluated from the measured masses of KOH and H_2O used to make up the solutions. For these experiments, the solution was contained within two sheets of polyethylene (3 mil) in an otherwise regular teflon cell set-up (Figure 2.11a). The need for polyethylene was that 2-20 M KOH solutions react corrosively with mylar sheets. Surface muons were used for the investigation and the asymmetries were normalized (equation 2.11) against that of CCl_4 in the same sample holder. In the case of pure KOH, the cell was filled with KOH pellets, where only a minute fraction of the muons would come to rest in the walls of the vessel or in the gas phase. The presence of some carbonate in the surface layer of the pellets exposed to air could be a source of uncertainty in that measurement. The muon yields (P_D) were found to change with the mole/mass/volume fractions of KOH in the manner shown in Figure 5.2. P_D is seen to increase from 0.62 to 0.79 as the medium changed from pure water to ca 50% KOH. Solid KOH pellets gave a P_D reading of 0.55.

5.B.2. Discussion.

The A_D values that one observes in a μSR experiment can only arise from contributions to one's histograms if they correspond to muon frequencies (ω_D) precessing with coherent initial phases. For example, equation (2.15) describes the amplitude contribution to A(t) from all muons which are (i) initially placed in stable diamagnetic species (μ^+_{aq}, MuOH and MuH) during thermalization in the muon track and (ii) also those diamagnetic species formed

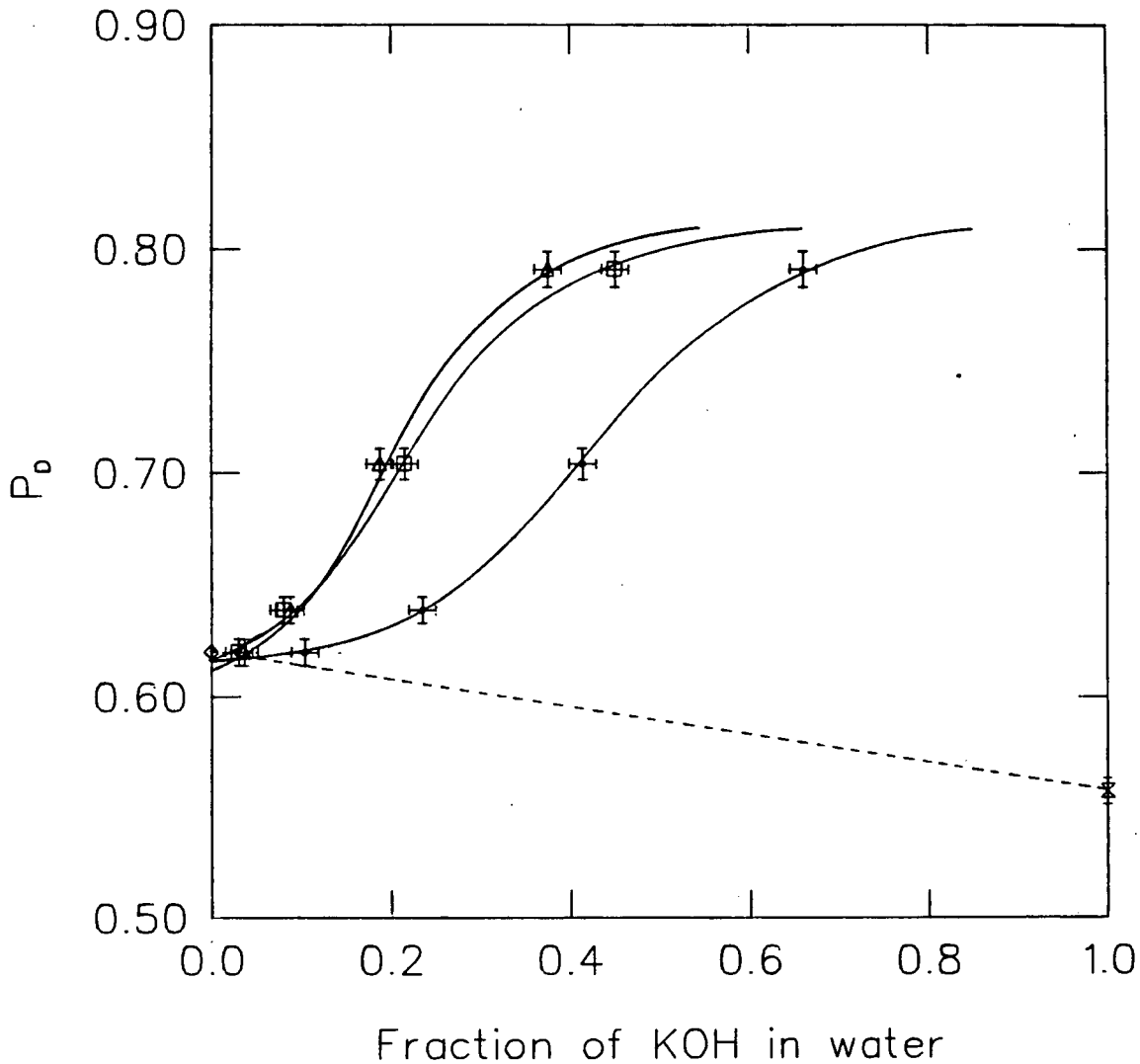

Figure 5.2: Variation of P_D with composition of KOH/H_2O solutions, plotted as mole (△), volume (□), and mass (●) fractions. The dashed line is the straight line connecting P_D in pure liquid H_2O with pure KOH pellets.

after thermalization - but only by reactions which are sufficiently fast to avoid dephasing by precession at another frequency (or depolarization due to magnetic interactions). Thus, for muons which initially appear as Mu atoms, they must be converted to diamagnetic species (such as MuOH) via chemical reaction with OH^- before dephasing or depolarization sets in, if they are to contribute to P_D at all. In the case of Mu atoms with parallel electron and muon spins (the so-called "triplets", ^TMu) coherence of the muon spin will be largely retained in the product if the reaction rate greatly exceeds the difference between the Mu and muon frequencies - which changes with magnetic field. For the "singlets" (^SMu), however, chemical conversion must precede depolarization of the muon spin by oscillations at the hyperfine frequency, ω_o [109]. This is independent of magnetic field below the "Paschen-Back" region (the region between $\omega_-(\sim\omega_e) \gtrsim \omega_o$ in Figure 2.5). In addition, Mu atoms can be "lost" (P_L) due to depolarization by encounters with radiation produced species during the non-homogeneous expansions of the terminal spur or of the entire track.

For reaction (5.3), since k_M is relatively small, all ^SMu will be depolarized by the hyperfine frequency (2.8×10^{10} s^{-1}) because it still greatly exceeds the value of $k_M[OH^-]$ even at 20 M (i.e. $k_M[OH^-] = 3.5\times10^8$ s^{-1}). However, at 80G, ^TMu depolarization ($\omega_M = 6.9\times10^8$ s^{-1}) covers the very time-scale over which reaction (5.3) proceeds. In fact, one can already predict qualitatively that P_D should increase in these concentrated KOH systems from "h" to a maximum of about [h+0.5(1-h)]: i.e. from 0.62 to 0.81, if h remains constant at 0.62. In this thesis, h represents the fraction of muons which

form stable diamagnetic species (before thermalization) via hot-atom abstraction or substitution reactions during collisional deexcitation following charge-exchange, or by thermalization as μ^+ ions. One must distinguish this use of h from h_D, which refers to a much latter point in time and was introduced to describe the yield of diamagnetic fractions emerging from the terminal spur in the spur model of Mu formation [43,52].

With regard to Mu formation, one has the following expectation. As the proton reaction [5.4],

$$H^+ + OH^- \longrightarrow H_2O \qquad (5.4)$$

is one of the fastest reactions known, with a rate constant of 1.4×10^{11} $M^{-1}s^{-1}$ [110], one would expect the analogous reaction of μ^+ with OH^- (5.5) to be far too fast for μ^+ to find an e^- in a

$$\mu^+ + OH^- \longrightarrow MuOH \qquad (5.5)$$

spur for Mu formation by thermal reaction. Therefore, one would expect that P_D for 2, 5, 10 or 20 M KOH all be 1.0 on the basis of the spur model. Similarly, it was noted previously be Walker et al. [48] that if the spur model should apply, then the observable Mu yield should have been reduced equally by μ^+ scavengers as by e^- scavengers, but no such reduction was found. As one can see from Figure 5.2, P_D does not approach 1.0 even at ~20M OH^-. This implies that the spur model does not apply for these systems.

We now continue the discussion of these results in terms of a hot model, one which describes h as the initial (hot) yield of diamagnetics and (1-h) as the initial yield of Mu. Various formalisms for the qualitative treatment of the exact time-dependence of muon polarizations have been given in references [4, 10, 16-18, 28]. Following Fleming et al. [28], the total muon polarization (Pres) extrapolated back to t=0 (the time at which Mu is formed) is given by equation (5.6),

$$\text{Pres} = \lim_{t\to\infty} P(t)\, \exp(-i\omega_D t) \tag{5.6}$$

where P(t) represents the time dependence of the entire muon ensemble including ^{T}Mu and ^{S}Mu converted to D. This P(t), of course, depends on the model of Mu reactions. In this chapter, the following model is proposed:

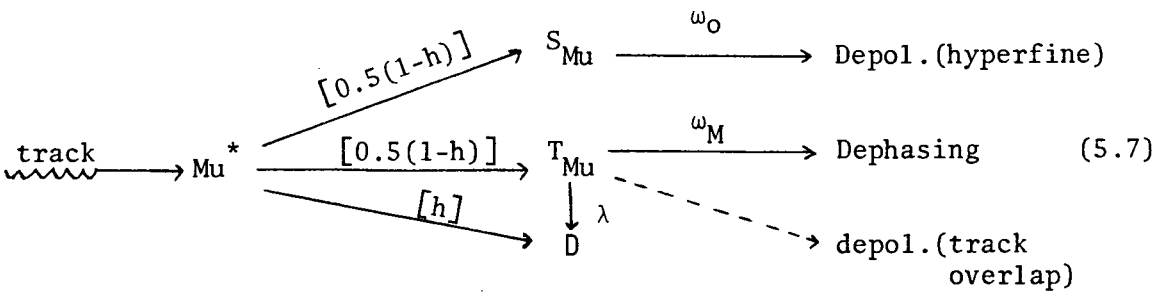

(5.7)

where Mu^* is a hot Mu atom and $\lambda = k_M[OH^-]$ for reaction (5.3). The dotted line represents depolarization of ^{T}Mu (P_L) via track overlap [51] and will not be included in the following derivation of P_D for reasons that will be explained later. Equation (5.7) is a single-step Mu reaction model (conversion of ^{T}Mu at 80G), since all ^{S}Mu will be depolarized through the hyperfine oscillations before reaction to D (as $\omega_o >> \lambda$), so that half of the Mu ensemble

is disregarded. By applying the complex muon polarization in free Mu-atoms at low fields (B<150G) [75], one obtains the total observable asymmetry as,

$$A_D(t) = A_D(o) + A_M(o) \int_o^t \lambda \cdot \exp - (\lambda + i\Delta\omega t')\, dt' \qquad (5.8)$$

where $\Delta\omega = \omega_D - \omega_M \simeq -\omega_M$. Integration of this equation to $t=\infty$ (since observation takes place long after the rapid motions of the μ^+ spin in Mu have settled down to the slow precession of the free μ^+-spin in a diamagnetic environment) for the ^{T}Mu ensemble, followed by normalization to fractional yields, gives equation (5.9). (See Appendix II).

$$P_D = h + 0.5(1-h)\, \{\lambda/(\lambda^2 + \omega_M^2)^{-\frac{1}{2}}\} \quad . \qquad (5.9)$$

Probably one would not expect h and k_M to be the same throughout the 0-20 M concentration range, but equation (5.9) is shown by the dashed line in Figure 5.3, calculated by keeping h=0.62 and $k_M = 1.7 \times 10^7\ M^{-1}s^{-1}$ for all concentrations. It can be seen very clearly that P_D calculated by equation (5.9) with h and k_M fixed does not correspond to the experimental values. There is a further channel by which ^{T}Mu may be lost (dashed line in equation (5.7)) represented by depolarization through intra-track encounteres of ^{T}Mu with paramagnetic species, as mentioned earlier. Such encounters are most important $\sim 10^{-8}$ sec after Mu formation, as the expanding track overlaps with Mu formed some 10 nm beyond it [51]. This extra decay mode will reduce P_D, but it is likely to compete with the conversion of Mu→D mainly in the lower portion of the concentration range. Therefore, this mode of Mu

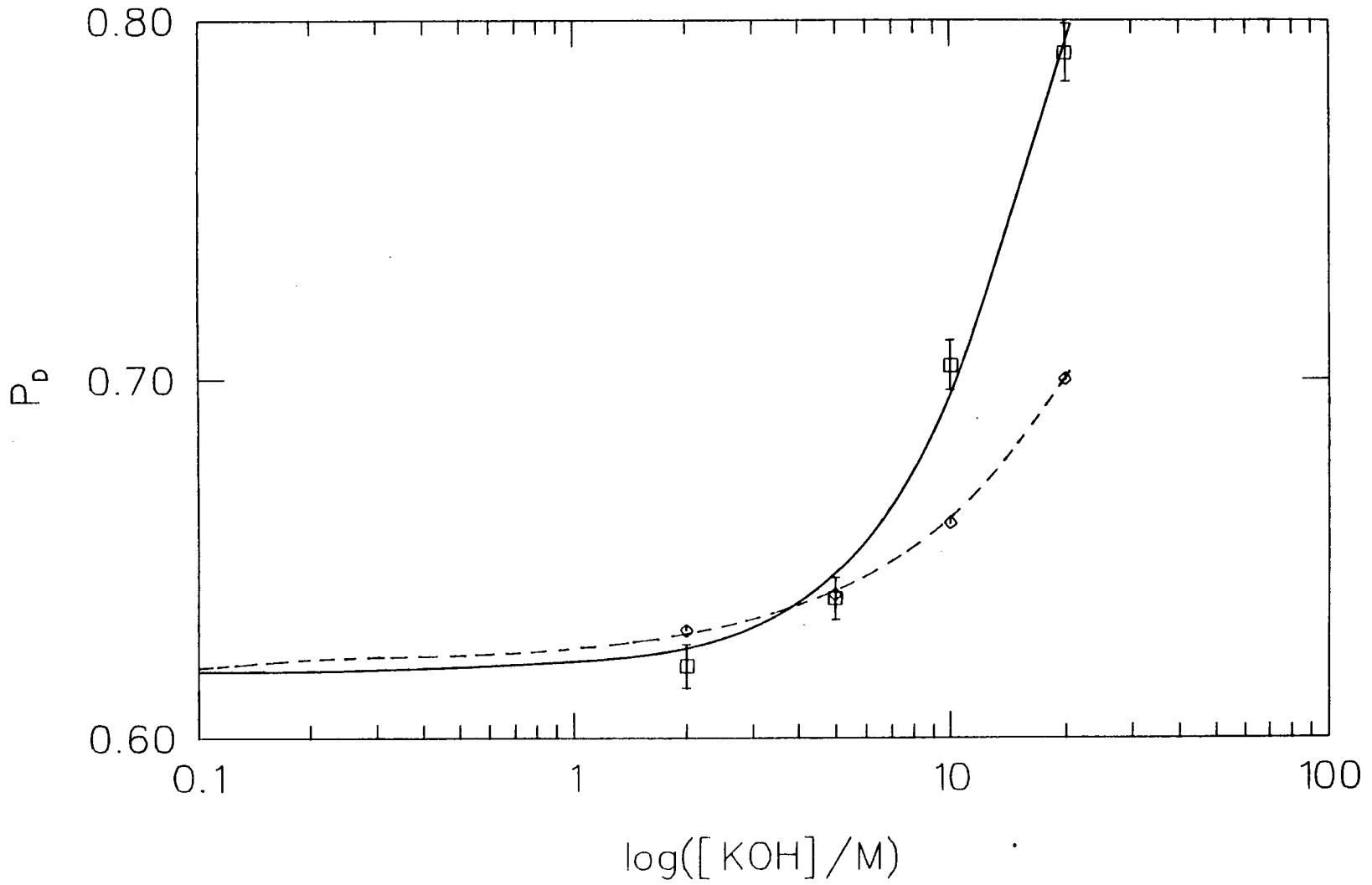

Figure 5.3: Plot of P_D against log [KOH]. The dashed line is calculated using equation (5.9) with h and k_M constant (see text). The solid line is that used to 'fit' to equation (5.9) with k_M or h variable - thereby giving the values in Table 5.4.

depolarization cannot account for the observed P_D being significantly larger than that calculated through equation (5.9) at the high concentrations.

However, it is interesting to note that if one allows the k_M value to change with $[OH^-]$ at greater than 1 M concentration, one finds that the data readily fit those of equation (5.9). A change of k_M at very high concentrations is expected in kinetic studies [111]. As shown by Table 5.4, in order for agreement between experimental and calculated P_D, k_M has to increase to about 7.0×10^7 $M^{-1}s^{-1}$ at 20 M KOH. This four-fold change in k_M is certainly not unreasonable for a solution in which the mass fraction of KOH reaches the 0.6 level. Alternatively, one could have obtained a good fit of the data to equation (5.9) if one allows h to change. The required variation of h with concentration is given also in Table 5.4. One would certainly expect h to change since the structural and chemical properties of water vary quite drastically when one third of its molecules are replaced by KOH. Therefore, by recognizing these factors at high concentrations, it is reasonable to conclude that the hot model given in equation (5.7) is not inconsistent with the observed enchancement in P_D.

5.C. Conclusion.

The muon yields in neopentane and concentrated aqueous KOH solutions point toward a general conclusion; that is, the findings seem to be at variance with the expections of a spur model of Mu formation.

TABLE 5.4

Variation of k_M or h required for equation (5.9) to fit the experimental P_D data.

$[OH^-]/M$	P_D (±0.01)	k_M' [a] $/10^7 M^{-1}s^{-1}$	h' [b]
0	0.62	1.7	0.62
2	0.62	1.7	0.61
5	0.64	1.7	0.62
10	0.70	3.3	0.66
20	0.79	7.0	0.73

Footnotes:

[a] k_M' are the values of k_M obtained by 'fitting' the experimental data to equation (5.9), by keeping h constant at 0.62 but allowing k_M to change with $[OH^-]$

[b] h' are the values of h (hot fractions) necessary to get the 'fitted' solid line if k_M is invariant at $1.7 \times 10^7 M^{-1}s^{-1}$.

CHAPTER 6

MUONIUM KINETICS IN AQUEOUS SOLUTIONS

In the M.Sc. thesis, the temperature dependence of various solutes reacting with Mu was investigated. It has been shown that Mu can undergo many types of reactions, such as abstraction, reduction, acid-base transfer, addition, substitution, and spin-conversion. With the establishment of a muon community at TRIUMF, many of these reactions involving water soluble inorganic and organic compounds were studied [3]. As mentioned in chapter 1, the comparison between Mu to H atom rate constants is an important step in understanding of kinetic isotope effects, quantum mechanical tunnelling and H atom reactions in general. In this chapter, two reactions will be discussed. Section A describes the acid-base reaction of Mu with hydroxide ion (OH^-_{aq}), while section B entails the Mu abstraction reaction with deuteroformate ions (DCO_2^-). Both of these will be compared to the HCO_2^- result from the M.Sc. work.

6.A. Muonium reaction with OH^-_{aq}.

In alkaline solutions, H atoms are converted into a species which reacts with scavengers in the same manner as radiation produced e^-_{aq} [112]. The reaction,

$$H + OH^-_{aq} \longrightarrow e^-_{aq} + H_2O \qquad (6.1)$$

was investigated by various groups [113, 114] in which it was identified as a proton transfer reaction. Also, it was used to evaluate the pK_a of the hydrogen atom [115] and it has some general interest since it demonstrated that

H and e^-_{aq} constituted a conjugate acid-base pair [116]. The rate constant (k_H) for equation (6.1) was determined by Neta et al. [117] as having a value of 1.5×10^7 $M^{-1}s^{-1}$. When compared to the analogous reaction for Mu,

$$Mu + OH^-_{aq} \longrightarrow e^-_{aq} + MuOH \; ; \qquad (6.2)$$

there was no kinetic isotope effect found [43, 87, 118]. This exact correspondence in rates therefore created an interest to study the temperature dependence of this "muon-transfer" reaction.

6.A.1. Results.

MSR measurements were carried out for four separate temperatures ranging from 1 to 84°C. Surface muons and the temperature cell (Figure 2.11b) were employed to extract k_M according to equation (2.16) using various values of $[OH^-]$, with the actual λ_o obtained in a separate experiment on pure water at that temperature (as λ_o changes slightly with temperature [71]). It should be noted that in Mu solution kinetics, since MSR measurements are accumulated over 4 muon lifetimes, solute concentrations must be chosen to bring λ^{-1} into the most accurate part of that range, namely ~1μsec. Figure 6.1 shows MSR histograms for λ_o and λ_M at 59°C for pure water and 0.01 M KOH, respectively. Table 6.1 gives the k_M's obtained for each of the four temperatures using different OH^- concentrations. These results are plotted (Figure 6.2) using the familiar Arrhenius expression (equation (2.17)) to obtain values of E_a and A, which are given in Table 6.2.

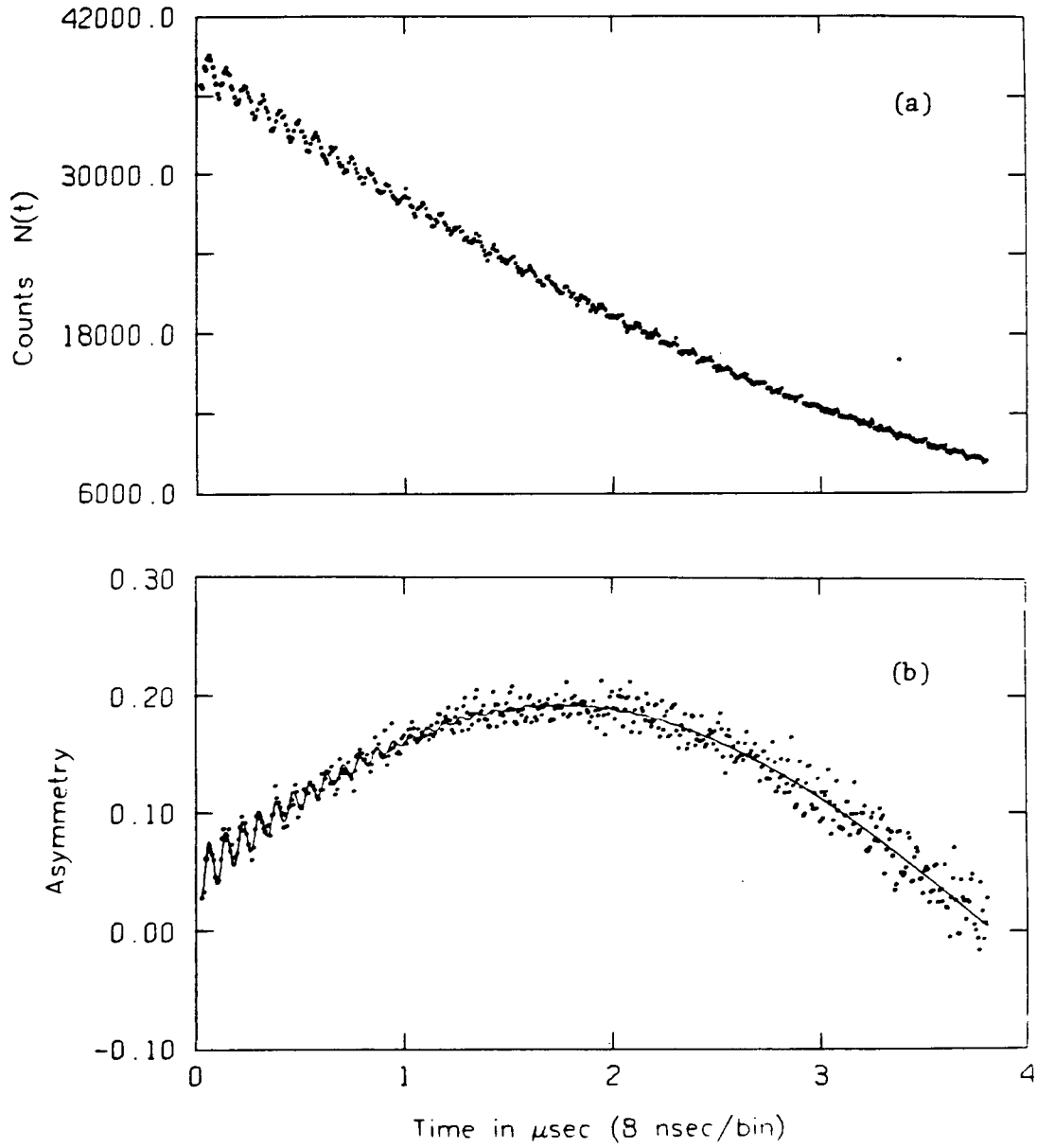

Figure 6.1: Typical MSR histograms showing the muonium signal at 8 gauss for (a) pure water at room temperature and (b) its decay at 0.01 M KOH at 59 C. The line drawn is the computer's best fit of the data points to equation (2.15).

TABLE 6.1

Second order rate constants (k_M) obtained from λ_M using equation (2.16) at various temperatures and OH^- concentrations.

$[OH^-]/10^{-3}M$	Temp/^oC	$\lambda_M/10^6 s^{-k}$	$k_M/M^{-1}s^{-1}$
1.60	84	0.97	3.8×10^8
7.49	59	1.62	1.7×10^8
49.9	22	1.15	1.7×10^7
82.5	1	0.93	7.8×10^6

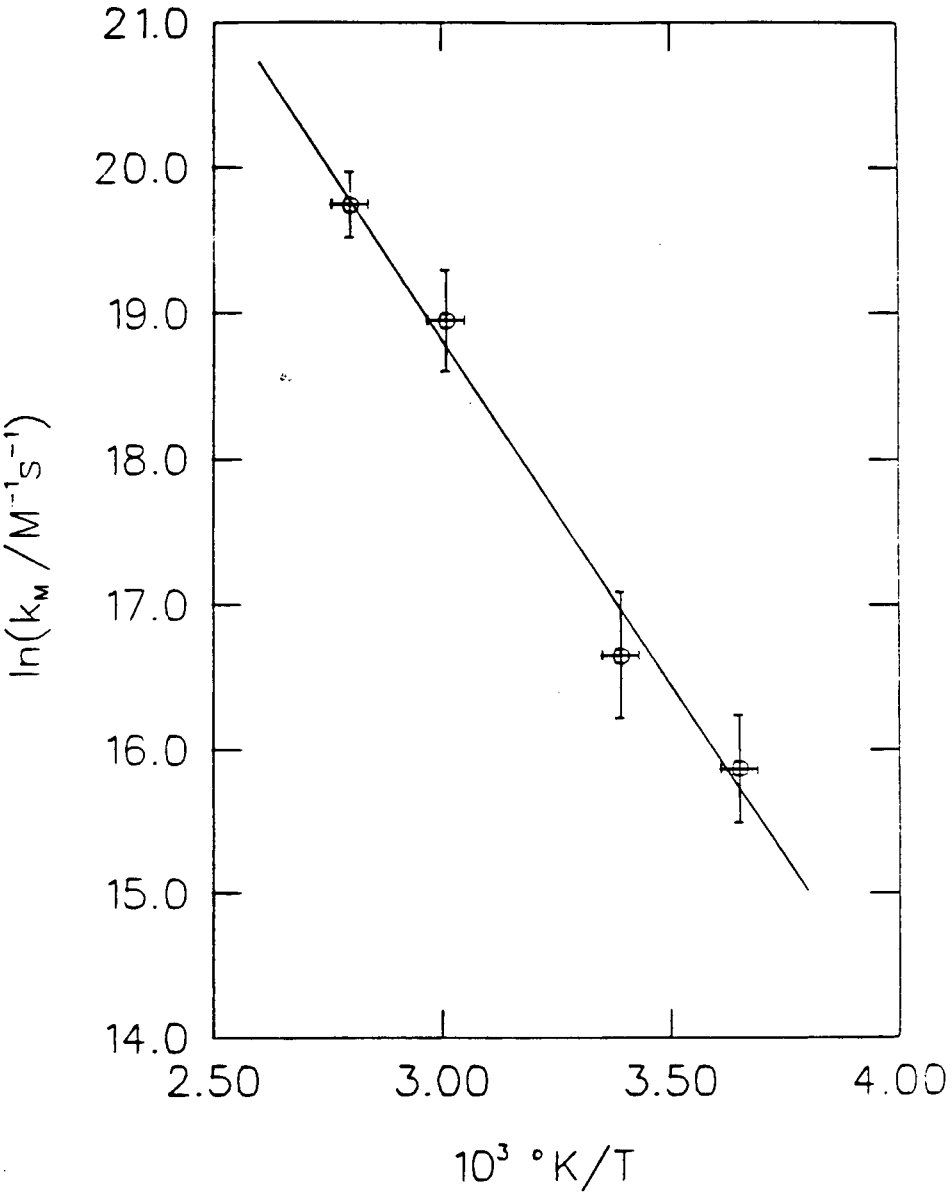

Figure 6.2: Arrhenius plot showing $\ln(k_M)$ versus T^{-1} for the $Mu+OH^-$ reaction.

TABLE 6.2

Arrhenius parameters obtained for k_M at ~ 295 K, and comparison with: (i) k_H [99], and (ii) reaction of Mu with HCO_2^- [70].

Reactant	$k_M/M^{-1}s^{-1}$	E_a/kJ mole^{-1}	$A/M^{-1}s^{-1}$	k_M/k_H
OH^-	1.7×10^7	40 ± 5	$(2.4\pm0.1)\times10^{14}$	1.1 ± 0.2
HCO_2^-	3.4×10^6	33 ± 2	4×10^{12}	0.01

6.A.2. Calculations and Discussion.

That there is no kinetic isotope effect (k_M/k_H) found for the OH^- reaction at room temperature (see Table 6.2), the only temperature where there is H data, agrees with the previous finding [43]. It suggests that the reaction mechanism is of the same type for Mu as for its H analogue (compare equation (6.1) and (6.2)), in which the net effect for Mu is the transference of a muon to the powerful base: muonium behaving as a "muonic acid".

The k_M value of 1.7×10^7 $M^{-1}s^{-1}$ at room temperature for the reaction of Mu with OH^- indicates that it is not a diffusion controlled reaction, since k_{diff} values of $\sim 2 \times 10^{10}$ $M^{-1}s^{-1}$ are usually found [3,99]. Certainly, the observed activation energy of 40 kJ $mole^{-1}$ (Table 6.2) reflects that the reaction greatly exceeds the E_a for diffusion of species in water, which is generally about 17 kJ $mole^{-1}$ [54,70]. Further, for diffusion controlled reactions, a plot of k_M/T against the inverse of viscosity should yield a straight line (see Smoluchowski's equation (1.10) in section 1.C.1.). This arises since k_M should be proportional to the relative diffusion constants, which in turn would show the temperature dependence of the viscosity [123,120]. Table 6.3 gives the viscosity (η) as a function of k_M/T, and as one can see from Figure 6.3, the plot of k_M/T versus $1/\eta$ does not yield a straight line. This corroborates the fact that the Mu reaction with OH^-_{aq} is not diffusion controlled. Instead, it is presumably activation controlled, as evident by the large activation energy obtained.

Following equation (1.1) in section 1.C.1., it is convenient to construct the following reaction scheme:

TABLE 6.3

Viscosity parameters as a function of temperatures for the reaction of Mu with OH^-_{aq}.

$T/^oC$	$(k_M/T)/M^{-1}s^{-1}K^{-1}$	$(1/\eta)^{\dagger}/10^{-2}$ poises
84	1.05×10^6	2.96
59	5.12×10^5	2.11
22	5.76×10^4	1.05
1	2.84×10^4	0.58

† η is the viscosity, obtained from reference [119].

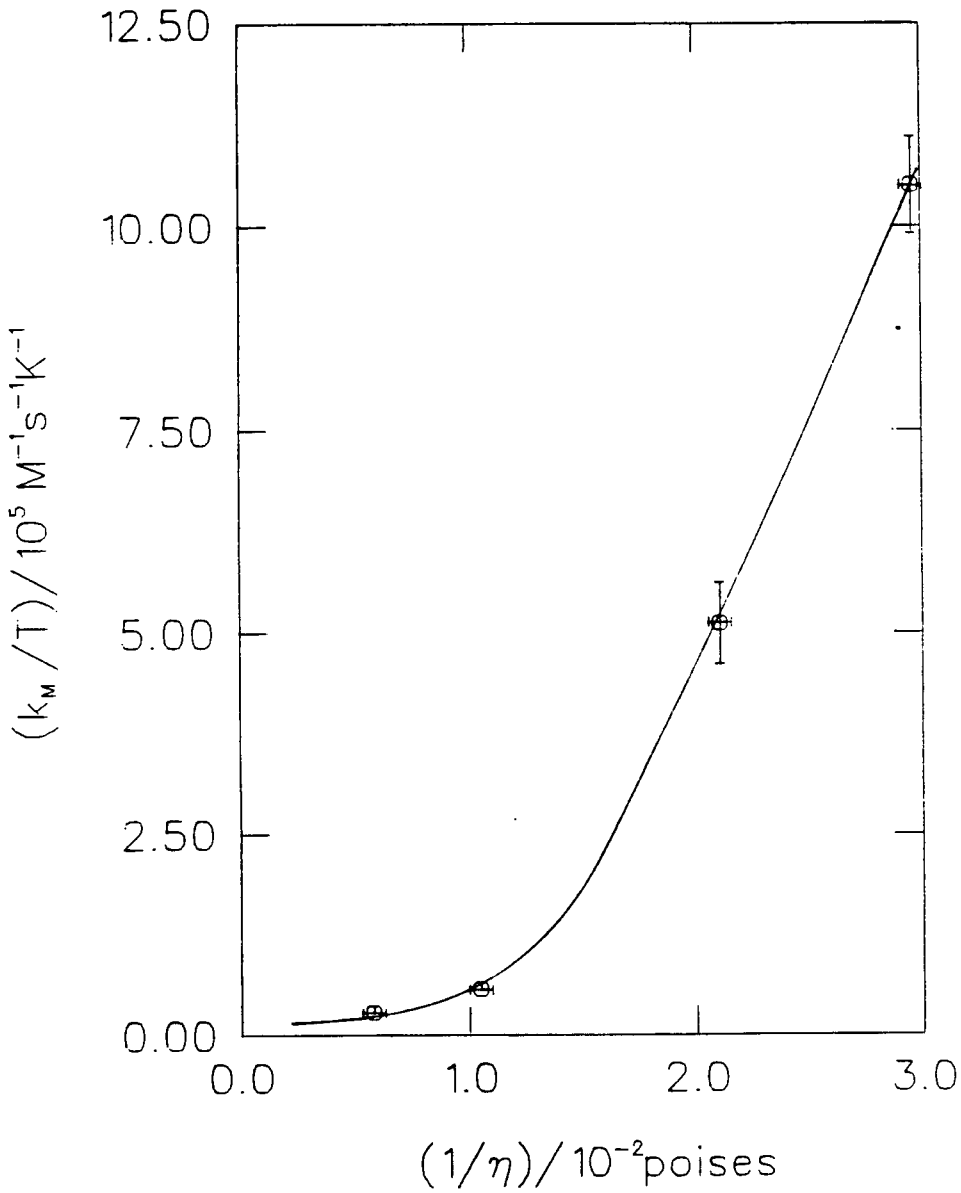

Figure 6.3: Plot of k_M/T versus the inverse of the viscosity for the $Mu+OH^-$ reaction.

$$Mu + OH^- \underset{k_b}{\overset{k_d}{\rightleftharpoons}} [Mu \ldots OH^-] \xrightarrow{k_p} MuOH + e^-_{aq} \qquad (6.3)$$

to describe bimolecular reactions in solution. The rate constants (k_d, k_p & k_b) are as described previously (see section 1.C.1.). In this case, the encounter-pair is the $[Mu...OH^-]$ complex formed by the diffusion of the two reacting species and caged momentarily by the solvent. Applying the steady state approximation to this encounter-pair, one obtains, as in equation (1.5), k_M equalling the composite of three parameters, $k_p k_d/(k_b+k_p)$. Since the OH^- reaction is $<< k_{diff}$, $k_b >> k_p$ (encounters seldom leading to reaction), one obtains $k_M \simeq k_p k_d/k_b$. Thus, the observed Arrhenius parameters may also be expected to be composites of: $A = A_p A_d/A_b$ and $E_a = E_p+E_d-E_b$. If one considers the establishment of the encounter-pair as equivalent to a pseudo-equilibrium controlled mainly by diffusive processes, then E_d and E_b should be small, and in any event comparable to each other in magnitude. In effect, E_a approximates E_p, the activation barrier of the slow rate-controlling step.

With these considerations pertaining to reaction (6.2), one sees that the muon-transfer step is characterized by an E_a of 40 kJ $mole^{-1}$. However, the unusually large value of A found (see Table 6.2), being a composite of $A_p A_d/A_b$, perhaps reflects the unique association of OH^- with the water structure. It is unfortunate that the Arrhenius parameters for the analogous H atom reaction (6.1) do not seem to be available for comparison. Instead, it is of interest to compare this $Mu+OH^-$ reaction with that of the $Mu+HCO_2^-$ reaction as given in Table 6.2. Here both E_a and A are smaller than with OH^- and there is a large (inverse) isotope effect. Towards formate, Mu is expected to

abstract the H atom - a reaction type in which H is generally much more efficient [3]. Indeed, one would not expect formate to be a sufficiently strong base to force Mu to undergo an acid-base transfer as in reaction (6.2).

6.B. Muonium abstraction with DCO_2^-.

In the M.Sc. thesis, the HCO_2^- reaction was studied as a function of temperature. For comparison, the DCO_2^- abstraction reaction will be described in this section. With these results, not only can one compare the isotope effect in which the isotope is the attacking species, but also the primary isotope effect in which the isotope is the atom to be transferred (abstracted). Abstraction reactions by hydrogen atoms have been well studied over the years. Indeed, Anbar et al. [121] have investigated H-D isotope effects on hydrogen abstraction by H atoms from 2-propanol, formate, methanol, and acetate. They concluded that the H-D isotope effect may be correlated with the reactivity of the given compound toward hydrogen abstraction by H atoms and speculated about the contribution of a tunnelling effect for these reactions. Now with Mu, tunnelling could be even more manifest due to the smaller mass. Therefore, a temperature-dependence study of $Mu+DCO_2^-$ can contribute towards further understanding of isotope effects in solution kinetics.

6.B.1. Results.

Surface muons were again used together with the temperature cell for these measurements. All DCO_2^- solutions were obtained by titration of formic-acid-d_2 (98 atom% D) with NaOH of known concentration, until the pH was about 7.

Table 6.4 and Figure 6.4 display the values of λ_M obtained for different concentrations of DCO_2^- at 80°C. The slope of the line gives k_M in accordance with equation (2.16). Values of k_M obtained in this way for the different temperatures are given in Table 6.5. These are then plotted in accordance with the usual Arrhenius treatment (Figure 6.5) to yield: $E_a = (39.0 \pm 3.2)$ kJ mole^{-1} and $A = (1.1 \pm 0.2) \times 10^{13}$ $M^{-1}s^{-1}$.

6.B.2. Discussion.

As with the OH^- reaction, the activation barrier for the DCO_2^- reaction is fairly large. By comparing it to the analogous H atom reactions, the mechanism is presumed to be the abstraction of deuterium from DCO_2^-.

$$Mu + DCO_2^- \longrightarrow MuD + CO_2^- . \qquad (6.4)$$

With such a low k_M (~1×10^6 $M^{-1}s^{-1}$) at room temperature, one expects this reaction to be activation controlled. Indeed, a plot of k_M/T versus $1/\eta$ (see previous section) gives a non-linear curve signifying that the reaction is not diffusion controlled.

Compared to the reaction of Mu abstracting H from HCO_2^- [70] (see Table 6.6), reaction (6.4) is expected to have a smaller k_M than HCO_2^- due to its larger E_a (39 kJ mole^{-1}). This can be qualitatively understood in terms of the height of a vibrationally adiabatic transition-state-theory barrier [70]. Table 6.6 shows that as the ratio of masses of abstracting/abstracted atom decreases, zero-point energy changes in the reactants and

TABLE 6.4

Muonium decay rate constants (λ_M) as a function of DCO_2^- concentration at 80°C.

$[DCO_2^-]/10^{-3}$ M	$\lambda_M/10^6 s^{-1}$
0.0 ± 0.0	0.36 ± 0.01
44.5 ± 1.0	1.80 ± 0.64
62.2 ± 1.0	1.30 ± 0.30
88.9 ± 1.0	2.13 ± 0.52

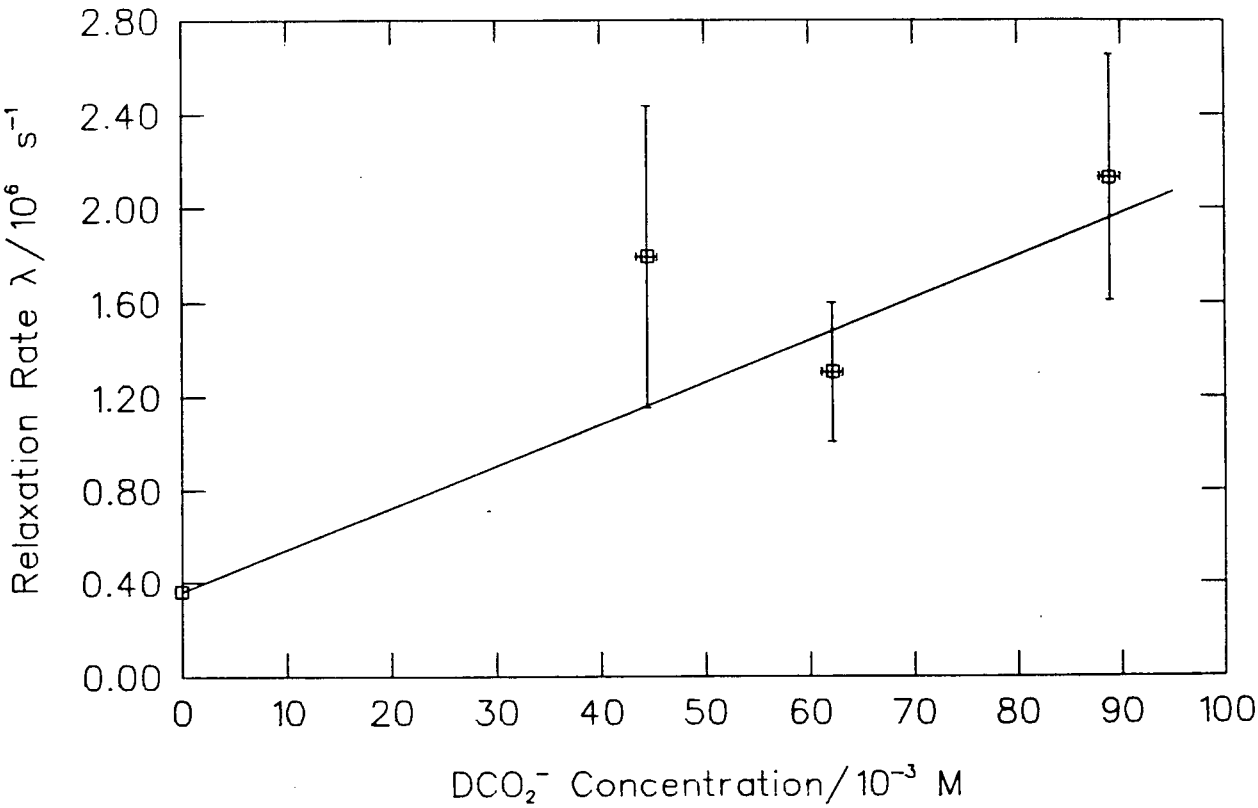

Figure 6.4: Plot of λ_M versus DCO_2^- concentration at 80 C.

TABLE 6.5

Second order rate constants (k_M) obtained from λ_M using equation (2.16) at four temperatures for the Mu + DCO_2^- reaction.

Temp/^oC	$k_M/M^{-1}s^{-1}$
1	$(4.3 \pm 0.8) \times 10^5$
22	$(9.9 \pm 2.3) \times 10^5$
60	$(8.5 \pm 0.8) \times 10^6$
80	$(1.8 \pm 0.3) \times 10^7$

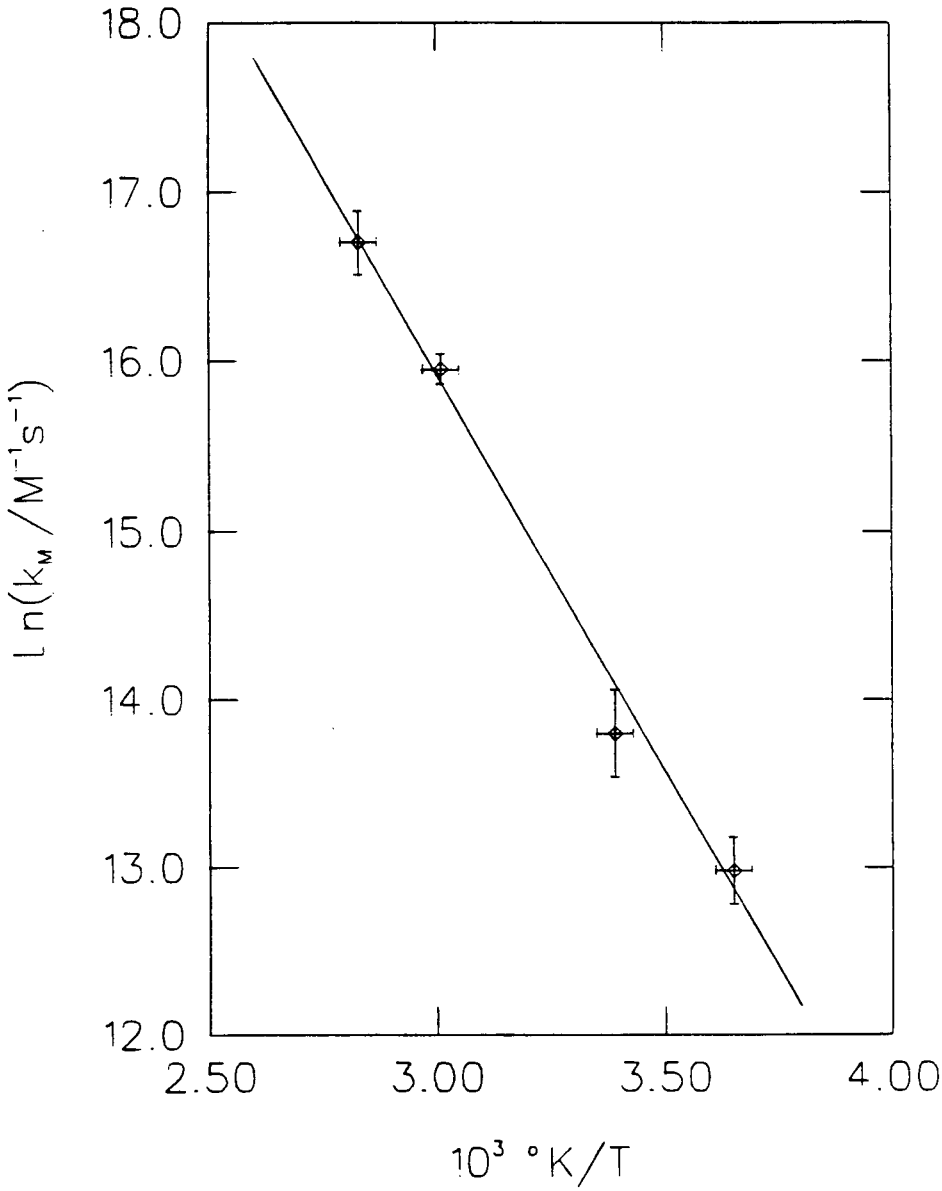

Figure 6.5: Arrhenius plot of the Mu+DCO_2^- reaction.

TABLE 6.6

Comparative kinetic parameters for various abstraction reactions.

Reaction	$^{\#}k/M^{-1}s^{-1}$	$m_1/m_2^{\dagger}$	k_M/k_H	k_H'/k_D'	E_a/kJ mole^{-1}	$A/M^{-1}s^{-1}$
$H + HCO_2^-$	1.2×10^8	1.00		5.2		
$H + DCO_2^-$	2.3×10^7	0.50				
$Mu + HCO_2^-$	3.4×10^6	0.11	0.03	3.4	33.4 ± 2.3	$(4.1\pm0.2)\times10^{12}$
$Mu + DCO_2^-$	9.9×10^5	0.056	0.04		39.0 ± 3.2	$(1.1\pm0.1)\times10^{13}$

† m_1 is the mass of the attacking atom (Mu or H) and m_2 is the mass of the abstracted atom (H or D).

\# k are the room temperature values, the H-atom values are from reference [99].

transition-states effectively cause a higher barrier, in line with the observed trend in reaction rates. However, it should be noted that (as pointed out in the M.Sc. thesis and reference [70]) the order of reaction rate is also the order of decreasing endothermicity. The trend in rates indicates that the probability of a light atom abstracting a heavier one is smaller than that of an atom abstracting an equivalent sized atom. The trend follows ones expectations based on simple mechanics of collisions.

Table 6.6 demonstrates two separate isotope effects. k_H'/k_D' refers to the case when the atom being abstracted is different, while k_M/k_H is for the case when the attacking atom is different. The trend for these two isotope effects are in opposite directions (e.g. $k_M/k_H < 1$, and $k_H'/k_D' > 1$). In the case of k_M/k_H, Roduner and Fischer [122] have concluded that this reverse isotope effect is due to quantum mechanical tunnelling in the abstraction reaction. However, it was argued [70] that such a tunnelling effect should also decrease the A-factor (as in NO_3^- [70]) and lower the observed activation energy. In the case of k_H'/k_D', smallish isotope effects (5.2 & 3.4) were obtained for the H and Mu abstractions from HCO_2^- and DCO_2^-. As mentioned in section 1.C.3., quantum mechanical tunnelling should give rise to curvature in Arrhenius plots, apparent decrease of A-factors (due to small E_a's), and large kinetic isotope effects. That none of these effects are apparent for the HCO_2^- and DCO_2^- implies tunnelling does not dominate the abstraction of H and D atoms in HCO_2^- and DCO_2^- by either H or Mu.

It is unfortunate that water has such a short liquid range in which to study isotope effects with solutes. This limitation could prevent the detection

of manifestations of quantum mechanical tunnelling. Perhaps this reflects the need to use non-polar media, such as hydrocarbons, some of which have much larger liquid ranges, to investigate kinetic isotope effects of Mu with various solutes.

CHAPTER 7

COLLABORATIVE WORKS

All projects up to and including chapter 6 are experiments of my own undertaking. In the present chapter, however, various other projects will be briefly reviewed which are investigations done in collaboration with Dr. Y. Ito & Mr. Y. Miyake (hydrocarbons), Dr. Y.C. Jean (model biological systems & solvent mixtures), and Dr. J.M. Stadlbauer (Mu kinetics of solutes in aqueous solutions). All of this work has now been published in various journals [33,34,36,38,39,40,41,49,74,93,123]. These projects were collaborative in the sense that the aforementioned research-associates were major investigators. Due to the nature of the TRIUMF beam-time system - one in which each group of experimenters is given on average one week of experimental time every 4 months - all projects must be done in close collaboration, with many people involved. The brief description of these projects reflects my relatively minor role in them.

7.A. MSR applications to model biological systems.

As mentioned in chapter 1, the MSR technique is being applied to study the chemical interactions of Mu atoms with some model biologically-important systems. For the M.Sc. thesis [71], the reaction of Mu with porphyrins (hemin and protoporphyrin [37]) was found to consist of a peripheral site attack at the π-system and of the central ion. The mechanisms were mainly through addition to the conjugated double bonds for the protoporphyrin and by reduction or partial spin conversion processes for the hemin solutions. For this Ph.D. thesis, other systems are being reported, namely micelles [39] and cyclodextrins [38]. An advantage of this MSR technique over some other

conventional techniques in biological studies is that it is a non-destructive method. Furthermore, since H atoms are involved in many fundamental biological processes, such as charge transfer, proton transfer, hydrogen bonding, etc; it follows that Mu atoms are ideal probes with which to study these complicated systems. Consequently, Mu can act as a direct probe inside giant molecules and extract information about the site of electron transfer and spin state of metallic ions. The first indication of this potential with Mu as a probe in biological application was revealed when Mu was used as a test of the spin state of transition metal ions in simple inorganic complexes in solution [30]. Perhaps the results given in this chapter will stimulate the biochemists' and biophysicists' interest in utilizing MSR as a means to study chemical dynamics in biological systems.

7.A.1. Muonium reactivity in cyclodextrins.

Cyclodextrins are doughnut-shaped molecules, formed by linking several units of D(+) glucose together in a ring. In this experiment, α and β-cyclodextrins were used. These are composed of six and seven glucose units, respectively. Each has a molecular diameter of 8 to 9 Å with central cavity radii of 5 and 7 Å. In aqueous solutions, they can support two distinct environments - the internal hydrophobic face along the central void and the external hydrophilic face on the sheath surface and beyond. They are well known for their ability to host various kinds of guest molecules, creating inclusion compounds that are important for catalysis or inhibition in many chemical and biological reactions, and also as models of enzyme active sites [124].

Surface muons were used for the MSR experiments. Chemicals were bought from the Aldrich Chemical Co. (highest purity) and were used without further purification. All samples were prepared fresh before experiment; in particular, iodine crystals were sublimed from analytical-grade reagents. The Mu rate constants (k_M) with I_2 and I_3^- (I_2+KI) in various solutions are shown in Table 7.1. By comparing to the analogous H atom reaction [99], the reactions in all media are presumed to be,

$$Mu + I_2 \longrightarrow MuI + I \quad (\text{or } \mu^+ + I_2^-) \qquad (7.1a)$$

and

$$Mu + I_3^- \longrightarrow \mu^+ + I^- + I_2^- \quad . \qquad (7.1b)$$

From Table 7.1, one can see that there is a tremendous increase of k_M (Mu + I_2) as the medium is made more hydrophobic (i.e. in the sequence water → methanol → n-hexane). However, when the I_2 is inside the hydrophobic enclosure of the cyclodextrin the value of k_M is almost unchanged from that of water. In fact, it is slightly reduced although not much beyond the given error bars. For the I_3^- reaction, there is a two- or three-fold decrease in k_M. Notice that Mu does not react significantly with either cyclodextrins or I^-.

The fact that Mu reacts faster with I_3^- than with I_2^- may be due to the larger size of I_3^-, particularly when one considers its coordination shell. This is expected since both reactions have k_M's corresponding to diffusion controlled rates [43]. The decrease of k_M when these are incorporated as

TABLE 7.1

Muonium reaction rate constants (k_M) with I_2 and I_3^- in various solutions at 295 K.

Solution ($[I_2]$ = 0.088 mM)	$k_M/10^{10} M^{-1} s^{-1}$
I_2 in water	1.7 ± 0.3
I_2 in methanol	16 ± 6
I_2 in n-hexane	29 ± 10
I_2 + α-cyclodextrin (1 mM) in water	1.2 ± 0.3
I_2 + β-cyclodextrin (2 mM) in water	1.4 ± 0.3
I_2 + I^- (0.16 mM) in water	5.9 ± 1.2
I_2 + I^- (0.2 mM) + α-cyclodextrin (1 mM) in water	2.5 ± 0.5
I_2 + I^- (0.2 mM) + β-cyclodextrin (2 mM) in water	2.1 ± 0.5
α- or β-cyclodextrin in water	~0.002
I^- in water	0.007 ± 0.001

guest molecules in cyclodextrins seems to reflect the shielding effect of the solute from encounters with Mu. It may also imply that there are significant van der Waals forces present between the guest (I_2 and I_3^-) and host molecules which causes the reduction in k_M. In any case, the cyclodextrin encasement does not seem to transmit Mu as if it were an active membrane-like enclosure. This is evident from the fact that I_2 in the presence of a hydrocarbon medium reacts extremely fast with Mu relative to that of water, and since the inside of the cyclodextrins have a hydrophobic environment, one could have expected an increase in rate. Although it is too early at this stage to extract formation constants from these data as in the case of positronium studies [125], one can at least conclude from these results that reactions are curtailed to a certain extent in these macromolecular sugar systems.

7.A.2. Muonium reactivity in micelles.

Micelles are formed by aggregation of surfactant molecules in aqueous solutions. These aqueous micellar systems contain two distinct environments, an internal hydrocarbon-like core and an external water-like shell. The importance of these systems has been recognized in many biological and industrial applications [126]. They can be used as the simplest models with which to investigate mechanisms of bio-membranes and energy storage and conversion media.

In these experiments, sodium octyl sulphate (NaOSA) was used above its critical micelle concentration (CMC) to provide a large (~50 monomer units)

internal hydrocarbon environment and negatively charged hydrophilic outer surface. Five solutes were chosen for the study, two of which (Ni^{2+}, $Fe(CN)_6^{3-}$) will be dissolved in the outer surface of the micelles and the others (I_2, phenol, and naphthalene) are much more soluble in hydrocarbon media than in water, so they should have been present only within a micelle. The values of k_M were determined for these solutes in pure water, in water containing NaOSA below its CMC, and in water containing an excess of micelles (above CMC). k_M was measured for the reaction between Mu and NaOSA when a value of 2×10^6 $M^{-1}s^{-1}$ was found; this is a negligible rate and cannot significantly contribute to k_M in these experiments. In fact, λ_o for equation (2.16) was taken to be the observed λ in the micelle solution in the absence of any solutes. The Mu reaction rate constants with these solutes in water, an organic solvent, and in NaOSA micellar aqueous solutions are given in Table 7.2.

For Ni^{2+} and $Fe(CN)_6^{3-}$, there was no observable change in k_M before and after CMC. This is expected since these two solutes are dissolved in the bulk aqueous medium, or the Guoy-Chapman region of the micelle. However, in the case of I_2 and phenol, a substantial increase (about two-fold) was found for k_M above CMC, and for naphthalene an increase of k_M by a factor of 6 was found above CMC. By comparing with data of H atom and positronium, the reactions of Mu with I_2 and phenol are at the diffusion controlled limit, whereas naphthalene is not. Perhaps the increase of k_M above CMC is due to a caging effect for these three solutes, and since k_M for naphthalene is in an activation controlled region, the observed increase can be greater for this solute than for I_2 or phenol.

TABLE 7.2

Reaction rate constants $k_M/10^{10}$ $M^{-1}s^{-1}$ of muonium in water, an organic solvent, and in NaSOA[a] micellar aqueous solutions, at 295 K.

Solute[b]	k_M (in water)	k_M (in CH_3OH or hexane)[e]	k_M[c] (below CMC)	k_M[d] (above CMC)	$\frac{k_M(\text{above})}{k_M(\text{below})}$
I_2	1.7 ± 0.3	16 ± 6	1.8 ± 0.3	4.1 ± 1.0	2.3
Phenol	0.8 ± 0.3	3.3 ± 1.0	0.9 ± 0.3	1.4 ± 0.3	1.5
Ni^{2+}	1.7 ± 0.3	...	1.5 ± 0.3	1.4 ± 0.3	1.0
$Fe(CN)_6^{3-}$	2.0 ± 0.5	...	2.2 ± 0.4	2.0 ± 0.4	1.0
Naphthalene	0.13 ± 0.03	13 ± 2	0.13 ± 0.03	0.80 ± 0.05	6.0

[a] NaOSA is sodium octyl sulphate, whose critical micelle concentration is 0.14 M. Naphthalene data refers to sodium dodecyl sulphate (NaLS).

[b] Solute concentrations were ~10^{-4} M.

[c] k_M measured in 0.05 M NaOSA aqueous solutions, except for naphthalene, where [NaLS] = 0.003 M.

[d] k_M measured in 0.19 M NaOSA aqueous solutions, except for naphthalene, where [NaLS] = 0.016 M.

[e] Hexane for naphthalene, methanol for I_2 and phenol.

However, the observed increase above CMC is not as large as that obtained in a pure hydrocarbon solvent (column 2 in Table 7.1). This means that the inner micellar core is of a sufficiently ordered nature such that it resembles a solid or very viscous environment [127], where reactions should be slower than that in a fluid hydrocarbon medium. A further important observation is that k_M is not decreased by enclosure of the solute in a micelle. Although the micelle is a thick sheath, it does not seem to impede Mu from reaching the solute in the micellar core. By analogy, this is similar to the efficient transmission of H atoms in radiobiological systems containing membranes of this type of composition. These results demonstrate the usefulness of Mu as a non-destructive and sensitive probe in large macromolecular and biological systems.

7.B. Studies with hydrocarbons.

Muon and muonium have been studied more extensively in water than in hydrocarbons. One difficulty with hydrocarbons lies in the reproducibility of purity in the sample. At times many attempts must be made before success can be realized for an experiment. This is especially relevant to MSR studies in these non-polar media. However, since the discovery of Mu atoms in various liquid hydrocarbons by Ito et al. [33], many successful experiments [34,35,49,74,107] have been carried out in collaboration by groups from TRIUMF and KEK. The μSR and MSR results of these works will be highlighted in this section with the emphasis on their implication for the model of Mu formation in condensed media.

7.B.1. Yields in liquid hydrocarbons.

There are many interests in liquid hydrocarbons. By extrapolating the values of P_M, P_D, and λ_o, intrinsic properties and mode of formation of Mu can be investigated and compared for non-polar and polar media. Also, there is particular relevance to the studies of biologically important materials such as micelles and cyclodextrins, as already alluded to.

The samples of hydrocarbons were all purified as described in chapter 2. The results are summarized in Tables 7.3 and 7.4. During the course of these experiments several samples of each liquid were studied following different purification procedures and with different rates of bubbling by helium gas in the target cells. It was clear that effects of both organic impurities (probably carbonyl compounds and unsaturated hydrocarbons) and residual O_2

TABLE 7.3

Results obtained for P_D, P_M, P_L and λ in n-hexane, c-hexane, tetramethylsilane (TMS), methanol, and water[a,b].

Liquid	P_D	P_M	P_L	$\lambda_o/10^6$ s^{-1}
n-Hexane	0.65 ± 0.02	0.13 ± 0.02	0.22 ± 0.04	1.0 ± 0.5
c-Hexane	0.69 ± 0.02	0.20 ± 0.02	0.11 ± 0.04	1.5 ± 0.4
TMS	0.53 ± 0.03	0.21 ± 0.02	0.26 ± 0.04	0.64 ± 0.07
Methanol	0.62 ± 0.01	0.23 ± 0.02	0.15 ± 0.02	2.3 ± 0.4 (0.74)[c]
d	(0.61)	(0.19)	(0.20)	(0.75)
Water	0.62 ± 0.01	0.20 ± 0.01	0.18 ± 0.01	0.25 ± 0.08
d	(0.62)	(0.19)	(0.19)	(0.25)

[a] P_D, P_M and P_L are the fractions of incident muons which are observed as diamagnetic species, free muonium atoms, or as neither of these ($P_L = 1 - P_D - P_M$), respectively. λ is the observed muonium spin relaxation rate constant.

[b] The values quoted are the mean of the values obtained independently from the left- and right-hand detectors. The error limits given cover the two values and each of their statistical errors only.

[c] Calculated for neat methanol from 20% methanol in water from Table 7.4.

[d] Mean values of the data published previously in refs. [24, 29, 42, 43].

TABLE 7.4

Results obtained for λ in solutions (plus parameters calculated therefrom).

Composition	λ/s^{-1}	λ_o(solvent)/s^{-1}	$k_M/M^{-1}s^{-1}$	Calculated λ_o(solute)/s^{-1}
20% (vol) methanol in water	5.1×10^5	3.6×10^5 [a]	3×10^4	0.74×10^6
1.9×10^{-4} M phenol in n-hexane	2.3×10^6	1.0×10^6	$7(\pm 2) \times 10^9$	--

[a] λ_o in the sample of water used was considerably larger than is normal in pure water.

contribute to the λ observed in all cases. It is especially important to bubble well since O_2 is about 100-times more soluble in hydrocarbons than in water. In general, λ usually decreased somewhat when the gas bubbling rate was increased. Therefore, it should be emphasized that the results presented here correspond to the longest-lived Mu signals obtained in each liquid. However, this effect of O_2 did not affect P_M or P_D. Also, once the Mu decay constant λ_o has been determined for a neat solvent, it was then used to make up solutions containing a solute to determine k_M (i.e. phenol in n-hexane in Table 7.4).

There are two points of interests from these results. The first involves the intrinsic Mu reactivity in these solvents (i.e. λ_o). It can be seen from Table 7.3 that none of the non-polar media has smaller λ than that of water (though neopentane now equals it). Perhaps this suggests (neglecting O_2 and impurity effects) that these λ's arises from a hydrogen abstraction reaction by Mu. Even considering these effects, the reported λ's for these non-polar media increase systematically in the series TMS/n-hexane/c-hexane, as the $-CH_3$ groups are replaced by $>CH_2$ groups. This trend is to be expected if these λ's arises from an H-abstraction reaction with Mu since the C-H bond strength of methylene is slightly less than that of methyl. In addition, the reactivity of Mu in hydrocarbons is demonstrated by the k_M result of phenol in n-hexane. The value of $(7\pm2)\times10^9$ $M^{-1}s^{-1}$ in n-hexane is some 3-times faster than the analogous reaction in water [29] suggesting that the enhanced reactivity seen for phenol embedded in micelle [39] may be due to the change from water to hydrocarbon as the environment for the reaction.

The second interest from these results in liquid hydrocarbons concerns the Mu formation mechanism. On the basis of the spur model, one expects the value of P_D and P_M to depend on both the chemical composition of the medium and their physical properties (such as dielectric constant and electron mobility). The comparison for these solutes are given in Table 7.5. It can be seen that P_M, P_D and P_L are essentially the same for both non-polar hydrocarbons and highly polar hydroxylic liquids. This strongly suggests that the formation of Mu by intraspur neutralization is not a dominant process. For example, Table 7.5 shows that P_M & P_D are essentially independent of electron escape probabilities in low LET spurs, and independent of the mobility of free electrons in these media. Such findings are contrary to the expectations of a spur model of muonium formation.

7.B.2. Temperature dependence of muonium in hydrocarbons.

In chapter 5, yields in solid and liquid neopentane were presented. Here, an extended temperature dependence is given for c-hexane and n-hexane. The experimental details for these experiments are the same as those described in section 5.A.1.

The results for c-hexane and n-hexane are displayed in Figures 7.1 and 7.2, respectively. For c-hexane, P_M could not be measured below -100°C due to a very large value of λ_M below that temperature. That the value of λ_M changes markedly at liquid/plastic-crystal, plastic/non-plastic(c-hexane), and liquid/solid transitions, indicates Mu is an excellent and sensitive probe to determine phase transitions for crystals. The increase in λ_M at

TABLE 7.5

Comparison of P_M and $(1-P_D)$ with properties of the liquid: (i) the fraction of electrons which escape intraspur neutralization in low LET radiolysis[a] (G_{fi}/G_t); (ii) the electron mobility (μ)[b]; and (iii) the static dielectric constant (ε).

Liquid	P_M	$(1-P_D)$	G_{fi}/G_t	μ	ε
Water	0.20	0.38	0.62	0.002	78
Methanol	0.23	0.38	0.38	0.0006	33
TMS	0.21	0.47	0.16	100	1.8
c-Hexane	0.20	0.31	0.03	0.4	1.8
n-Hexane	0.13	0.35	0.03	0.08	1.8

[a] G_{fi} is the free ion yield [103] and G_t the total ionization yield taken to be 4.5 (±0.5) in all cases.

[b] μ is in $cm^2V^{-1}s^{-1}$, data from Allen [102].

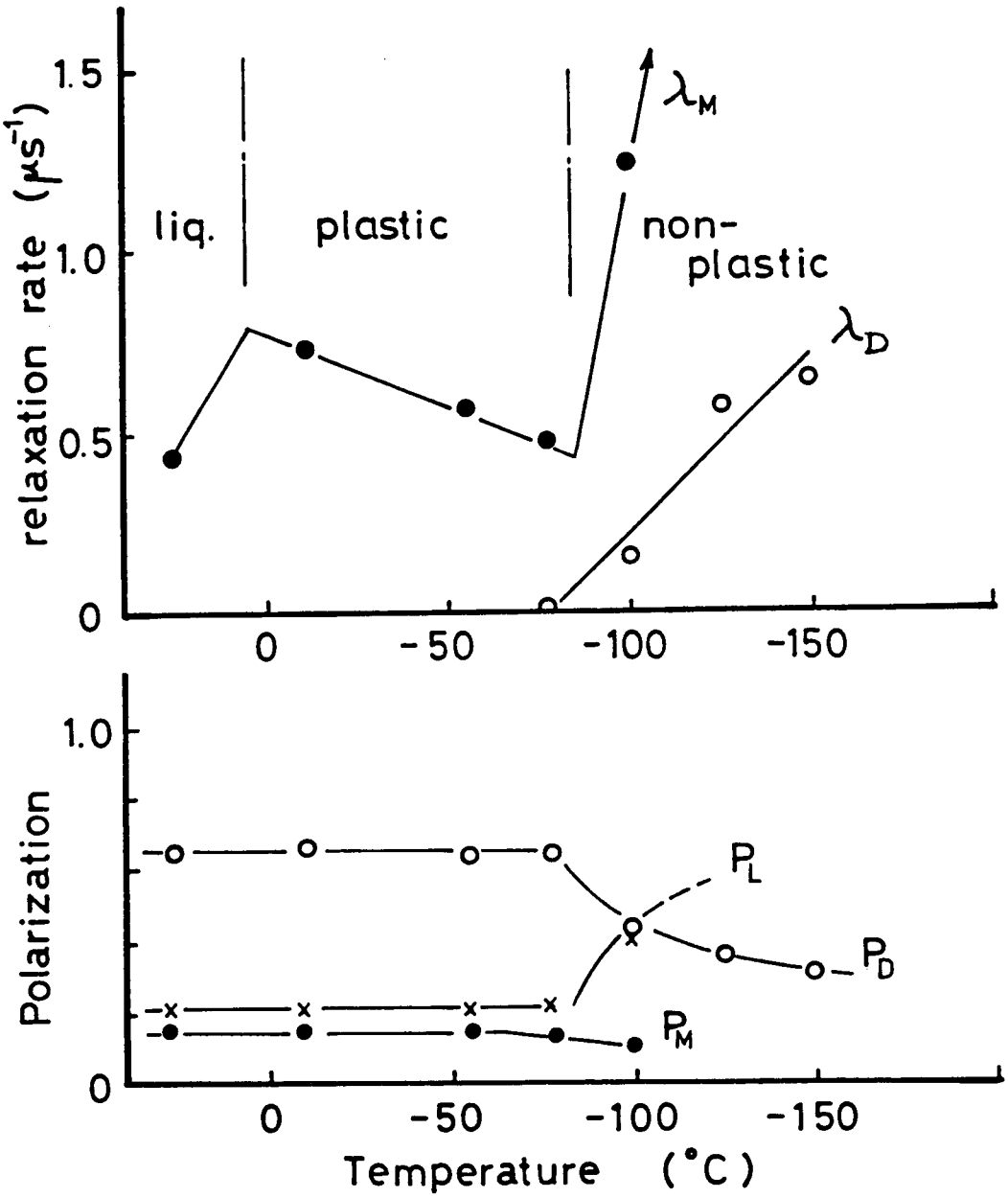

Figure 7.1: Muonium and diamagnetic muon parameters for cyclohexane from room temperature down to -150 C. P_M, P_D and P_L are the muonium, diamagnetic muon and lost polarization, respectively. The lines are drawn to aid the eye.

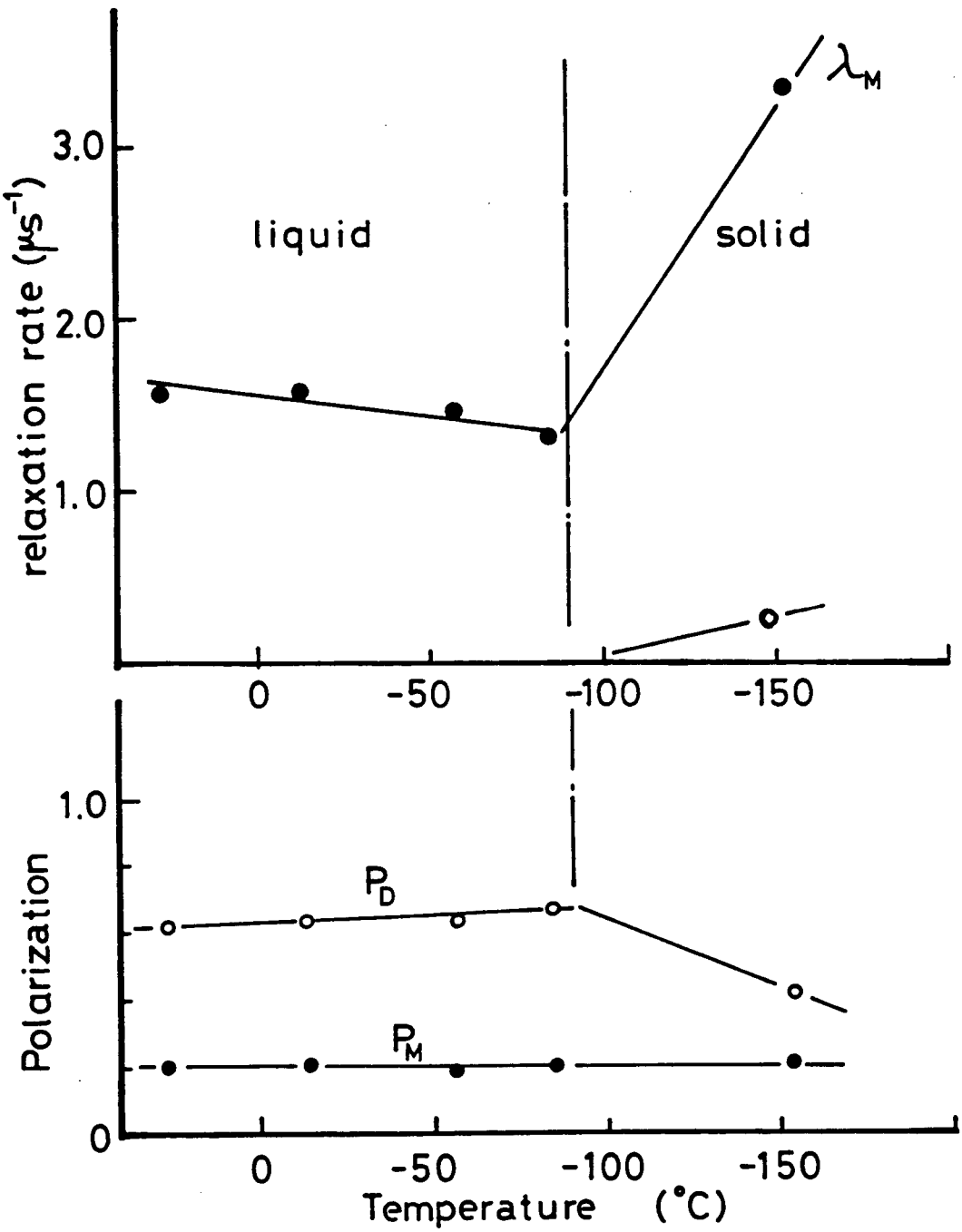

Figure 7.2: Muonium and diamagnetic muon parameters for n-hexane from room temperature down to -150 C. The notations are the same as in Figure 7.1. Note that there is no solid phase corresponding to plastic crystals.

the solid phases can be explained in terms of increased dipole-dipole interactions. That is, as a liquid these interactions are isotropic; however, at lower temperature, the random magnetic fields of surrounding nuclear spins becomes anisotropic due to solidification with resulting interaction with the Mu dipole, thereby causing an increase in λ_M. A similar explanation can also be applied to the observed increase of λ_D for c-hexane.

For both c-hexane and n-hexane, the yields of P_M and P_D do not change significiantly in the solid phase. There is no disappearance of P_L, as in ice [43]. These results resemble that in neopentane (Table 5.3). Again, the expanding track model can be used to rationalize P_L by postulating that there may not be any suitable trapping sites available for Mu in these hydrocarbons even at these low temperatures (see section 5.A.2.).

7.B.3. Effect of external electric fields on the μSR of liquid hydrocarbons and fused quartz.

For positronium (Ps=bound state of e^+ and e^-), its formation mechanism is commonly based upon a spur reaction model [128]. Indeed, the spur model of Mu formation [43] is a copy of that Ps mechanism. The spur model of Ps formation assumes that a positron thermalizes in its own terminal radiation spur, where it can combine with one of the excess electrons to form a Ps atom. This model explains well the experimental results that good electron scavengers are also good inhibitors of Ps formation [129]. More relevant to this section, it explains the fact that the application of an external

electric field (EEF) inhibits Ps formation efficiently [130]. Therefore, an analogous experiment can be investigated for Mu to test the spur model.

A special teflon cell was constructed for the experiment. Thin tungsten meshed sheets (0.05 mm thick, 30 mesh), which were attached to the mylar films of a regular teflon cell, served as the electrodes. Less than 1 nA current was passing between the electrodes, therefore there were no side effects on the transverse magnetic field. For the experiments with the organic liquids, only A_D was measured. A_M was not attempted due to the difficulties mentioned in section 7.B.1. The presumption here was that if the combination of μ^+ and e^- occurs it should be hindered by the EEF, thus more of the μ^+ will eventually precess as diamagnetic muon thereby increasing A_D. To study the effect of EEF on A_M, fused quartz was chosen. Quartz is a suitable material since it has a large P_M value and the technical part of this particular experiment (as compared to an organic liquid) would not be difficult.

In the organic liquid experiments up to 20 kV/cm was applied, while up to 60 kV/cm was used for fused quartz. Such fields should easily separate μ^+ from e^- in a typical low LET spur, sufficiently that an increase in A_D should be seen in accordance with the spur model. It can be seen clearly from Tables 7.6 and 7.7 that there were no changes observed for A_D or A_M in all the liquids studied or for fused quartz, when an EEF was applied. Again, it is entirely in accord with the hot model. Since the muon is in a charged state only when its energy is relatively high, the EEF will have no effect on its charge-exchange processes. Furthermore, an EEF should not influence the hot reactions of Mu, or its thermalization.

TABLE 7.6

Effect of EEF on A_D and A_M in fused quartz.

E (kV/cm)	A_D	A_M
0	0.0925 ± .0013	0.101 ± .001
15	0.0937 ± .0018	0.100 ± .001
30	0.0925 ± .0015	0.101 ± .001
45	0.0969 ± .0014	0.100 ± .001

TABLE 7.7

Effect of EEF on A_D in various liquids (the statistical errors are between 0.001 and 0.002 in all cases).

	Left		Right	
Liquid	E = 0	E = 20 kV/cm	E = 0	E = 20 kV/cm
n-hexane	0.223	0.223	0.238	0.238
c-hexane	0.236	0.233	0.243	0.246
benzene	0.088	0.091	0.095	0.096
CS_2	0.105	0.105	0.121	0.122
$CC\ell_4$	0.338		0.334	

7.B.4. μSR studies with solvent mixtures.

It has already been shown [4,28] that P_D in a wide variety of common liquids varies from 0.17 (for benzene) to 1.0 (for $CC\ell_4$), while water and saturated hydrocarbons have P_D values of ~0.63. There have been unsuccessful attempts to correlate these P_D data with various physical and chemical properties of the liquids [28]. There does not seem to be any consistent correlation with such properties as dipole moment, density, polarizibility, dielectric constant or ionization energy. Some systematic trends were evident [28], however. For example, P_D has been found to be less than 0.5 only in molecules containing π-bonds, and the greater the degree of conjugation the smaller is P_D, with benzene being the extreme. Also, P_D increases with the number of halogen substitutions in organic compounds, with $CC\ell_4$ being the upper extreme. It was thus decided to study solvent mixtures, in particular mixtures of c-hexane, benzene, and $CC\ell_4$ and to determine P_D values to compare the hot and spur models of muon fates.

Regular cells containing these solvent mixtures were placed in front of a surface muon beam to collect left and right histograms. The results are given in Figure 7.3 as plots of P_D against volume fraction of $CC\ell_4$, or c-hexane, in benzene. The volume fraction is the best representation of these results since it most closely reveals the fraction of time the muon spends in contact with each ingredient during its slowing-down process.

Although these results cannot give any indications of why $CC\ell_4$ and benzene should have the largest and smallest P_D values, they do however provide some information about the mechanism of Mu formation in liquids.

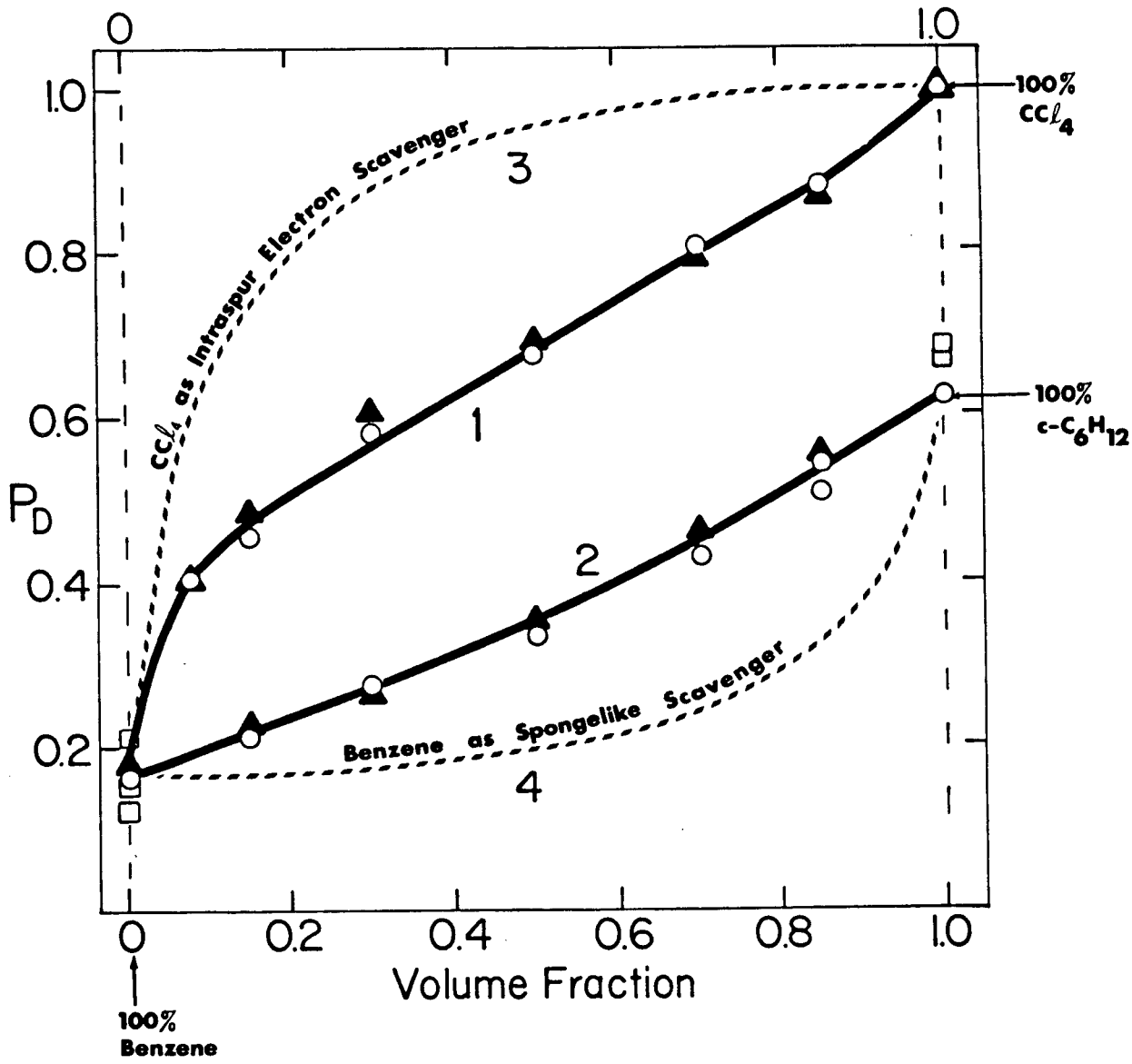

Figure 7.3: Plots of P_D against volume fraction of $CC\ell_4$ or cyclohexane in benzene (1) for $CC\ell_4$-benzene mixtures and (2) for cyclohexane-benzene mixtures: (○) data points obtained on the left-hand side detector; (▲) data from the right-hand side detector; (□) data taken from ref. [28]. The dotted curve 3 is expected on the basis of a spur model with $CC\ell_4$ as an intraspur electron scavenger, and curve 4 is expected if benzene protects cyclohexane by energy transfer or sacrificial scavenging.

For $CC\ell_4$, the fact that P_D=1 can be explained, through the spur model, by the fact that $CC\ell_4$ is an excellent electron scavenger, therefore giving $CC\ell_4^-$ and then $C\ell^-$+$CC\ell_3$, which are long-lived. Thus an ion, rather than an electron, would be available for neutralization by μ^+, as in (7.2),

$$\mu^+ + C\ell^- \text{ (or } CC\ell_4^-) \longrightarrow MuC\ell \text{ (or } CC\ell_3). \qquad (7.2)$$

This neutralization, due to $CC\ell_4$'s low dielectric constant, would occur over considerable distances and therefore up to times when the original spur has virtually dispersed due to diffusion. But, if such intraspur reactions are responsible for P_D=1.0 in $CC\ell_4$, then they should also be equally effective when the spurs are partly composed of benzene molecules (e.g. 0.5 mole fraction $CC\ell_4$ in benzene) because $CC\ell_4$ would equally scavenge all electrons initially. Thus, on the basis of the spur model, one should have obtained a pronounced curve, such as that sketched as curve 3 in Figure 7.3. The fact that the experimental data points (curve 2) for these $CC\ell_4$-benzene mixtures is linear rather than following curve 3 indicates once again that the spur process plays a minor role in the Mu formation mechanism.

A similar argument can be applied to the benzene-cyclohexane mixtures. The delocalized π-bonding of benzene should be effective in reducing P_D of cyclohexane when they are mixed together. If a "sponge-like"-protection by benzene is operative [131], then one should have obtained a curve such as 4 in Figure 7.3. The disagreement between curve 2 & 4 and the fact that

curve 2 is approximately linear implies that there is a one-step intramolecular process for these mixtures. These results are not inconsistent with the expectation of a hot model of Mu formation.

7.C. Muonium solution kinetics.

Since the discovery of Mu in water by Percival et al.[24], many reactions of Mu interacting with various solutes in aqueous solutions have been studied by groups from TRIUMF [29,30,70] and SIN [87]. Chapter 6 detailed the kinetics of Mu reacting with DCO_2^- and OH^-. In this section, more recent results including Mu reactions with vinyl monomers [41,93], nickel cyclam [40], and cyanides [123] will be briefly described. The discussion will be mainly focused upon kinetic isotope effects (k_M/k_H), its relevance to H atom studies, applications for polymer initiation rates, and the use of Mu as a sensitive probe for paramagnetism in solutions. The MSR technique was used for all these experiments, including the temperature-dependence measurements. Mainly a surface muon set-up was used, with backward muons on occassions. All quoted values of k_M have realistic probable errors of ±25%.

7.C.1. Muonium addition to vinyl monomers.

As already seen in chapter 4, Mu radicals can be observed in benzene, styrene, and their mixtures. These species are formed by Mu addition reactions. This section describes Mu additions to aqueous solutions of styrene, methylmethacrylate (MMA), acrylonitrile (AN), acrylic acid (AA), and acrylamide (AM). Also, MRSR experiments were carried out to obtain A_μ in order to identify the mode of reaction.

The A_μ-value for styrene has already been shown to be independent of magnetic field (Figure 2.6). By comparing its value of 214 MHz to analogous radicals observed by ESR, one identifies the mechanism as Mu addition to the vinyl bond of styrene (see chapter 4). This contradicts the suggestion by Swallow [132], based on band labelling studies, that H adds to styrene's vinyl bond 15% of the time and to the ring 85% of the time. However, one must realize that the radical adducts observable in MRSR are in the time window of 10^{-7} to 10^{-5} sec, therefore it is quite likely that the observed radicals are not the primary ones but rather the most stable ones after intramolecular rearrangements. This same conclusion has also been reached during the discussion section in chapter 4.

Table 7.8 lists the hyperfine coupling constants for the various monomers in neat solutions. With the exception of MMA, all monomers gave one observable Mu radical. The comparison with A_p confirms the assumption that Mu is indeed adding across the vinyl bond of these monomers as shown here by equation (7.3):

TABLE 7.8

Hyperfine Coupling Constants.

Monomer	Mu-R		H-R
	A_μ/MH_2	A'_μ/MHz	A_p/MHz
Styrene	213.4	67.0	56.0
MMA	270	84.8	73
	276	87.0	71.2
AN	280.4	88.1	64.4
AA	319.3	100.3	70.8
Benzene	514.6	161.6	133.7

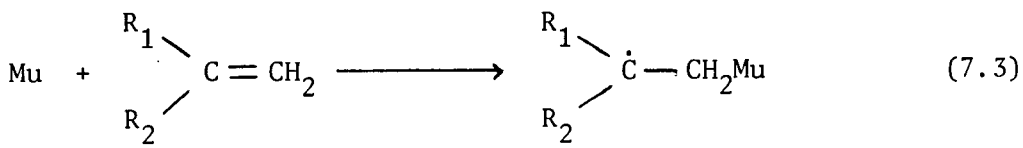

(7.3)

where R_1 and R_2 vary through H, C_6H_5, $CONH_2$, CO_2H, CH_3, CN & CO_2CH_3 depending on the monomer. In the case of MMA, the two radicals have been assigned as the cis and trans forms where Mu adds at the CH_2-group end of the carbon-carbon double bond. This is analogous to the assignment by Roduner et al. [133] for ethylmethacrylate. As one can clearly see, the radical assignments in Table 7.8 identifies the Mu reactions with these monomers as that of an addition reaction.

Table 7.9 lists the reaction rate constants (k_M) for the various monomers. Maleic acid is included for comparison as a non-acrylic compound. Due to the scarcity of H atom data, k_M/k_H ratios were obtained for only AN, AM, and maleic acid. With the exception of styrene, all k_M's are near the diffusion controlled limit (~2×10^{10} $M^{-1}s^{-1}$). The low value of k_M for styrene (1.1×10^{9} $M^{-1}s^{-1}$) indicates that the large π-delocalization stabilizes the molecule and hence reduces its reactivity toward Mu. For the other monomers, k_M increases from 9.5×10^{9} $M^{-1}s^{-1}$ in the order MMA<AN<AA<AM. This trend can be explained on a steric argument. For example, MMA should have the smallest k_M since it has the least accessible double bond due to the "blocking" effect of its α-methyl group. For the three straight chain 3-carbon conjugated monomers, Mu (which acts like a nucleophile) should encounter less electron shielding and react faster with AM or AA due to the electron withdrawing

TABLE 7.9

Reaction rate data of monomers at 295 K.

Monomer	$k_M/10^{10} M^{-1} s^{-1}$	k_M/k_H †
Styrene	0.11 ± 0.01	-
Methylmethacrylate	0.95 ± 0.19	-
Acrylonitrile	1.14 ± 0.20	2.8
Acrylic acid	1.55 ± 0.25	-
Acrylamide	1.90 ± 0.13	1.1
Maleic acid	1.1 ± 0.1	1.4

† k_H obtained from reference [99], data only available for AN, AM and maleic acid. Maleic acid data was added as comparison.

CO group on these molecules; whereas it would be slower with AN.

When comparing with k_H, AM's isotope effect of 1.1±0.4 indicates that there is little mass effect in this type of reaction. As these reactions are near the diffusion controlled limit, the question arises as to whether the Stokes-Einstein relationship holds for small particles like Mu or H, or whether the isotope effect should be 3, as with AN, because the mean velocity of Mu (with mass 1/9 H) is three times faster than that of H. At this stage, due to the lack of H atom data, judgement is reserved on the kinetic effect in these addition reactions. That the H atom data is of such scarcity indicates the strong need for the Mu chemist to supply information on the initiation of polymerization of monomers by the simplest of atoms, the hydrogen atom.

7.C.2. Spin conversion reaction of muonium with nickel (II) cyclam.

The first observation of electron-spin exchange (or spin flip) interactions of Mu was by Hughes in 1960's [10] studying Mu reactions with O_2 and NO in the gas phase. Jean et al.[30] have investigated interactions of various paramagnetic ions and found that Mu reacted with a low-spin complex (diamagnetic $Fe(CN)_6^{4-}$) at ~10^{-8} $M^{-1}s^{-1}$, while in a high-spin state (paramagnetic Fe_{aq}^{2+}) it reacted at ~10^{10} $M^{-1}s^{-1}$. In this section will be described the reaction of Mu with a metal complex (nickel (II) cyclam) in two spin states, interchanged merely by altering the ionic strength of the solution by addition of an inert salt. Nickel cyclam, (1,4,8,11-tetraazacyclotetradecane)-nickel(II), is an excellent system for such a study since it switches from being an octahedral (paramagnetic, d^8) configuration in aqueous ammonia to a square-planar (diamagnetic) structure in solution containing perchlorate or sulphate.

In the equilibrium between the paramagnetic (P) and diamagnetic (D) species of Ni-cyclam, Mu reacts with each with different k_M's, represented by:

$$Mu + P \xrightarrow{k_P} \text{products} \qquad (7.4a)$$

$$Mu + D \xrightarrow{k_D} \text{products}. \qquad (7.4b)$$

The overall k_{obs} can be equated with $k_P[P]+k_D[D]$, which leads to the following relationship [40]:

$$(\lambda-\lambda_o) = k_P[Ni]F_P + k_D[Ni](1-F_P), \qquad (7.5)$$

where F_P is the fraction of complex ions in the paramagnetic state. Therefore, a plot of $(\lambda-\lambda_o)/[Ni]$ versus F_P, shown by Figure 7.4, should give k_D as its intercept and (k_P-k_D) as the slope.

Unfortunately, Figure 7.4 does not give a straight line. Nevertheless, the intercept at $F_P=0$ from the three low F_P points gives $k_D \leq 5\times10^8$ $M^{-1}s^{-1}$, which seems to be a reasonable value, being some 100-times slower than the diffusion controlled limit (as with Fe(II), for instance). k_D can be a result of a reduction reaction (Ni(II)→Ni(I)) of the diamagnetic product, of which the analogous H atom reaction has a value of 2×10^5 $M^{-1}s^{-1}$ [99]. It could also be a reaction between Mu and the ligand (abstraction of H) since the blank solution of the cyclam ligand also gives a k_M of less than 5×10^8 $M^{-1}s^{-1}$.

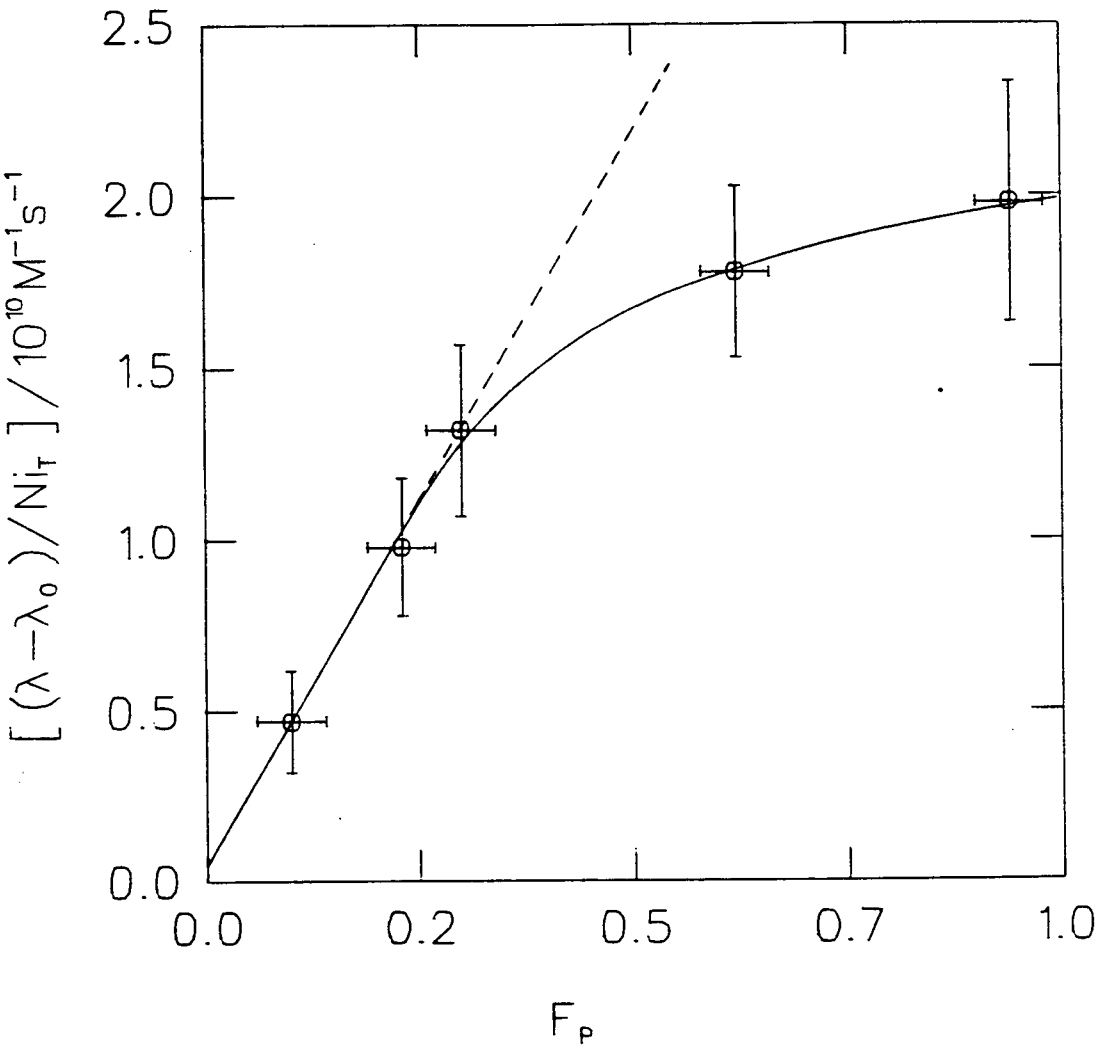

Figure 7.4: Plot of the observed rate constant, given as $(\lambda-\lambda_o)/[Ni]$, as a function of the fraction of nickel-complex species in the paramagnetic state (F_P). [Ni] is the total Ni complex in solution. The two highest data points were obtained in aqueous NH_3 solution, where the axial ligands will be NH_3, whereas the lower three points correspond to H_2O ligands in the axial position of the paramagnetic component.

An intriguing question is the non-linearity of Figure 7.4 at the high F_p data points. In any case, it is clear that k_p is much greater than k_D. Using the initial slope at the three low F_p-points, one obtains $k_p=4.5\times10^{10}$ $M^{-1}s^{-1}$. Two reasons can be invoked to explain the non-linearity. The first arises from the fact that NH_3 had to be added to induce the change to a paramagnetic state for the two high F_p data points. The second could be a result of the presence of a five-coordinate intermediate, which, like pentacyanonickelate [134], could be diamagnetic. In any event, the results imply k_p for the interaction of Mu with the paramagnetic complex to be ~4.5×10^{10} $M^{-1}s^{-1}$ when H_2O is the axial ligand and ~2×10^{10} $M^{-1}s^{-1}$ for NH_3 as the axial ligand. This experiment further demonstrates the potential of using the "triplet" to "singlet" conversion of muonium as a probe of paramagnetism and as a monitor of spin-exchange interactions.

7.C.3. Muonium addition to cyanides.

In section 7.C.1., the observed isotope effects of 1.1 and 2.8 for acrylamide and acrylonitrile prompted more extensive investigations into Mu addition reactions. Here, both organic and inorganic cyanides were selected for study. Similar to ESR studies [135,136], one expects Mu to add across the C≡N bond of these cyanide molecules. An MSR technique employing surface muons was used to extract the k_M's; also a temperature-dependence study was carried out for cyanoacetate and tetracyanocadmate(II) ($Cd(CN)_4^{2-}$) to determine their Arrhenius parameters.

Table 7.10 lists the kinetic data for these cyanides and other relevant Mu rate constants. By applying Smoluchowski's equation (1.10) (see also chapter 6) for the cyanoacetate and $Cd(CN)_4^{2-}$ reactions, it was found that $Cd(CN)_4^{2-}$ exhibited diffusion controlled behaviour while cyanoacetate demonstrated activation controlled behaviour. This was reflected by the activation energies of 35 and 15 kJ $mole^{-1}$ [70] obtained for cyanoacetate and $Cd(CN)_4^{2-}$, respectively. Because the C≡N bond system is stronger than the C=C double bond of the monomers, with more electron density to shield the nucleophilic Mu from the target C atom, one expects the cyanide rate constants to be smaller than those for the monomers (Table 7.9). Indeed, Table 7.10 gives the cyanide k_M's ranging from 5.1×10^7 to 1.7×10^{10} $M^{-1}s^{-1}$. These data suggest that the reactions of Mu with organic nitriles and cyanide to be activation controlled while it is diffusion controlled for $Cd(CN)_4^{2-}$. The peculiarity of the $Cd(CN)_4^{2-}$ can possibly be explained by a size effect increasing the collision cross-section and making available four CN^- groups on each encounter. Another possibility is that the cadmium complex stabilizes the radical product to a much higher degree than the other cyanide reactants, thereby lowering the reaction barrier.

Also listed in Table 7.10 are the kinetic isotope effects, k_M/k_H, for the solutes studied. That k_M/k_H has values of 0.7 and <7 for the inorganic cyanides supports the idea that addition reactions, being primarily electronic in nature, should have little or no mass effect, as exemplified by the monomer experiments in section 7.C.1. However, both the organic nitriles react much faster with Mu than H giving k_M/k_H of 24 for cyanoacetate and 19

TABLE 7.10

Kinetic data of cyanide system with some associated Mu rate constants.

Solute	$k_M/M^{-1}s^{-1}$	Ea/kJ $mole^{-1}$	k_M/k_H
cyanoacetate	7.7×10^7	35 ± 2	24
acetonitrile	5.1×10^7		19
cyanide	3.0×10^9		0.7
tetracyanocadmate(II)	1.7×10^{10}	15 ± 2	<7[a]
acetic acid	$\sim 3.8 \times 10^6$		
cadmium(II)	8.5×10^5		

[a] k_H was reported in reference [99] as $>2.4 \times 10^9$ $M^{-1}s^{-1}$.

for acetonitrile. Percival et al. [43] have found a similar isotope effect of 40±10 for reaction of Mu with acetone in water, the only other organic addition reaction studied to date. These data, rather than clarifying the questions of Mu addition isotope effects, reflects the necessity for more kinetic information; particularly activation controlled addition reactions with organic solutes.

CHAPTER 8

SUMMARY AND CONCLUSION

This Ph.D. thesis is, in a sense, a continuation - a more in-depth investigation - of muonium chemistry resulting from the M.Sc. thesis. Therefore it seems appropriate to now present a brief summary of all work during my graduate years at U.B.C. and TRIUMF.

From the magnetic field dependence study in chapter 3 and the temperature-dependence of λ_o from the M.Sc. work, it has now been verified that Mu does not react with water to any significant extent. Instead, the natural relaxation of Mu in water (λ_o) is simply an experimental artifact, due to a combination of magnetic field inhomogeneities and the physical phenomenon of Mu-frequency beating. Perhaps the use of the two-frequency MSR technique can be applied to study the origin of λ_o in other solvents.

For the first time, muonium radicals were observed and identified through their combined MRSR precession frequencies in high transverse magnetic fields in mixtures. Thus, pure benzene, pure styrene and a full range of their mixtures were studied, all as liquids at room temperature. In styrene, it was found that there was only one radical formed, one resulting from Mu addition to the vinyl bond of styrene, while there was no net insertion of Mu into the phenyl ring as in benzene. In benzene-styrene mixtures, the radicals obtained in each pure liquid were both present, so no slow (10^{-9} - 10^{-5} sec) intermolecular exchange occurs; but strong selectivity was found with the formation of the radical from styrene being about eight-times more probable than the radical from benzene. Further, the selectivity result from chapter 4 implies either that the radical precursor is epithermal, or that the effect is due to the tunnelling ability of the light Mu atom, or there is intramolecular rearrangement.

To specifically investigate the hot and spur Mu formation mechanisms, muon and muonium yields in neopentane (liquid & solid) and concentrated OH^- solutions were studied. First, the observed long-lived Mu signal in neopentane further substantiated the conclusion reached in chapter 3, that λ_o in pure, unreactive, solvents is a physical artifact rather than a chemical reaction. Second, both P_M and P_D results in neopentane and concentrated OH^- solutions seem to be at variance with the expectations of a spur model of Mu formation.

In muonium solution kinetics, many reactions were investigated. In the M.Sc. thesis, it was shown from temperature dependence studies of k_M that Mu reacted at diffusion controlled rates with MnO_4^-, maleic acid and Ni^{2+} (E_a ~ 17 kJ mole^{-1}), and at an activation controlled rate with HCO_2^- (E_a ~ 33 kJ mole^{-1}). On the other hand, the low E_a (8 kJ mole^{-1}) obtained for NO_3^- was explained via quantum mechanical tunnelling contributions or alternative (competitive) reaction paths. In this Ph.D. thesis, the reaction of Mu with OH_{aq}^- was found to be relatively slow due to a substantial activation energy (E_a ~ 40 kJ mole^{-1}). When compared to H atom result, there was no kinetic isotope effect at room temperature. The reaction was identified as activation controlled and it was concluded that Mu behaves as a "muonic acid" in this acid-base transfer reaction. As with the OH^- reaction, the abstraction of Mu with DCO_2^- gave a large E_a of 39 kJ mole^{-1} as if it is primarily activation-limited. When compared with HCO_2^-, the isotope effects (k_M/k_H and k_H'/k_D') implied that quantum mechanical tunnelling does not dominate the abstraction of H and D atoms in HCO_2^- and DCO_2^- by either H or Mu. Furthermore, collaborative works (section 7.C.) describing reactions of Mu with

cyanides, vinyl monomers, and nickel cyclam have shown that there is almost no mass-effect in addition reactions. But, more importantly, these solution kinetics results demonstrated the potential of using Mu in polymer initiation kinetics due to its unique characteristic as a sensitive and non-destructive probe. It is hoped that these kinetic studies will be extended to non-polar (hydrocarbon) solutions and hence to a wider temperature range. In this way the effect of quantum mechanical tunnelling can be more easily manifest, as in either Arrhenius curvatures or relative primary isotope effects.

In the M.Sc. thesis, the study of Mu reaction with O_2(aq) showed that the reaction did not involve any long range encounter. Unfortunately, the nature of the reaction, spin conversion or chemical reduction, could not be determined with the transverse field technique. However, the study did demonstrated the importance of residual O_2 in muonium kinetics. Since H atoms are involved in some of the most fundamental processes in biological systems, the MSR technique was also applied to study a few model biological systems. The macromolecules investigated were porphyrins (M.Sc.), cyclodextrins and micelles (Ph.D.). The results again demonstrated the potentially sensitive nature of the muonium atom as a nuclear probe. Hopefully, this will inspire future practical applications of this novel technique to other biological systems.

Last, but not least, hydrocarbons were investigated to expand the study of Mu beyond aqueous media. These systems included various neat hydrocarbons, with studies of λ_o and various muon yields, their temperature dependence,

the effect of EEF, and muon yields in solvent mixtures. All of the results tend to point toward the fact that Mu formation does not occur primarily via spur processes. Rather, the results are consistent with those expected to result from a 'hot' mechanism. Also, the use of an 'expanding-track' model explains the results of P_L in polar media and at phase boundaries.

Almost all results in both the M.Sc. and Ph.D. thesis seem to be in conflict with the spur model of Mu formation. It is interesting that the analogous model in positronium studies [129] is now gaining wide acceptance. Then, one should ask, why does a spur model apply to Ps but not to Mu? This can be explained by realizing that there are several important differences between the muon and positron at the end of their radiation tracks. First, according to estimates by Mozumder [45], the linear energy transfer (LET) of the positron greatly exceeds that of the muon (~two orders of magnitude) during their last few hundred eV of kinetic energy. Therefore, it is much more reasonable for the e^+ to create its own terminal spur relative to the muon. Indeed, the last spur of the muon is actually created by a secondary electron, and it is difficult to envisage the muon donating all of its remaining kinetic energy in one last ionization process. This is probably why an expanding track model [51] can more readily explain the missing fractions in various liquids. A second difference between Ps and Mu spur processes originates from the ionization energy (I_p) of these two species. The I_p of Ps (6.8 eV) is less than that of the molecules of a typical medium (eg. I_p ~ 9-12 eV), whereas that of Mu is higher (I_p(Mu) = 13.6 eV), therefore one would expect the muon to continue extracting electrons from the medium

down to thermal energies; however, the positron cannot undergo the capture step of such charge-exchange cycles during its last few eV of energy. A third factor concerns the relative thermalization distance of e^+ and μ^+ after formation of their terminal spur. However, it is not so clear whether or not this favours intraspur Ps formation over Mu [51]. With all these arguments and conflicting results, based on radiation chemistry effects, the spur model of Mu formation [43] should be seriously revised. Yet it is unfortunate that the hot model of Mu formation is so simple and vague that it cannot be tested as severely as is the case with the spur model.

At present, the muon community is rapidly expanding into many new areas of research, even into emission spectroscopic studies [3]. For certain, Mu will continue to be useful as an isotope of hydrogen until the complicated picture of H atom chemistry is sorted out. It is hopeful that one can someday evaluate the pK_a of Mu and to determine its standard reduction potential, to observe its tunnelling at low temperatures, to study its precession in hydrogen-bonded structures, to evaluate the solvation energy of μ^+, and to reach a consensus on the mechanism of Mu formation. To carry out such research at TRIUMF, the present apparatus, electronics, and counter set-up must be improved. For example, effects such as unstable cell geometry, magnetic field inhomogeneity, small positron solid angle detection, and electronic resolution all contribute to uncertainties in μSR, MSR and MRSR measurements. It is hoped that an all-purpose liquid chemistry apparatus employing a closed-He-gas-flow cryostat situated between a pair of high resolution "tip-pole" magnets (range ~ 5kG) and improved timing resolution circuitry will be built by the

future generations of μSR scientists to not only remedy the above problems, but also to facilate the study of Mu-substituted radicals, which is one of the most exciting and rapidly-growing fields in muon science. With such improvements, one can be assured that the μSR/MSR/MRSR technique will be both a productive and useful tool in many areas of scientific research.

REFERENCES

1. V.W. Hughes, D.W. McColm, K. Ziock and R. Prepost, Phys. Rev. A1, 595 (1970).

2. S. Weinberg, Sci. Am., 244(6), 64 (1981).

3. D.C. Walker, J. Phys. Chem., 85, 3960 (1981).

4. J.H. Brewer, K.M. Crowe, F.N. Gygax and A. Schenck, in "Muon Physics", eds., V.W. Hughes and C.S. Wu, Academic Press, New York, (1975).

5. J.H. Brewer and K.M. Crowe, Ann. Rev. Nucl. Part. Sci., 28, 239 (1978).

6. R.L. Garwin, L.M. Lederman and M. Weinrich, Phys. Rev., 105, 1415 (1957).

7. J.L. Friedman and V.L. Telegdi, Phys. Rev., 105, 1681 (1957).

8. C.S. Wu, E. Ambler, R.W. Hayward, D.D. Hoppes and R.P. Hudson, Phys. Rev., 105, 1413 (1957).

9. V.W. Hughes, D.W. McColm, K. Ziock and R. Prepost, Phys. Rev. Lett., 5, 63 (1960).

10. V.W. Hughes, Annu. Rev. Nucl. Sci., 16, 445 (1966).

11. A.I. Babaev, Ya. Balats, G.G. Myasishcheva, Yu. V. Obukhov, V.S. Rogonov and V.G. Firsov, Sov. Phys. - JETP, 23, 583 (1966).

12. V.G. Firsov and V.M. Byakov, Sov. Phys. - JETP, 20, 719 (1965).

13. V.G. Firsov, Sov. Phys. - JETP, 21, 786 (1965).

14. G.A. Swanson, Phys. Rev., 112, 580 (1958).

15. (a) R.M. Mobley, J.M. Bailey, W.E. Cleland, V.W. Hughes and J.E. Rothberg, J. Chem. Phys., 44, 4354 (1960).

    (b) R.M. Mobley, Ph.D. Thesis, Yale University, 1967.

16. V.G. Nosov and I.V. Yakovleva, Nucl. Phys., 68, 609 (1965).

17. I.G. Ivanter and V.P. Smilga, Sov. Phys. - JETP, 77, 301 (1968).

18. I.G. Ivanter and V.P. Smilga, Sov. Phys. - JETP, 23, 796 (1969).

19. K.M. Crowe, J.F. Hague, J.E. Rothberg, A. Schenck, D.L. Williams, R.W. Williams and K.K. Young, Phys. Rev., D5, 2145 (1972).

20. J. Bailey, W. Barth, G. von Bochmann, R.C.A. Brown, F.J.M. Farley, M. Giesch, H. Jostlein, S. van der Meer, E. Picasso and R.W. Williams, Nuov. Cim., 917, 369 (1972).

21. D. Favast, P.M. McIntyre, D.Y. Stowell, V.L. Telegdi, R. de Voe and R.A. Swanson, Phys. Rev. Lett., 27, 1336 (1971).

22. J.H. Brewer, K.M. Crowe, F.N. Gygax, R.F. Johnson, D.G. Fleming and A. Schenck, Phys. Rev., A9, 495 (1974).

23. J.H. Brewer, Ph.D. Thesis, University of California. Lawrence Berkeley Laboratory Report LBL-950 (1972) unpublished.

24. P.W. Percival, H. Fisher, M. Camani, F.N. Gygax, W. Rüegg, A. Schenck, H. Schilling, H. Graf, Chem. Phys. Lett., 39, 33 (1976).

25. P.W. Percival, Radiochimica Acta, 26, 1 (1979).

26. E. Roduner, P.W. Percival, D.G. Fleming, J. Hochmann and H. Fischer, Chem. Phys. Lett., 57, 37 (1978).

27. D.G. Fleming, J.H. Brewer, D.M. Garner, A.E. Pifer, T. Bowen, D.A. Delise and K.M. Crowe, J. Chem. Phys., 64, 1281 (1976).

28. D.G. Fleming, D.M. Garner, L.C. Vaz, D.C. Walker, J.H. Brewer and K.M. Crowe, in "Positronium and Muonium Chemistry", ed. H.J. Ache, Adv. Chem. Series, 175, 279 (1979).

29. Y.C. Jean, J.H. Brewer, D.G. Fleming, D.M. Garner, R.J. Mikula, L.C. Vaz and D.C. Walker, Chem. Phys. Lett., 57, 293 (1978).

30. Y.C. Jean, J.H. Brewer, D.G. Fleming and D.C. Walker, Chem. Phys. Lett., 60, 125 (1978).

31. Y.C. Jean, J.H. Brewer, D.G. Fleming, D.M. Garner and D.C. Walker, Hyperfine Interactions, 6, 410 (1979).

32. Y.C. Jean, D.G. Fleming, B.W. Ng and D.C. Walker, Chem. Phys. Lett., 66, 187 (1979).

33. Y. Ito, B.W. Ng, Y.C. Jean and D.C. Walker, Can. J. Chem., 58, 2395 (1980).

34. Y. Ito, B.W. Ng, Y.C. Jean and D.C. Walker, Hyperfine Interactions, 8, 355 (1981).

35. B.W. Ng, J.M. Stadlbauer, Y.C. Jean and D.C. Walker, Can. J. Chem., 61, 671 (1983).

36. Y.C. Jean, B.W. Ng and D.C. Walker, in "Applications of Nuclear and Radiochemistry", ed. by R.M. Lambrecht and N. Morcos, p. 543, Pergamon Press, New York (1982).

37. Y.C. Jean, B.W. Ng and D.C. Walker, Chem. Phys. Lett., 75, 561 (1980).

38. Y.C. Jean, B.W. Ng, Y. Ito, T.Q. Nguyen and D.C. Walker, Hyper. Inter. 8, 351 (1981).

39. Y.C. Jean, B.W. Ng, J.M. Stadlbauer and D.C. Walker, J. Chem. Phys. 75, 2879 (1981).

40. J.M. Stadlbauer, B.W. Ng and D.C. Walker, J. Am. Chem. Soc. 105, 752 (1983).

41. J.M. Stadlbauer, B.W. Ng, Y.C. Jean, Y. Ito and D.C. Walker, Can. J. Chem., 59, 3261 (1981).

42. P.W. Percival, E. Roduner and H. Fischer, Chem. Phys., 32, 353 (1978).

43. P.W. Percival, E. Roduner and H. Fischer, Adv. Chem. Ser., 175, 335 (1979).

44. P.W. Percival, Hyperfine Inter., 8, 325 (1981).

45. A. Mozumder, in "Advances in Radiation Chemistry", ed. by M. Burton and J.L. Magee, Vol. 1, p. 1, Wiley, New York (1969).

46. O.E. Mögensen, J. Chem. Phys., 60, 998 (1974).

47. P.W. Percival, J.C. Brodovitch and K.E. Neman, Chem. Phys. Lett., 91, 1 (1982).

48. D.C. Walker, Y.C. Jean and D.G. Fleming, J. Chem. Phys., 70, 4534 (1979).

49. Y.C. Jean, B.W. Ng, J.H. Brewer, D.G. Fleming and D.C. Walker, J. Phys. Chem., 85, 451 (1981).

50. D.C. Walker, Y.C. Jean and D.G. Fleming, J. Chem. Phys., 72, 2902 (1980).

51. D.C. Walker, Hyperfine Int., 8, 329 (1981).

52. P.W. Percival, Hyperfine Int., 8, 315 (1981).

53. P.W. Percival, J. Chem. Phys., 72, 2901 (1980).

54. M.J. Pilling, "Reaction Kinetics", Oxford Univ. Press, (1975).

55. A.M. North, "The Collision Theory of Chemical Reactions in Liquids", London, (1964).

56. E.A. Moelwyn-Hughes, "Physical Chemistry", p. 1211, Pergamon Press, Oxford (1964).

57. M.V. Smoluchowski, Z. Phys. Chem., 92, 129 (1917).

58. I. Kirshebaum, in "Physical Properties and Analysis of Heavy Water", ed. by H.C. Urey and G.M. Murphy, p. 33, McGraw, London (1951).

59. N. Bjerrum, Z. Phys. Chem., 108, 85 (1924); 118, 252 (1925).

60. J.N. Brönsted, Z. Phys. Chem., 102, 169 (1922); 115, 337 (1925).

61. W.H. Rodebush, J. Chem. Phys., 1, 440 (1933); 3, 242 (1935); 4, 744 (1936).

62. O.K. Rice and H. Gerschenowitz, J. Chem. Phys., 2, 853 (1934).

63. S. Glasstone, K.J. Laidler and H. Eyring, "The Theory of Rate Processes", New York, McGraw-Hill, (1941).

64. H. Eyring, J. Chem. Phys., 3, 107 (1935).

65. M.G. Evans and M. Polanyi, Trans. Faraday Soc., 31, 875 (1935).

66. S.G. Entelis and R.P. Tiger, "Reaction Kinetics in the Liquid Phase", John Wiley & Sons, New York, (1976).

67. R.P. Bell, Proc. R. Soc., A 139, 466 (1933).

68. P.W. Atkins, "Physical Chemistry", p. 897, N.Y., (1978).

69. E. Roduner and H. Fischer, Hyper. Int., 6, 413 (1979).

70. B.W. Ng, Y.C. Jean, Y. Ito, T. Suzuki, J.H. Brewer, D.G. Fleming and D.C. Walker, J. Phys. Chem., 85, 454 (1981).

71. B.W. Ng, M.Sc. Thesis, University of British Columbia (1980).

72. B.W. Ng, J.M. Stadlbauer and D.C. Walker, "Muon spin rotation involving muonium at high pH", J. Phys. Chem., in press.

73. B.W. Ng, J.M. Stadlbauer, Y. Ito, Y. Miyake and D.C. Walker, "Muonium radicals in styrene-benzene mixtures", Hyper. Inter., in press.

74. Y. Miyake, B.W. Ng, J.M. Stadlbauer, Y. Ito, Y. Tabata and D.C. Walker, "Temperature dependence of muonium in hydrocarbons", Hyper. Inter., in press.

75. D.M. Garner, Ph.D. Thesis, University of British Columbia, Vancouver, 1979.

76. J.D. Bjorken and S.D. Drell, in "Relativistic Quantum Mechanics", p. 261, McGraw-Hill, New York, (1964).

77. D.G. Fleming, D.M. Garner, J.H. Brewer, J.B. Warren, G.M. Marshall, G. Clark, A.E. Pifer and T. Bowen, Chem. Phys. Lett., 48, 393 (1976).

78. J.H. Brewer, Hyperfine Int., 8, 831 (1981).

79. A.E. Pifer, T. Bowen and K.R. Kendall, Nucl. Instr. Methods, 135, 39 (1976).

80. E. Roduner and H. Fischer, Chem. Phys., 54, 261 (1981).

81. F. James and M. Ross, MINUIT, CERN Computer 7600 Interim Programme Library, (1971).

82. E. Roduner, G.A. Brinkman and P.W.F. Louwrier, Chem. Phys., 73, 117 (1982).

83. A. Hill, G. Allen, G. Stirling and M.C.R. Symons, J. Chem. Soc. Fara. Trans. 1, 78, 2959 (1982).

84. S.J. Rzad, P.P. Infelta, J.M. Warman and R.H. Schuler, J. Chem. Phys. 52, 2971 (1970).

85. H.A. Schwarz, J. Phys. Chem., 73, 1928 (1969).

86. R.F. Kiefl, J.B. Warren, G.M. Marshall, C.J. Oram and C.W. Clawson, J. Chem. Phys., 74, 308 (1981).

87. P.W. Percival, E. Roduner, H. Fischer, M. Camani, F.N. Gygax and A. Schenck, Chem. Phys. Lett., 47, 11 (1977).

88. K. Nagamine, K. Nishiyama, J. Imazato, H. Nakayama, M. Toshida, Y. Sakai, H. Sato and T. Tominaga, Chem. Phys. Lett., 87, 186 (1982).

89. D.L. Baulch, D.D. Drysdale and A.C. Lloyd, High temperature reaction data, Leeds University, Leeds, 3, (1968); 4 (1969).

90. E. Roduner, Ph.D. Thesis, Universität Zürich, 1979.

91. L.B. Wall and R.B. Ingalls, J. Chem. Phys., 41, 1112 (1964).

92. C.H. Bamford and C.F.H. Tipper, "Comprehensive Chemical Kinetics", Vol. 14, New York, Elsevier, (1975).

93. J.M. Stadlbauer, B.W. Ng, Y.C. Jean, Y. Ito and D.C. Walker, in "Initiation of Polymerization", ed. F.E. Bailey, Jr., Adv. Chem. Series, 212, 35 (1983).

94. E. Roduner, "Formation of Muonium substituted free radicals" μSR83 conference proceedings, Hyperfine Interactions, (in press).

95. P.W. Percival and J. Hochmann, Hyperfine Interactions, 6, 421 (1979).

96. S.F.J. Cox, A. Hill and Roberto De Renzi, J. Chem. Soc., Fara. Trans. I, 78, 2975 (1982).

97. P. Smith, J.T. Pearson, P.B. Wood and T.C. Smith, J. Chem. Phys., 43, 1535 (1965).

98. J.A. Kerr and M.J. Parsonage, "Evaluated Kinetic data in gas phase addition reactions", Butterworths, London, (1972).

99. M. Anbar, Farhatazia and A.B. Ross, Natl. Stand. Ref. Data Ser., Natl. Bur. Stand., 51, (1975).

100. E. Roduner, G.A. Brinkman and P.W.F. Louwrier, "Relative rate constants for the formation of Muonic radicals in liquid aromatic systems", μSR83 conference proceedings, Hyper. Inter., (in press).

101. J-P. Dodelet and G.R. Freeman, Can. J. Chem., 50, 2667 (1970).

102. A.O. Allen, NSRDS-NBS, 58 (1976).

103. A.O. Allen, NSRDS-NBS, 57 (1976).

104. R.C. Livingstone, W.G. Rothschild and J.J. Rush, J. Chem. Phys., 59, 2498 (1973).

105. H. Namba, K. Shinsaka and Y. Hatano, J. Chem. Phys., 70, 5331 (1979).

106. T.J. Hardwick, J. Phys. Chem., 65, 101 (1961).

107. Y. Ito, Y. Miyake, Y. Tabata, K. Nishiyama and K. Nagamine, Chem. Phys. Lett., 93, 361 (1982).

108. E.W.R. Steacie and R.E. Rebbert, J. Chem. Phys., 21, 1723 (1953).

109. R.J. Mikula, Ph.D. Thesis, University of British Columbia, Vancouver, 1981.

110. M. Eigen and L. de Maeyer, Z. Elektrochem., 59, 986 (1955).

111. G. Czapski and E. Peled, J. Phys. Chem., 77, 898 (1973).

112. J. Jortner and J. Rabani, J. Am. Chem. Soc., 83, 4868 (1961).

113. S. Nehari and J. Rabani, J. Phys. Chem., 67, 1609 (1963).

114. M.S. Matheson and J. Rabani, Radiation Res., 19, 180 (1963).

115. J.H. Baxendale, Radiation Res. Suppl., 4, 139 (1964).

116. (a) D.C. Walker, Quant. Rev., 21, 79 (1967).

(b) E.J. Hart and M. Anbar in "The Hydrated Electron", p. 191 (1970).

117. P. Neta and R.H. Schuler, J. Phys. Chem., 76, 2673 (1972).

118. E.V. Minaichev, G.G. Myasischcheva, Yu.V. Obukhov, V.S. Roganov, G.I. Savel'er, V.P. Smilga and V.G. Firsov, Soviet Physics JETP, 39, 946 (1974).

119. CRC Handbook of Chemistry and Physics, 59, (1979).

120. A.L.F. Lazzarini and E. Lazzarini, J. Inorg. Nucl. Chem., 42, 953 (1980).

121. M. Anbar and D. Meyerstein, J. Phys. Chem., 68, 3184 (1964).

122. E. Roduner and H. Fischer, Hyperfine Interact., 6, 413 (1979).

123. J.M. Stadlbauer, B.W. Ng, Y.C. Jean and D.C. Walker, J. Phys. Chem., 87, 841 (1983).

124. R.J. Rergeron, J. Chem. Ed., 54, 204 (1977).

125. Y.C. Jean and H.J. Ache, J. Phys. Chem., 81, 2093 (1977).

126. H.J. Fendler and E.J. Fendler, "Catalysis in Micellar and Macromolecular Systems", Academic Press, New York, (1975).

127. C. Bucci, P.R. Crippa, G.M. de'Munari, G. Guidi, M. Manfredi, R. Tedeschi, A. Vecli and P. Podini, Hyper. Inter. 6, 425 (1979).

128. O.E. Mögensen, J. Chem. Phys. 60, 998 (1974).

129. (a) O.E. Mögensen, Hyper. Inter., 6, 365 (1979).

(b) O.E. Mögensen, Chem. Phys. Lett., 65, 511 (1979).

130. Y. Ito and Y. Tabata, Proc. 5th Intern. Conf. Positron Annihil., 325 (1979).

131. J.P. Manion and M. Burton, J. Phys. Chem., 56, 560 (1952).

132. A.J. Swallow, Adv. in Chem. Ser., 82, 499 (1968).

133. E. Roduner, W. Strub, P. Burkhard, J. Hochmann, P.W. Percival, H. Fischer, M. Ramos and B.C. Webster, Chem. Phys., 67, 275 (1982).

134. R.A. Penneman, R. Bain, G. Bilbert, C.H. Jones, R.S. Nyholm and G.K.N. Reddy, J. Chem. Soc., 2266 (1963).

135. P. Neta and R.W. Fessenden, J. Phys. Chem., 74, 3362 (1970).

136. D. Behar and R.W. Fessenden, J. Phys. Chem., 76, 3945 (1972).

137. P.W. Percival and H. Fischer, Chem. Phys., 16, 89 (1976).

APPENDIX I

CORRECTIONS FOR MU-RADICAL AMPLITUDES

For μSR and MSR experiments, it is sufficient to obtain P_D's and P_M's by normalizing against $CC\ell_4$ as given by equations (2.11) and (2.12). However, for MRSR experiments, since the observed radical frequencies are so much higher than those in the above techniques (at least 10 times faster oscillations), there arises a need for corrections of the observable amplitudes before normalizing against $CC\ell_4$. The two corrections are, the finite response time (timing resolution) of the detection system and the pre-set number of bins per cycle in the spectrum. Both of these can cause apparent reductions in the amplitudes that one is trying to observe. Depending on the limitations of these two effects, amplitudes at frequencies greater than 200 MHz can be dramatically reduced or seriously obscured.

I.a. Effect of timing resolution of the detector system on the amplitude of sinusoidal oscillations.

Consider a wave of type $\cos(\omega t)$ (or $\sin(\omega t)$) and that at t=0 it fluctuates with a Gaussian distribution of standard deviation τ. This represents the detector response time (or the limit of the measuring instrument) and is commonly called the "jitter" in one's system. This jitter is assumed to be Gaussian since most random noise phenomena are of that nature. This Guassian distribution is displayed by Figure I-1 and is represented by the following expression:

$$f(t) = \frac{A}{\tau} \cdot \exp(-t^2/2\tau^2) \qquad (I\text{-}1)$$

where A is a factor so that f(t) is normalized to 1 (i.e. $\int_{-\infty}^{\infty} f(t)dt=1$).

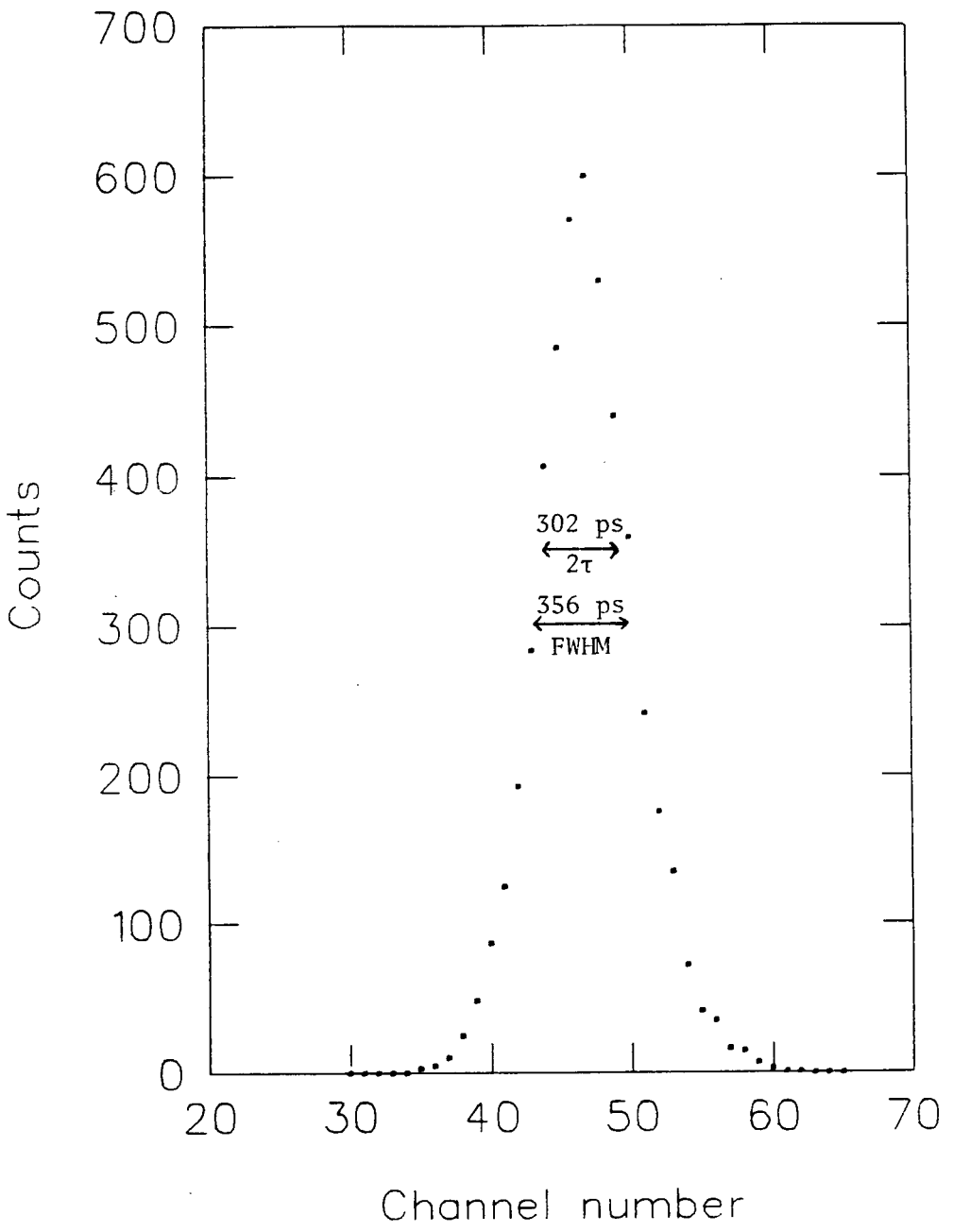

Figure I-1: Timing resolution curve of Positronium system by measuring the two γ's emitted from a ^{60}Co source. The curve is Gaussian in nature and is represented by equation (I-1).

As a matter of convenience, 2τ is defined as the timing resolution (Δt) of one's system in this thesis. Notice that the value of full width half maximum (FWHM) is slightly greater than that of 2τ.

To determine the effect of how this jitter, equation (I-1), affects the amplitude of a sinusoidal oscillation, one can physically superpose this jitter on top of an oscillation and watch its effects as it moves along the sinusoidal wave. Mathematically, this is equivalent to doing a convolution of the two functions. Therefore, let's define a sinusoidal oscillation by the following expression,

$$S(t) = \cos(\omega t) \ . \tag{I-2}$$

To perform the convolution, one integrates f(t') on S(t) over dt' from $-\infty$ to ∞,

$$I(t) = \int_{-\infty}^{\infty} S(t + t')\ f(t')\ dt' \ ; \tag{I-3}$$

or

$$I(t) = \int_{-\infty}^{\infty} \cos\{\omega(t+t')\} \cdot \frac{A}{\tau} \cdot \exp(-t'^2/2\tau^2)\ dt' \ . \tag{I-4}$$

The integration can be easily carried out to yield,

$$I(t) = \cos(\omega t)\ e^{\frac{-\tau^2\omega^2}{2}} \left\{ \int_{-\infty}^{\infty} f(t' + i\tau^2\omega)^2\ dt' \right\} . \tag{I-5}$$

Notice the integral in wiggly brackets is simply the original Gaussian jitter f(t) except with a phase shift in time.

Since $f(t)$ and $f(t' + i\tau^2\omega)$ are both normalized to one as mentioned previously, the effect $I(t)$ is again just a simple Gaussian function with an exponential decay of $\exp(-\tau^2\omega^2/2)$. For example,

$$I(t) = \exp(-\tau^2\omega^2/2)\cos(\omega t), \qquad \text{(I-6)}$$

where $\omega = 2\pi\nu$, and ν $(=1/T)$ is one's observable frequency in the μSR, MSR or MRSR experiment. Notice that the derivation is the same for a sine function. This observable amplitude fraction, $I''(t) = \exp\{-2\pi^2(\tau/T)^2\}$, is plotted against $2\tau/T$ in Figure I-2. It can be clearly seen that as T approaches Δt, it will not be observable in the Fourier transform (i.e. at $2\tau/T = 1$, $I''(t) \simeq 0$). This means that the following relationship should be seen for amplitudes of various frequencies

$$A_{OBS} = A_{REAL} \cdot \exp\left\{-\frac{1}{2}(\pi\nu\Delta t)^2\right\}. \qquad \text{(I-7)}$$

There are two ways in which one can check or obtain equation (I-7). One is to simply produce a timing resolution curve of the system using muons and beam positrons. This is done by using the muon as the start pulse and the beam e^+ as the stop pulse. The two signals are fed into a high resolution multi-channel analyzer (MCA), and a "T_0" curve can be obtained. This was carried out for the backward muon set-up with the forward and perpendicular histograms. The forward-T_0-calibration curve is shown in Figure I-3. Since this is a Gaussian distribution, one can plot ln N(t) versus t^2 to obtain Δt. In this case, $\Delta t = 0.80$ nsec (FWHM = 0.94 nsec) was obtained for the forward

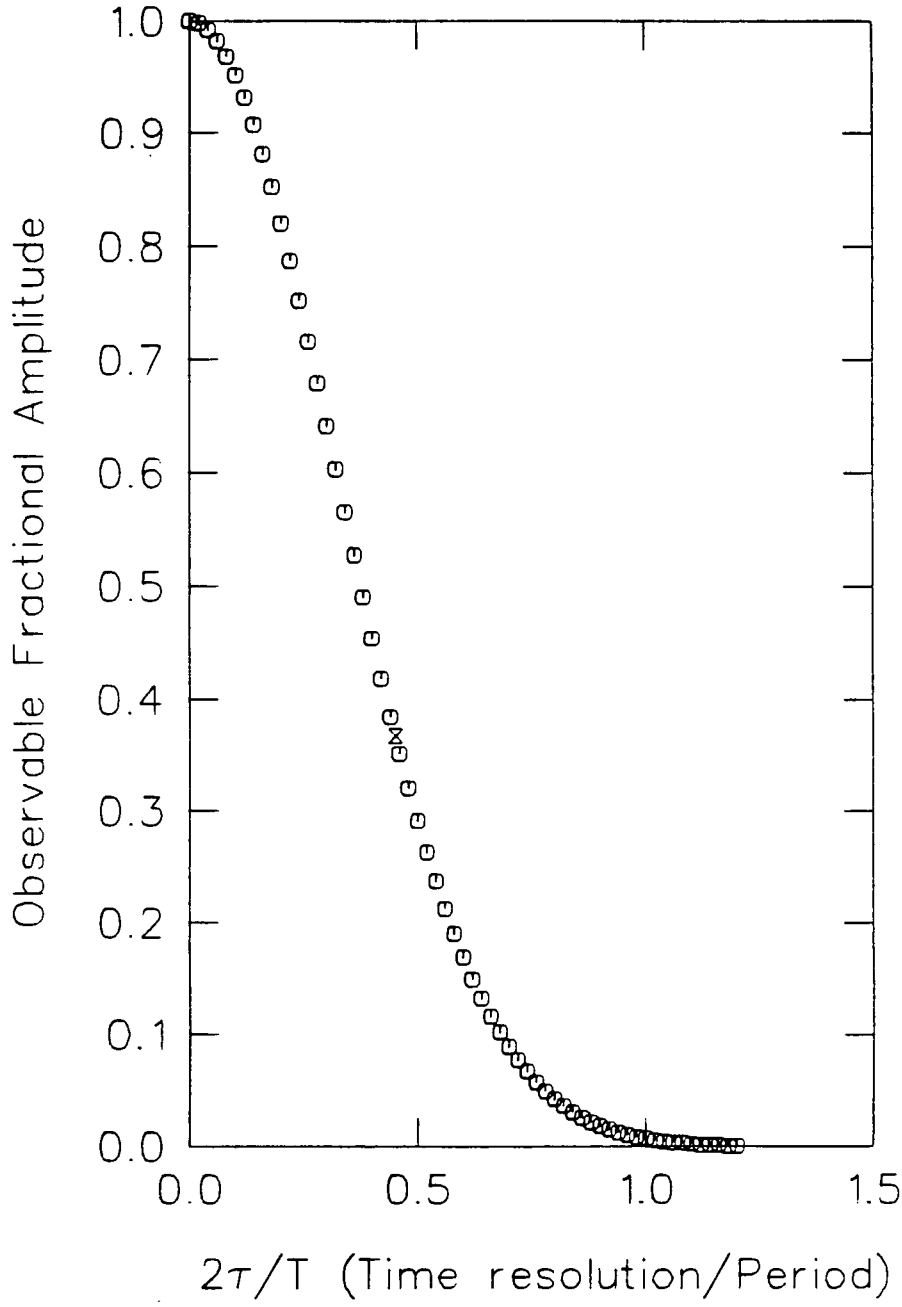

Figure I-2: The effect of timing resolution (2τ or Δt) on a sinusoidal function. The observable fractional amplitude $\exp\{-2\pi^2(\tau/T)^2\}$ is plotted against $2\tau/T$.

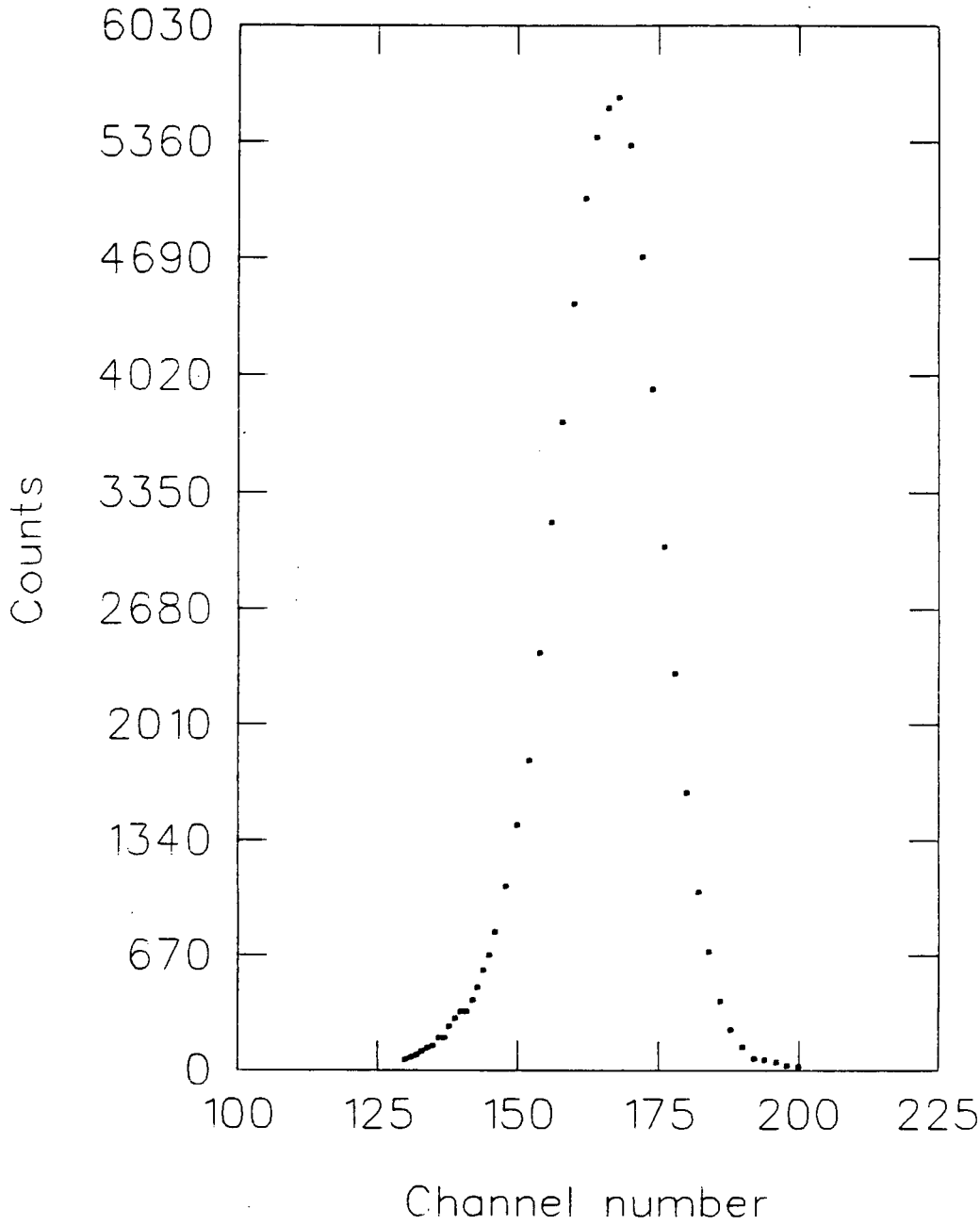

Figure I-3: T_o-calibration or timing resolution curve of the forward histogram for backward muon set-up.

histogram, while Δt = 0.97 nsec (FWHM = 1.14 nsec) for the perpendicular histogram. It was experimentally impossible to obtain the Δt-value for the backward spectrum. However, this T_0-method of getting Δt is only approximate since the clock of the detection system was not included in the calibration.

Another method of obtaining the relationship between the dependence of amplitude on Δt is by empirically measuring A_M of quartz as a function of magnetic field. Since A_M of quartz is large ($P_M \simeq 0.80$), then in effect, I"(t) can be easily determined as a function of frequency. This is a more accurate method compared to the above T_0-MCA technique since the exact electronic logic, experimental set-up, and computer software are being used to obtain the A_M functional dependence on magnetic field. The timing resolution curve is given in Figure I-4. When fitted with equation (I-7), (i.e. ln $A_{M(obs)}/A_{M(real)}$ versus $(freq.)^2$), Δt value of 1.24 nsec was obtained for the forward histogram, while 1.31 nsec for both the perpendicular and backward histograms. This shows that the jitter is Gaussian and the reduction effect can be described approximately by equation (I-7). However, for the correction due to timing resolution, the line drawn in Figure I-4 was used to obtain the true A_M values for the radicals. This is shown in Table 4.2.

I.b. Effect of packing factor on amplitudes.

Due to the limitation imposed by the clock (1GHz oscillator, 1 ns/bin absolute accuracy), the effect of packing factor (number of nsec per bin) on amplitude signal was investigated. The Mu-signal in water at 9G (raw packing factor = 2 ns/bin) was fitted with various packing factors (up to 68 ns/bin) using equation (2.6). The effect is plotted in Figure I-5. It can be seen

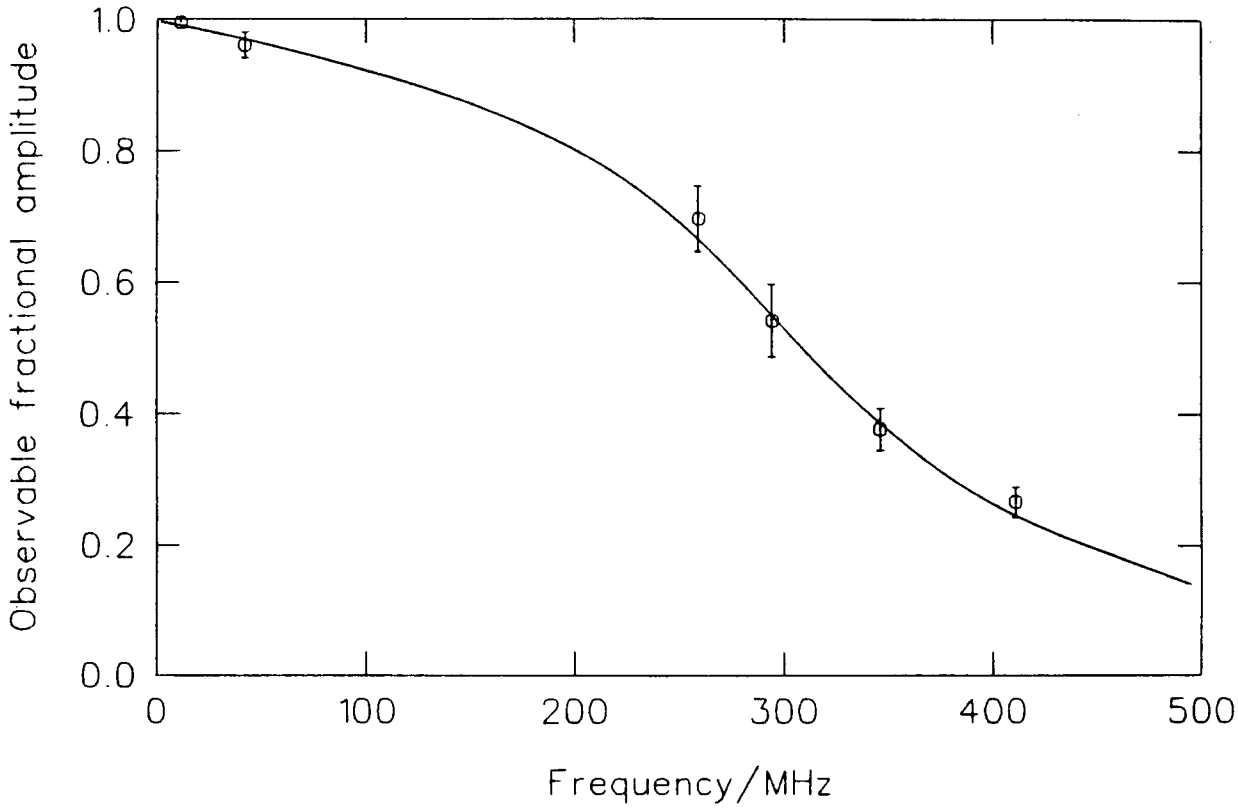

Figure I-4: Timing resolution curve of backward muon set-up using quartz as the emperical measurement. Its observable A_M is plotted against frequency (ν). The solid line is drawn by eye. The points are averages of the forward, perpendicular and backward histograms.

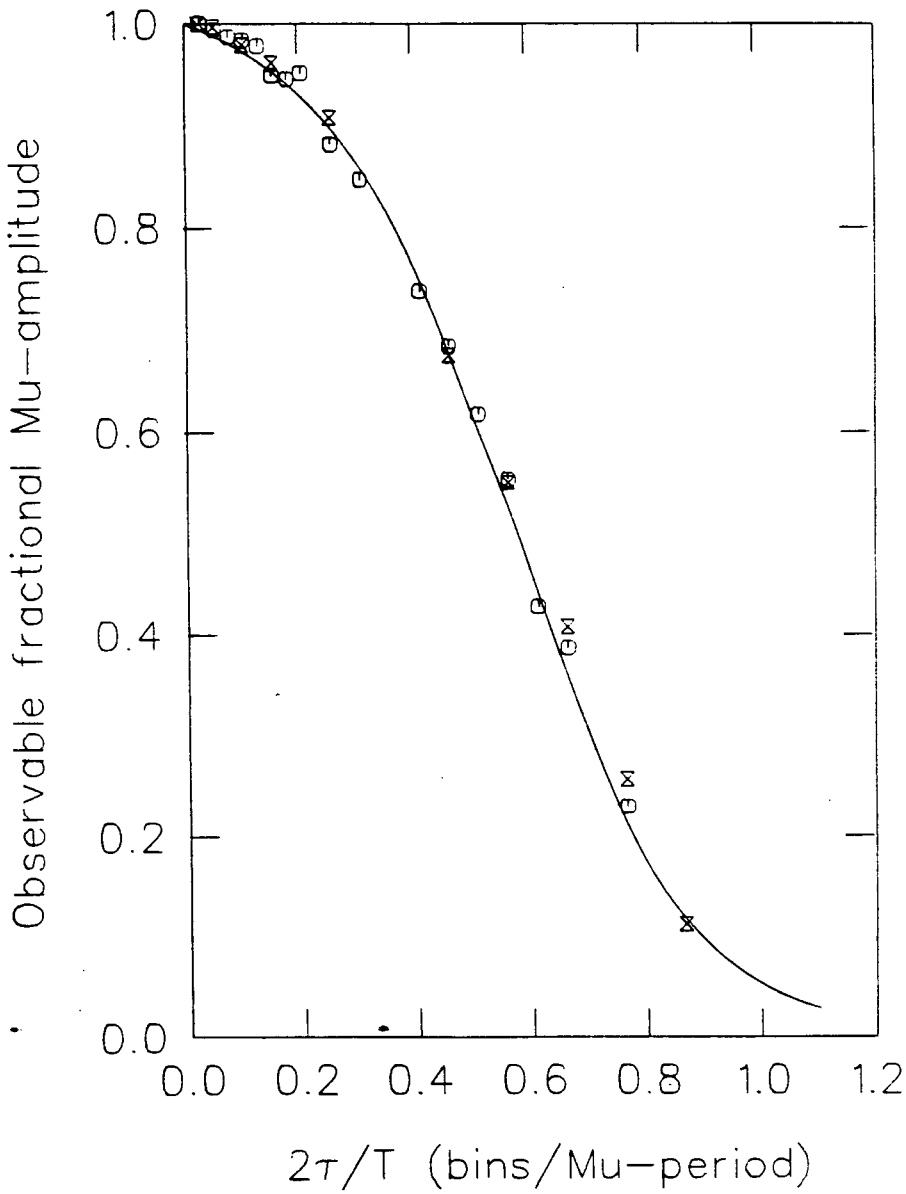

Figure I-5: Effect of bins/oscillation period on amplitude. The observable Mu-amplitude at 9G is plotted against $2\tau/T$ (bins/Mu-period).

that the functional dependence resembles that of equation (I-7). As a matter of fact, considering statistical effects at high packing factors, the distribution is Gaussian from 100% A_M down to 50%. For MRSR experiments, 1ns/bin packing was used for the radical spectra. Therefore, Figure I-5 is used as a further (in addition to I.a.) small correction to the amplitudes at various frequencies. This is given in Table 4.2.

I.c. Other effects.

Besides the above two corrections, additional effects such as density of sample and muon stops in target walls should be considered. The first effect arises from the fact that higher-energy decay positrons contain "higher asymmetries" of the total muon polarization than lower-energy positrons [4]. This means that high density materials (by degrading low energy positrons more) therefore create an apparently larger asymmmetry relative to low density materials. The second effect depends on collimater size up to the sample container, in this case, pyrex glass. In this thesis, backward muons are collimated to 20 mm and its their energy adjusted by a water degrader so that the muons will stop in the middle of the sample; therefore muons will only stop in the front glass of the sample container. It is estimated that these two effects, density and muon stops in glass, are very small for the MRSR experiments with benzene and styrene. In addition, the two effects tend to cancel each other out. This is corroborated by the fact that μSR experiments using $CC\ell_4$, H_2O, and the mixtures gave the same P_D values for all three histograms. This indicates that correction is not needed for these two effects.

APPENDIX II

RESIDUAL POLARIZATION OF A SINGLE-STEP MU REACTION MECHANISM

In section 5.B.2., an expression for the expected P_D-values for a single-step Mu reaction mechanism was given as equation (5.9). The derivation leading up to that expression was based upon some classical and intuitive arguments. In this appendix, a formal derivation based on the formalism by Fleming et al. [28] will be presented. Other references [4,137] should be read by those who wish to fully understand the complete derivation of muon polarization and its time dependence in transverse magnetic fields.

II.a. Residual polarization in liquids.

The residual polarization (P_{res}) is defined as the amplitude and phase of the diamagnetic μ^+-molecule extrapolated back to t=0, the time at which Mu is initially formed. The observable signal (to a good approximation) is the real part of P(t) [75], the exact (complex) time dependent polarization of the entire muon ensemble. Since an observation on the μSR timescale takes place long after the rapid motions of the μ^+-spin in Mu have settled down to the slow precession of the free μ^+-spin in a diamagnetic environment, one can say that one observes at t=∞. For example,

$$P_{OBS}(t) = \lim_{t\to\infty} (Re)\ P(t)\ . \qquad \text{(II-1)}$$

Experimentally, the signal is fitted to an expression of the form,

$$P_{OBS}(t) = |P_{res}|\ \cos(\omega_D t + \phi)\ , \qquad \text{(II-2a)}$$

$$\text{or} \qquad P_{OBS}(t) = Re\ \{P_{res} \cdot e^{i\omega_D t}\}\ ; \qquad \text{(II-2b)}$$

where $\tan\phi = \{Im(P_{res})/Re(P_{res})\}$. By equating (II-1) and (II-2b), one has

$$P_{res} = \lim_{t\to\infty} P(t) \cdot \exp(-i\omega_D t) \ . \qquad \text{(II-3)}$$

Notice here that P(t) depends on the method by which Mu reacts. In this case, the following derivations will be for a single step Mu reaction mechanism.

II.b. Implication of Mu reaction kinetics on P_{res}.

Since one essentially receives one muon at a time [3] into a sample, the problem of Mu kinetics, measured one at a time, can be equated with a "steady-state" approximation. Also, one can assume pseudo first-order kinetics in treating the Mu decay constant λ as proportional to concentration S ([S]): thus,

$$\lambda = k[S] + \lambda_o \ . \qquad \text{(II-4)}$$

There are two obvious limits for λ in relation to P_{res}. (i) If $\lambda >> \omega_o$, the muon spins will not have moved appreciably before the Mu reacts, then there will be no depolarization of the muon spins. This gives

$$P_{res} = 1 \ . \qquad \text{(II-5)}$$

(ii) If $\lambda << \omega_M$, then the reaction at randomly distributed times will leave the muons with randomly oriented spins, therefore causing complete depolarization

of the muon spins,

$$P_{res} = 0 . \qquad \text{(II-6)}$$

II.c. The ensemble of muon polarization in a single-step Mu reaction mechanism.

The ensemble of muon polarization at time t is formally given by,

$$P(t) = \sum_q f_q P_q(t) , \qquad \text{(II-7)}$$

where q represents the "fate" of a fraction f_q of the muon ensemble, and $P_q(t)$ gives the polarization at time t of that fraction. In a single-step Mu reaction mechanism, there are two types of fates:

$$Mu \longrightarrow Mu \text{ (unreacted)} \qquad \text{(II-8a)}$$

$$Mu \longrightarrow D . \qquad \text{(II-8b)}$$

In (II-8a), muons in still uncombined Mu atoms at time t (i.e. free Mu atoms) have

$$P_1(t) = e^{-\lambda t} \tilde{P}_D(t) , \qquad \text{(II-9)}$$

where $\tilde{P}_D(t)$ represents the complex μ^+ polarization in free Mu atoms. $\tilde{P}_D(t)$ will be given in the next section. On the other hand, in (II-8b), those muons in diamagnetic products following reaction at times $t'<t$ have

$$P_2(t) = \int_o^t \lambda e^{-\lambda t'} \tilde{P}_o(t') e^{i\omega_D(t-t')} dt' . \qquad \text{(II-10)}$$

P(t) is the sum of $P_1(t)$ and $P_2(t)$. In the limit of $t\to\infty$, (i.e. all Mu atoms eventually react), $P_1(t) = 0$. Therefore, substituting equation (II-10) into (II-3), one has an expression of P_{res} for a single-step Mu reaction mechanism.

$$P_{res} = \lambda \int_o^\infty \tilde{P}_o(t') e^{-(\lambda+i\omega_D)t'} dt' . \qquad \text{(II-11)}$$

II.d. The general expression of P_{res} for all fields.

In order to evaluate the P_{res} expression in (II-11), $\tilde{P}_D(t')$ must be calculated. According to the notations of Fleming et al. [28], $\tilde{P}_D(t)$ is given by equation (II-12).

$$\tilde{P}_D(t) = \tfrac{1}{2}[c^2(e^{i\omega_{12}t} + e^{-i\omega_{34}t}) + s^2(e^{i\omega_{23}t} + e^{i\omega_{14}t})] \qquad \text{(II-12)}$$

where:

$$c = \frac{1}{\sqrt{2}}\left[1 + \frac{x}{\sqrt{1+x^2}}\right]^{\frac{1}{2}} \qquad \text{(II-12a)}$$

$$s = \frac{1}{\sqrt{2}}\left[1 - \frac{x}{\sqrt{1+x^2}}\right]^{\frac{1}{2}} \qquad \text{(II-12b)}$$

and

$$x = B/B_o . \qquad \text{(II-12c)}$$

The frequencies, ω_{12}, ω_{34}, ω_{23} & ω_{14} are as defined in chapter 2 (Figure 2.5). Substituting equation (II-12) into (II-11) and integrating gives the analytical

expression for P_{res} at all fields in accordance with (II-13),

$$P_{res} = \frac{\lambda}{2}\left\{\frac{c^2}{\lambda+i(\omega_D-\omega_{12})} + \frac{c^2}{\lambda+i(\omega_D+\omega_{34})} + \frac{s^2}{\lambda+i(\omega_D-\omega_{23})} + \frac{s^2}{(\lambda+i(\omega_D-\omega_{14})}\right\} \tag{II-13}$$

II.e. Different field limits of P_{res}.

Now one has an analytical solution to P_{res} for a single-step Mu reaction mechanism. Before evaluating equation (II-13), one should consider the different field limits and their implications for reactions of various rate constants.

II.e.1. $B \lesssim 10G$.

At low magnetic fields ($B \lesssim 10G$), $x \simeq 0$, $c \simeq s \simeq 1/\sqrt{2}$, $\omega_{12} \simeq \omega_{23} \simeq \omega_M$; and $\omega_{34} \simeq \omega_{14} \simeq \omega_o$, equation (II-13) becomes

$$P_{res} = \frac{\lambda}{2}\left[\frac{1}{\lambda - i\Delta\omega}\right], \tag{II-14}$$

where $\Delta\omega=\omega_D-\omega_M$. For practical applications, the absolute magnitude of equation (II-14) can be rewritten as

$$|P_{res}| = (P_x^2 + P_y^2)^{-\frac{1}{2}}, \tag{II-15}$$

where

$$P_x = (Re)P_{res} = \frac{1}{2}\left[\frac{\lambda^2}{\lambda^2 + \Delta\omega^2}\right], \tag{II-15a}$$

and

$$P_y = (\mathrm{Im})P_{res} = \frac{1}{2}\left[\frac{\lambda\Delta\omega}{\lambda^2 + \Delta\omega^2}\right] . \qquad \text{(II-15b)}$$

II.e.2. $10G < B < 150G$.

In the case up to 150G where $x \lesssim 0.1$, equation (II-13) becomes

$$P_{res} = \frac{\lambda}{2}\left[\frac{1}{\lambda - i\omega_M} + \frac{\lambda^2}{\lambda^2 + \omega_o^2}\right] \qquad \text{(II-16)}$$

noting that $\omega_M >> \omega_D$.

By defining P_x and P_y as in (II-15), one obtains

$$|P_{res}| = \frac{1}{2}(\lambda^4 + \lambda^2\omega_M^2)^{\frac{1}{2}} / (\lambda^2 + \omega_M^2) . \qquad \text{(II-17)}$$

There are several interesting but qualitative features of equations (II-16) and (II-17). For extremely fast reactions ($\lambda >> \omega_o >> \omega_M$),

$$P_{res} \longrightarrow 1 ; \qquad \text{(II-16a)}$$

that is, all Mu atoms react at $t \simeq 0$ and therefore the polarization has no chance to change from its initial value. However, for normal reagent concentrations ($\lambda << \omega_o$),

$$P_{res} \longrightarrow \frac{1}{2}\left(\frac{1 + i\omega_M\tau}{1 + \omega_M^2\tau^2}\right) ; \qquad \text{(II-16b)}$$

where $\tau(=1/\lambda)$ is defined as the mean chemical lifetime of a thermal Mu atom. But when the reaction is still much faster than Mu precession ($\omega_M\tau<<1$), then

$$|P_{res}| \longrightarrow \frac{1}{2} ; \qquad \text{(II-17a)}$$

whereas if the opposite is true (i.e. $\omega_M\tau>>1$), then

$$|P_{res}| \longrightarrow 0 . \qquad \text{(II-17b)}$$

These qualitative features can be easily checked for one's Mu-reaction mechanism without going into any sophisticated (and tiring) calculations with equation (II-13).

II.f. Inclusion of Hot-atom reactions.

So far one has only been talking about those muons which thermalize as free Mu atoms. However, one must consider those epithermal Mu* atoms that react at "hot-times" ($\sim 10^{-12}$ sec, $t\simeq 0$) and have no opportunity for depolarization, or muons which do not form Mu. These muons contribute a constant unrotated fraction h (as defined in section 5.B.2) to the overall residual polarization, while the contribution (equation (II-13)) from thermal reactions of Mu atoms gives a fraction of (1-h). Therefore, the overall P_{res} or P_D is given by equation (II-18).

$$P_D = P_{res}\ (\text{overall}) = h + (1-h) \cdot P_{res}\ [\text{equation (II-13)}] . \qquad \text{(II-18)}$$

II.g. Application of P_{res} to muon yields in concentrated OH^- solutions.

In order to arrive at equation (5.9) in section 5.B.2., one simply substitutes the P_{res} expression for less than 150G (equation (II-17)) into equation (II-18) because $\lambda << \omega_o$. This gives the expression for the single-step Mu reaction in concentrated OH^- solutions as

$$P_D = h + 0.5(1-h)\ \{\lambda/(\lambda^2 + \omega_M^2)^{-\frac{1}{2}}\} \quad . \qquad \text{(II-19)}$$

PUBLICATIONS

(1) B.W. Ng, Y.C. Jean, Y. Ito, T. Suzuki, J.H. Brewer, D.G. Fleming and D.C. Walker, 1981, "Diffusion and activation-controlled reactions of muonium in aqueous solutions", J. Phys. Chem., vol. 85, p. 454.

(2) B.W. Ng, J.M. Stadlbauer, Y.C. Jean and D.C. Walker, 1983, "Muonium atoms in liquid and solid neopentane", Can. J. Chem., V.61, p.671.

(3) B.W. Ng, J.M. Stadlbauer and D.C. Walker, 1983, "Muon spin rotation involving muonium at high pH", J. Phys. Chem., in press.

(4) B.W. Ng, J.M. Stadlbauer, Y. Ito, Y. Miyake, and D.C. Walker, "Muonium radicals in styrene-benzene mixtures", Hyper. Inter., in press.

(5) Y.C. Jean, D.G. Fleming, B.W. Ng and D.C. Walker, 1979, Chem. Phys. Lett., V.66, p.187.

(6) Y.C. Jean, B.W. Ng and D.C. Walker, 1980, Chem. Phys. Lett., vol.75. p.561.

(7) Y. Ito, B.W. Ng, Y.C. Jean and D.C. Walker, 1980, Can. J. Chem., V.58. p.2395.

(8) Y.C. Jean, B.W. Ng, J.H. Brewer, D.G. Fleming, and D.C. Walker, 1981, J. Phys. Chem., vol.85, p.451.

(9) Y. Ito, B.W. Mg, Y.C. Jean and D.C. Walker, 1981, Hyperfine Interactions, vol.8, p.355.

(10) Y.C. Jean, B.W. Ng, Y. Ito, T.Q. Nguyen and D.C. Walker, 1981, Hyperfine Interactions, vol.8, p.351.

(11) Y.C. Jean, B.W. Ng, J.M. Stadlbauer, and D.C. Walker, 1981, J. Chem. Phys., vol.75, p.2879.

(12) J.M. Stadlbauer, B.W. Ng, Y.C. Jean, Y. Ito and D.C. Walker, 1981, Can. J. Chem., vol.59, p.3261.

(13) J.M. Stadlbauer, B.W. Ng and D.C. Walker, 1983, J. Am. Chem. Soc., vol.105, p.752.

(14) J.M. Stadlbauer, B.W. Ng, Y.C. Jean and D.C. Walker, 1983, J. Phys. Chem., vol.87, p.841.

(15) Y.C. Jean, B.W. Ng and D.C. Walker, 1982, in "Applications of Nuclear and Radiochemistry", p.543.

(16) J.M. Stadlbauer, B.W. Ng, Y.C. Jean, Y. Ito and D.C. Walker, 1983, in "Initiation of Polymerization", p.35.

(17) J.M. Stadlbauer, B.W. Ng, Y.C. Jean, Y. Ito and D.C. Walker, 1983, Hyperfine Interactions, in press.

(18) Y. Miyake, Y. Tabata, Y. Ito, B.W. Ng, J.M. Stadlbauer and D.C. Walker, 1983, Chem. Phys. Lett., in press.

(19) Y. Miyake, B.W. Ng, J.M. Stadlbauer, Y. Ito, Y. Tabata and D.C. Walker, 1983, "Temperature dependence of Muonium in hydrocarbons", Hyperfine Interactions, in press.

(20) J.M. Stadlbauer, B.W. Ng, R. Ganti and D.C. Walker, 1983, "Muonium addition reactions to aromatic solutes: application of the Hammett equation in the production of muonium-radicals", J. Am. Chem. Soc., submitted.